

**STRUCTURAL AND SPECTROSCOPIC ANALYSIS OF PROLINE-
BASED DEEP EUTECTIC SOLVENTS AND THEIR INTERACTIONS
WITH ALPHA-LACTALBUMIN PROTEIN**

By

Raisul Awal Mahmood

In the partial fulfillment of the requirement for the degree

of

MASTER OF SCIENCE IN CHEMISTRY



Department of Chemistry

**BANGLADESH UNIVERSITY OF ENGINEERING AND
TECHNOLOGY (BUET),**

DHAKA-1000

November 2021

**Bangladesh University of Engineering and Technology (BUET), Dhaka-1000
Department of Chemistry**



Certification of Thesis

A thesis on

**STRUCTURAL AND SPECTROSCOPIC ANALYSIS OF PROLINE-BASED DEEP
EUTECTIC SOLVENTS AND THEIR INTERACTIONS WITH ALPHA-
LACTALBUMIN PROTEIN**

By

Raisul Awal Mahmood

Roll No.: 1018032701, Session: October-2018, has been accepted as satisfactory in partial fulfillment of the requirements for the degree of Master of Science (M.Sc.) in Chemistry and certify that the student has demonstrated satisfactory knowledge of the field covered by this thesis in an oral examination held on November 09, 2021.

Board of Examiners

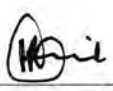
1. Dr. Md. Shakhawat Hossain Firoz

Professor
Department of Chemistry
BUET, Dhaka-1000.


Supervisor & Chairman

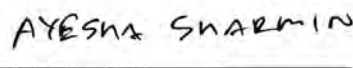
2. Dr. Md. Abdur Rashid

Head
Department of Chemistry
BUET, Dhaka-1000


Member (Ex-officio)

3. Dr. Ayesha Sharmin

Associate Professor
Department of Chemistry
BUET, Dhaka-1000


Member

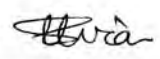
4. Dr. Md. Ayub Ali

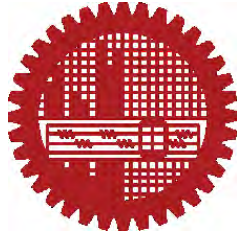
Assistant Professor
Department of Chemistry
BUET, Dhaka-1000


Member

5. Dr. Muhammed Shah Miran

Professor
Department of Chemistry
University of Dhaka, Dhaka -1000


Member (External)



CANDIDATE'S DECLARATION

It is hereby declared that this thesis or any part of it has not been submitted elsewhere for the award of any degree or diploma.

Raisul Awal

Raisul Awal Mahmood

ACKNOWLEDGEMENTS

In the first place, I am infinitely grateful to Almighty creator who gives me the physical and mental ability, patience, strength, and courage continuously to complete this research work and to prepare this manuscript as a thesis for the fulfillment of the degree of Master of Science in the Department of Chemistry at Bangladesh University of Engineering and Technology (BUET), Dhaka Bangladesh.

I warmly and sincerely show my gratitude to my respected supervisor **Dr. Md. Shakhawat Hossain Firoyz**, Professor, Department of Chemistry, Bangladesh University of Engineering and Technology (BUET), for allowing me to work in the group of *nano*Chemistry Research Laboratory. Besides, I want to show my cordial gratitude to my respected co-supervisor **Dr. Mohammad A. Halim** who gives me the freedom to work in his computational research group, *The Red-Green Research Centre*. In this research, he has encouraged me to learn and teach me the best guidance in the field of computational chemistry. I also express my greatest thanks to **Md. Sajjadur Rahman** and **Md. Ackas Ali** for helping me in this research work.

I would like to convey my thankfulness to all teachers including Professor **Dr. Md. Abdur Rashid**, **Dr. Al-Nakib Chowdhury**, and **Dr. Nazrul Islam**, Associate professor **Dr. Abu Bin Imran**, Associate Professor **Dr. Ayesha Sharmin**, Assistant professor **Dr. Chanchal Kumar Roy**, and Assistant Professor **Dr. Md. Ayub Ali** for their guidance and encouragement during my research work.

My warmest appreciation goes to all of my friends specially **Sadnan Chowdhury**, **Md. Yeasin Arafat Tarek**, **Sumaia Afroz Mim**, and all other friends for their cooperation, fruitful discussion and for their cordial help during my study period, and all sorts of encouragement throughout my university life. I also give my heartiest thanks to my all seniors especially **Syed Abdul Monim**, **Akter H. Reaz**, **Md Amzad Hossain** who give me continuous guidance, support, and knowledge.

I am highly obliged to all members of the board of examiners for their valuable suggestions and comments. I am also very much thankful to the CASR, BUET for providing financial support to complete this research work.

I am very grateful to my parents for their unquestioned trust, support, and love, understanding, and sacrifice. They have encouraged me more than I could ever have hoped for. Without their careful assistance, it would not possible to complete my Master's study.

With love and affection
Raisul Awal Mahmood

Table of Contents

	Page No.
Graphical Abstract	01
Abstract	01
CHAPTER 1	
INTRODUCTION	02
1.1 Fundamental of Deep Eutectic Solvents (DES)	02
1.2 Theoretical approach	13
1.3 Potential energy surface (PES) and global minimum energy structure	16
1.4 Basis set and its classification	19
1.5 Electronic structure theory	21
1.6 Problem statement and present approach	22
CHAPTER 2	
COMPUTATIONAL METHODOLOGY	25
2.1 Preparation of Deep Eutectic Solvent (DES) components	25
2.2 Molecular Dynamics (MD) Simulation of DES components	25
2.2.1 Required number of molecules of L-Proline and Urea for MD simulation	25
2.2.2 YASARA Dynamics tool for MD simulation	26
2.3 Analyses of MD simulation results of DES components	27
2.3.1 Analyses of 50 ns L-Proline and urea DES micro-structures	27
2.3.2 Non-bonding interaction of DES components	27
2.3.3 Selection of the best pair and isolation of 1:1 L-Proline: Urea DES clusters	29
2.3.4 Finalization of the best structures from 1:1 L-Proline: Urea DES clusters	30
2.3.5 QM calculation of the final structures of 1:1 L-Proline: Urea DES clusters	31
2.4 MD simulation of 1:1 D-Proline: Urea DES of 200 pairs	32
2.5 Analyses of 200 pairs of D-Proline: Urea DES	32
2.5.1 Analysis of 50 ns 1:1 D-Proline: Urea DES micro-structures	32

2.5.2 Non-bonding interaction of 1:1 D-Proline: Urea DES clusters	33
2.5.3 Finalization of the best structures from 1:1 D-Proline: Urea DES clusters	35
2.5.4 QM calculation of final structures of 1:1 D-Proline: Urea DES clusters	36
2.6 Protein preparation	37
2.7 YASARA Dynamics tool for protein MD simulation in DES solvents	37
2.8 Parameters for protein MD simulation in DES solvents	38
CHAPTER 3	
RESULTS AND DISCUSSION	39
3.1 QM calculation of 1:1 L-Proline: Urea and 1:1 D-Proline: Urea cluster conformers	39
3.1.1 Structural geometry and hydrogen bond analysis by DFT calculation	39
3.1.2 Thermochemistry calculation	41
3.1.2 Molecular electrostatic potential, HOMO-LUMO and NBO charge	42
3.1.3 Calculated IR spectra analysis	46
3.1.4 Calculated VCD spectra analysis	49
3.2 MD simulation results of DES-protein complex	52
3.2.1 Impact on the backbone structure of alpha-lactalbumin	52
3.2.2 Effect on the compactness of alpha-lactalbumin	53
3.2.3 Variation of solvent accessible surface area of alpha-lactalbumin	55
3.2.4 Impact on the flexibility of alpha-lactalbumin	57
3.2.5 Changes in secondary structure of alpha-lactalbumin	58
CHAPTER 4	
CONCLUSIONS AND FUTURE ASPECTS	65
4.1 Conclusion	65
4.2 Future Aspects of this Research	65
REFERENCES	67 – 74

List of Figures

Figure No.	Figure Caption	Page No.
Figure 1.1	Schematic illustration of the phase diagram of a eutectic point on two-component mixtures	02
Figure 1.2	Simulation structure of (CPL/TBACl) + H ₂ S + CH ₄ DES obtained from GROMACS. Color code – white: hydrogen; grey: carbon; blue: nitrogen; yellow: sulfur; and green: chloride	04
Figure 1.3	(a) Simulation snapshots of ethaline-water mixtures at equilibration describing the structural arrangement of hydrogen bond donors (ethylene glycol and water molecules) in 0.5-w, 2-w, 10-w, and 20-w ethaline-water mixtures; (b) Isodensity surfaces around the central choline cation for 0.5-w, 2-w, 10-w, and 20-w ethaline-water mixtures	06
Figure 1.4	The lowest energy cluster conformers of 1:1 L-Men/AA DES are (a) conformer A, (b) conformer B, (c) conformer C, and (d) conformer D, optimized at the ω B97XD/6-311G (d,p) level of theory	07
Figure 1.5	(a) Crystal structure of HP-36 (PDB: 1VII). The locations of helix 1 (residues 4–8), helix 2 (15–18), and helix 3 (23–32) are also indicated. (b) Folded conformations are FOLD1–FOLD3. (c) Unfolded conformations are UNFOLD1–UNFOLD10	09
Figure 1.6	Spatial density maps of (a) Gdm ⁺ and (b) urea within 5 Å of the protein in 2 M denaturant solution at T = 300 K; (c) Interaction of Gdm ⁺ with Asp52 and Glu35; (d) Interaction of urea with Trp63 and Thr118	10
Figure 1.7	Interactions between (a) Gln23, (b) Thr267, (c) Glu269, and (d) Lys271 with urea, choline and chloride ions in Reline at 300 K	11
Figure 1.8	(a) RMSD of C α atoms of HEWL backbone with its crystal structure; (b) the radius of gyration of HEWL; (c) root-mean-square fluctuations of C α atoms of each residue averaged over the last 100 ns in the presence of water, 50/50 reline/water, 75/25 reline/water, and pure reline	12
Figure 1.9	Geometry optimization by force field methods - (a) the change in energy of a molecule with the changes of bond lengths and bond angles; (b) dihedral angles (torsional angles) effect on molecular geometries and energies and (c) variation of the energy of a molecule with separation of nonbonded atoms or groups	14-15
Figure 1.10	(a) Geometric parameters (such as q ₁ , q ₂ , q ₃ ,) in a cartesian coordinate system where the PES lies; (b) A potential energy surface (PES) where given input structure is turned to optimized	17-18

	structure and (c) The lowest energetically structure is the global energy minimum where the optimized structure is obtained	
Figure 2.1	Optimized structures of (a) L-Proline, (b) D-Proline, (c) Urea in the gas phase calculated at pm6 level of theory. The asterisk (*) sign indicates the chiral center	25
Figure 2.2	50 ns simulation snapshot (structure) of (a) 50:50 ratio, (b) 100:100 ratio, (c) 150:150, (d) 200:200 and (e) 250:250 ratio obtained from MD simulation in the gas phase	26
Figure 2.3	50 ns simulation structures of (a) 50:50, (b) 100:100, (c) 150:150, (d) 200:200 and (e) 250:250 ratios of L-Proline: Urea in the gas phase obtained from molecular dynamics (MD) simulation showed hydrogen bond interaction form	27
Figure 2.4	A total of 11 clusters of 1:1 L-Proline: Urea DES were isolated from 200:200 ratio in the gas phase.	29
Figure 2.5	Total 50 ns Energy (kJ/mol) vs Time (ns) plot of 200:200 of L-Proline: Urea obtained from the analysis of MD simulation results which shows equilibrium at 30 – 50 ns	30
Figure 2.6	Single point (SP) energy calculation of 11 clusters of 1:1 L-Proline: Urea clusters and the chosen three clusters at 39.2, 40.8 and 42.2 ns were highlighted after reaching equilibrium at 30 – 50 ns	31
Figure 2.7	50 ns simulation structure of 200:200 of L-Proline: Urea in the gas phase obtained from molecular dynamics (MD) simulation	33
Figure 2.8	Total 58 clusters of 1:1 D-Proline: Urea DES were isolated from 200:200 ratio in the gas phase	33 – 35
Figure 2.9	Total 50 ns Energy (kJ/mol) vs Time (ns) plot of 200:200 of L-Proline: Urea obtained from the analysis of MD simulation results which shows equilibrium at 30 – 50 ns	35
Figure 2.10	Single point (SP) energy calculation of 11 clusters of 1:1 L-Proline: Urea clusters and the chosen three clusters at 31.3, 32.0 and 46.3 ns were highlighted after reaching equilibrium at 30 – 50 ns	36
Figure 2.11	Crystal structure of alpha-lactalbumin (PDB ID: 1hfx, resolution 1.90Å) obtained from https://www.rcsb.org/structure/1hfx . The different colors indicate the different domains of the protein	37
Figure 2.12	Initial simulation soup of Alpha-lactalbumin in (a) L-Proline: Urea DES, (b) 20% water-DES and (c) 40% water-DES (d) D-Proline: Urea DES and (e) Physiological solution where the magenta color indicates the L-Proline and orange color indicates the urea molecules.	38
Figure 3.1	Optimized structures of (a) L1, (b) L2, and (c) L3 cluster conformers of 1:1 L-Proline: Urea DES calculated at B3LYP-	39

	D3/6-311+g(d,p) level of theory. The dotted bonds indicate the hydrogen bonding interactions	
Figure 3.2	Optimized structures of (a) D1, (b) D2, and (c) D3 cluster conformers of 1:1 D-Proline: Urea DES calculated at B3LYP-D3/6-311+g(d,p) level of theory. The dotted bonds indicate the hydrogen bonding interactions	40
Figure 3.3	Molecular electrostatic potential (MEP) surface of (a) L1, (b) L2, (c) L3 cluster, (d) L-Proline and (e) Urea calculated at B3LYP-D3/6-311+g(d,p) level of theory highlighting the regions to interact through hydrogen bonding. The red region is the negative electrostatic potential and the blue region is the positive electrostatic potential	42
Figure 3.4	Electrostatic potential (ESP) surface map of (a) D1, (b) D2, (c) D3 cluster, (d) D-Proline and (e) Urea calculated at B3LYP-D3/6-311+g(d,p) level of theory highlighting the regions to interact through hydrogen bonding. The red region is the negative electrostatic potential and the blue region is the positive electrostatic potential	43
Figure 3.5	Frontier molecular orbitals (HOMO-LUMO) with an energy gap of (a) L1, (b) L2, (c) L3 cluster, (d) L-Proline and (e) Urea calculated at B3LYP-D3/6-311+g(d,p) level of theory. The yellow regions indicate the positive isosurfaces and the blue regions indicate the negative isosurfaces	44
Figure 3.6	Frontier molecular orbitals (HOMO-LUMO) with an energy gap of (a) D1, (b) D2, (c) D3 cluster, (d) D-Proline, and (e) Urea calculated at B3LYP-D3/6-311+g(d,p) level of theory. The yellow regions indicate the positive isosurfaces and the blue regions indicate the negative isosurfaces	44
Figure 3.7	Calculated IR spectra of urea, L-Proline, L1, L2, and L3 clusters at (a) Low-frequency region and (b) High-frequency region at B3LYP-D3/6-311+G(d, p) level of theory in the gas phase	48
Figure 3.8	Calculated vibrational circular dichroism (VCD) spectra of L-Proline, L1, L2, and L3 clusters at (a) Low-frequency region and (b) High-frequency region at B3LYP-D3/6-311+G(d, p) level of theory in the gas phase	49
Figure 3.9	Calculated vibrational circular dichroism (VCD) spectra of D-Proline, D1, D2, and D3 clusters at (a) Low-frequency region and (b) High-frequency region at B3LYP-D3/6-311+G(d, p) level of theory in the gas phase	50
Figure 3.10	Analysis of 500ns simulation for alpha-lactalbumin by the root mean square deviation (RMSD) values for C- α atom in Proline-based DES solvents	52

Figure 3.11	Analysis of 500ns simulation for alpha-lactalbumin by Radius of gyration (R_g) in Proline-based DES solvents	53
Figure 3.12	Analysis of 500ns simulation for alpha-lactalbumin by solvent accessible surface area (SASA) in Proline-based DES solvents	54
Figure 3.13	Polar (Hydrophilic) and apolar (Hydrophobic) surface area of 500 ns simulation structure of alpha-lactalbumin in Proline-based DES solvents	55
Figure 3.14	Analysis of 500ns simulation for alpha-lactalbumin by root mean square fluctuations (RMSF) in Proline-based DES solvents	56
Figure 3.15	RMS fluctuation of residues (a) Leu8 – Ser9, (b) Asp14 – Leu15, (c) Asp20 – Thr22, (d) His32 – Tyr36, (e) Asp84 – Asp87, (f) Leu110 – Cys111 and (g) Cys120 – Glu121 of alpha-lactalbumin over the simulation of 500 ns	57
Figure 3.16	The superimposed structure (in Figure) also shows the structural changes of all conformers in different domains	58
Figure 3.17	Conformational changes of alpha-lactalbumin in L-Proline: Urea DES, 20% water-L Proline: Urea DES, 40% water-L Proline: Urea DES, D-Proline: Urea DES, and physiological solution.	59
Figure 3.18	Analysis of (a) Percentage of secondary structure contents and (b) Visual changes of alpha-lactalbumin in L-Proline: Urea DES, D-Proline: Urea DES, 20% water, 40% water, and physiological solution at 500ns	59
Figure 3.19	Analysis of (a) Percentage of secondary structure contents and (b) Visual changes of alpha-lactalbumin in L-Proline: Urea DES, D-Proline: Urea DES, 20% water, 40% water, and physiological solution at 500ns	61
Figure 3.20	Interaction between the residues of protein and DES components shows that H-bonds dominate the residues by the urea and L-Proline	62
Figure 3.21	Interaction between the residues of protein and DES components with the presence of 20% water shows that <i>urea-water-proline</i> or <i>urea-proline-water</i> dominate the residues of the protein	63
Figure 3.22	Interaction between the residues of protein and DES components with the presence of 40% water shows that <i>urea-(water)_{cluster}-proline</i> or <i>urea-proline-(water)_{cluster}</i> dominate the residues of the protein	64

List of Tables

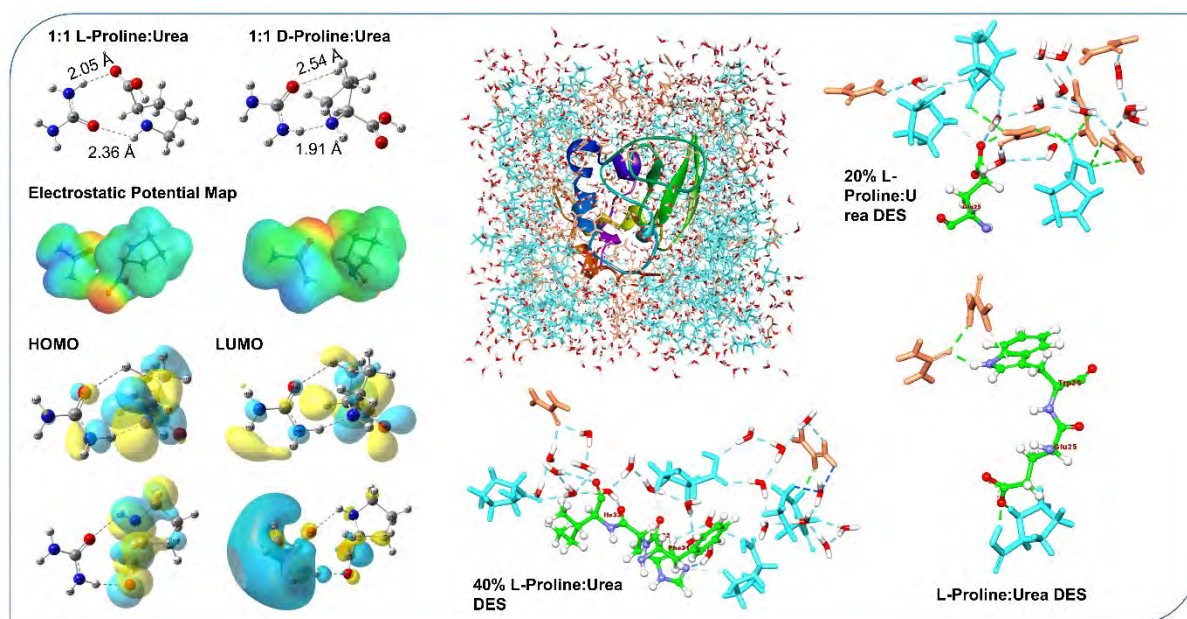
Table No.	Table Caption	Page No.
Table 1	Types of different types of DES solvent systems	03
Table 2	Required number of molecules of L-Proline and urea for 50, 100, 150, 200, and 250 pairs for MD simulation in the gas phase	26
Table 3	H-bond distances of (a) 50, (b) 100, (c) 150, (d) 200 and (e) 250 pairs of L-Proline and urea of 1:1 L-Proline: Urea DES cluster conformers	27-29
Table 4	Explanation of theoretical method, B3LYP-D3/6-311+G(d,p) level of theory that was used for studied DES	32
Table 5	Required number of molecules of D-Proline and urea of 200 pairs of 1:1 D-Proline: Urea for MD simulation in the gas phase	32
Table 6	The required number of molecules of L-Proline, urea, D-Proline, and water molecules for DES-protein MD simulation	37
Table 7	Selected H-bond distances of 1:1 L-Proline: Urea and 1:1 D-Proline: Urea DES calculated at D3-B3LYP/6-311+G (d,p) level of theory	40
Table 8	Change in Gibbs Free Energies, Enthalpies and Electronic Energies of (a) 1:1 L-Proline: Urea and (b) 1:1 D-Proline: Urea DES calculated at D3-B3LYP/6-311+G (d,p) level of theory	41
Table 9	NBO Charges of (a) L1, L2, and L3 clusters of 1:1 L-Proline: Urea DES (b) D1, D2, and D3 clusters of 1:1 D-Proline: Urea DES calculated at B3LYP-D3/6-311+g(d,p) level of theory. ($N_{3(\text{Pro})} = N_3$ atom of Proline in 1:1 L-Proline: Urea DES)	45
Table 10	Calculated vibrational frequencies of the major functional groups of 1:1 L-Proline: Urea DES cluster conformers and their relative wavenumber changes (%) in the DES with respect to urea and L-Proline	46
Table 11	Calculated vibrational frequencies of the major functional groups of 1:1 D-Proline: Urea DES cluster conformers and their relative wavenumber changes (%) in the DES with respect to urea and D-Proline	47
Table 12	Calculated IR and VCD intensities of the characteristic functional groups of L1, L2, and L3 clusters of 1:1 L-Proline: Urea DES	49
Table 13	Calculated IR and VCD intensities of the characteristic functional groups of D1, D2, and D3 of 1:1 D-Proline: Urea DES	51
Table 14	The polar and apolar surface area of 500 ns simulation structure of alpha-lactalbumin in L-Proline DES, 20% water-L Proline DES, 40% water- L Proline: Urea DES, D-Proline: Urea DES, and physiological solution	56

Table 15	Percentage of secondary structure contents (α -Helix, β -Sheet, β -Bridge, Turn, Coil and 3_{10} -Helix) of alpha-lactalbumin in L-Proline: Urea DES, 20% water, 40% water, D-Proline: Urea DES, and physiological solution at 500ns	60
----------	--	----

List of Abbreviations of Technical Symbols and Terms

1. *DES*: Deep eutectic solvent
2. *THDES*: Therapeutic deep eutectic solvent
3. *HBD*: Hydrogen bond donor
4. *HBA*: Hydrogen bond acceptor
5. *ChCl*: Choline chloride
6. *BO*: Born-Oppenheimer
7. *MM*: Molecular Mechanics
8. *PES*: Potential energy surface
9. *QM*: Quantum Mechanics
10. *LCAO*: Linear Combination of Atomic Orbitals
11. *MO*: Molecular orbital
12. *STO*: Slater-type orbital
13. *GTO*: Gaussian-type orbital
14. *HF*: Hartree-Fock
15. *MP*: Møller–Plesset
16. *CC*: Couple Cluster
17. *CCSD*: Coupled cluster single-double
18. *CCSD(T)*: Coupled cluster single-double (Triplet)
19. *DLPNO-CCSD(T)*: Domain-based Local Pair-Natural Orbital Coupled Cluster single-double (Triplet)
20. *DFT*: Density function theory
21. *LSDA*: Local Spin Density Approximation
22. *B3LYP*: Becke 3-parameter Lee–Yang–Parr
23. *B3LYP-D3*: Becke 3-parameter Lee–Yang–Parr with dispersion correction
24. *PBE*: Perdew–Burke–Ernzerhof
25. *MD*: Molecular Dynamics
26. *RDF*: Radial distribution function
27. *SDF*: Spatial density function
28. *MMFF*: Merck Molecular Force Field
29. *GAFF*: General Amber Force Field
30. *M06*: Minnesota 06
31. *NBO*: Natural bond orbital
32. *CHELPG*: Charges from electrostatic potentials using a Grid-based method
33. *IR*: Infra-Red
34. *VCD*: Vibrational circular dichroism
35. *YASARA*: Yet Another Scientific Artificial Reality Application
36. *GROMACS*: Groningen machine for chemical simulations
37. *COSMO-RS*: Conductor like screening model for real solvents
38. *RMSD*: Root mean square deviation
39. R_g : Radius of gyration
40. *SASA*: Solvent accessible surface area
41. *RMSF*: Root mean square fluctuation
42. *AMBER*: Assisted Model Building with Energy Refinement
43. *PME*: Particle-mesh Ewald
44. *SPE*: Single point energy
45. *MEP*: Molecular electrostatic potential
46. *HOMO*: Highest occupied molecular orbital
47. *LUMO*: Lowest unoccupied molecular orbital

GRAPHICAL ABSTRACT



ABSTRACT

This work represents the computational approaches using molecular dynamic (MD) simulations and quantum calculations to elucidate the proline-based Deep Eutectic Solvents (DES) L-Proline: Urea and D-Proline: Urea in 1:1 molar ratios. The most stable DES clusters are established by an MD simulation study followed by a quantum calculation with the B3LYP-D3/6-311G+(d,p) level of theory. By observing the orientation and vibrational spectra, the responsible H-bonds of 1:1 L-/D-Proline: Urea are $\text{NH}_{\text{L-Pro}} \dots \text{HN}_{\text{Urea}}$, $\text{CO}_{\text{Urea}} \dots \text{HC}_{\text{L-Pro}}$, $\text{OH}_{\text{L-Pro}} \dots \text{OC}_{\text{Urea}}$ and $\text{CO}_{\text{Urea}} \dots \text{HN}_{\text{L-Pro}}$, probed by NBO charge transfer, HOMO-LUMO, and electrostatic potential map analyses. The changes in Gibb's free energy (ΔG), electronic energy (ΔE), and enthalpy (ΔH) give evidence of the spontaneity of DES formation. Calculated IR and vibrational circular dichroism (VCD) signatures give the characteristics spectra that support the hydrogen bond formation of DES cluster conformers. In L-/D-Proline: Urea DES, the selected protein, alpha-lactalbumin gets stabilized. After 20% and 40% water insertion into DES-protein, this stabilizing gets deteriorated. In 20% water, the protein destabilizes most because the water molecules lodge in the DES microstructures producing *urea-(water)_{cluster}-proline* or *urea-proline-(water)_{cluster}* while 40% of water cleave the DES forming *urea-(water)_{cluster}-proline* or *urea-proline-(water)_{cluster}* by which DES-protein system stabilize and thus, water molecules dominate the DES-protein interactions.

KEYWORDS: *Deep eutectic solvents, Molecular dynamics simulation, Density functional theory, Vibrational circular dichroism, Non-covalent interaction.*

CHAPTER 1

INTRODUCTION

“No human investigation can be called real science if it cannot be demonstrated mathematically” - Leonardo da Vinci

1.1 Fundamentals of Deep Eutectic Solvents (DES)

The emergence of deep eutectic solvents (DES) has started in 2001 when Abbott et al discovered a eutectic temperature at 12 °C when 33 mol % choline chloride is combined with 67 mol% urea [1-2]. The field has expanded over the years and the number of DES solvents is rising accordingly.

By definition, DES is a eutectic mixture of hydrogen bond donor (HBD) and hydrogen bond acceptors (HBA) which cause melting point depression (**Figure 1.1**) compared to the melting point of individual components [3]. For example, the most common example of DES is Reline solution which is the mixture of choline chloride and urea (ChCl: Urea) at 1:2 molar ratio. The melting points of the components are 303°C for choline chloride and 134°C for urea. When these components are mixed at 1:2 molar ratio, a DES is obtained with a eutectic point at 12°C [4]. This unique behavior lowers the melting point of DES which is generally caused by the presence of strong non-covalent bonding interactions. The non-bonding interactions such as dipole, hydrogen bond, alkyl-alkyl interactions, halogen bonds, and Van der Waals forces are the major reason for the depression of the melting point between DES components.[5-7].

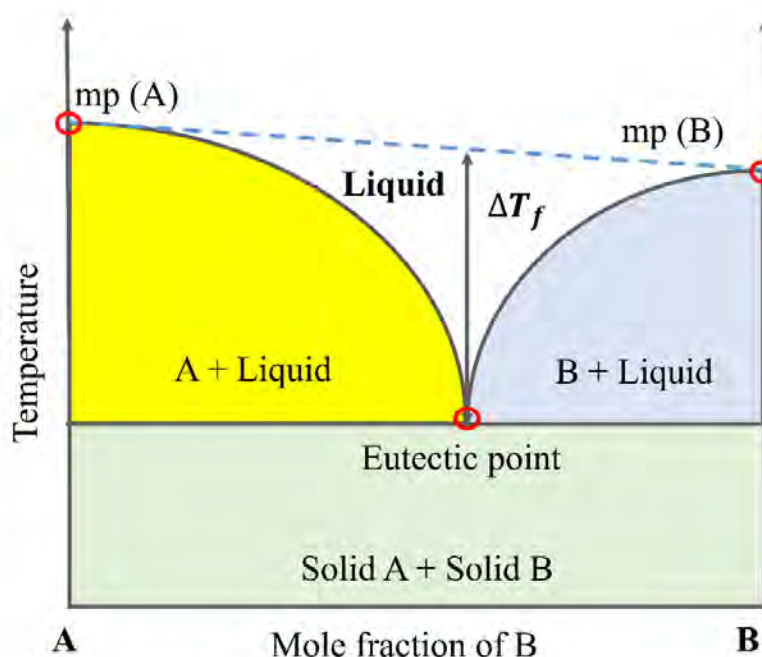


Figure 1.1: Schematic illustration of the phase diagram of a eutectic point on a two-component mixtures.

Four major types of DES are found –

Type	DES mixtures	Examples
I	Quaternary ammonium salt + metal salt	ChCl:ZnCl ₂ ; ChCl:SnCl ₂ ; FeCl ₃ :1-butyl-3-methylimidazolium chloride
II	Quaternary ammonium salt + hydrated metal salt	ChCl:CrCl ₃ .6H ₂ O; ChCl:CaCl ₂ .6H ₂ O; ChCl:Zn(NO ₃) ₂ .4H ₂ O
III	Quaternary ammonium halide + neutral HBD	ChCl:Urea (<i>reline</i>); ChCl:ethylene glycol (<i>ethaline</i>); ChCl:glycerol (<i>glyceline</i>)
IV	Metal salt + neutral HBD	ZnCl ₂ :Urea; ZnCl ₂ :Acetamide; ZnCl ₂ :Ethylene glycol; ZnCl ₂ :1,2-Hexanediol

Table 1: Four different types of DES solvent systems [4].

Among these four types of DES, type III DES solvents are the most common and extensively used. DESs have an easy preparation methodology, are low cost, biodegradable and non-toxic compared to ionic liquids (ILs) [8]. These solvents can be used in several applications such as bio-catalytic processes, electrochemical applications, dissolutions, separations, organic synthesis, and several biomedical areas [9-29].

Extraction: The solvent extraction method by using DES can efficiently eliminate hazardous materials. Petroleum-based fuels containing large amount of sulfur compounds can be extracted using reline (1:2 ChCl/Urea) and ethaline (1: ChCl/glycol) DES solvents [14], [18], [24]–[27]. It was found that the oxidized form petroleum fuels strongly interact with DES components whether unoxidized fuels show negligible interaction. This phenomenon indicates the extraction of petroleum-based fuels [27]. Marcos et al. investigated that DES involving ethylene glycol, glycerol, levulinic acid, phenylacetic acid, malonic acid, and urea with ChCl can be used to extract aromatic sulfur compounds from fossil fuel. The group showed that 1:3 ChCl:levulinic acid DES showed the most effective performance in the extraction process [16]. Employing MD simulation hydrogen sulfide (H₂S) gas can also be extracted from natural gas using 1:1 CPL/TBABr, 1:1 CPL/TBACl, 1:2 ChCl/urea, and 1:6 MTPPBr/MEA. It is probed that DES can separate the H₂S has from natural like such as CH₄ [18]. Another group et al. showed that lower alcohols such as ethanol, 1-pentanol, 1-butanol can be extracted from their azeotropic mixtures using 2:1 menthol: lauric acid and 1:1 menthol: decanoic acid by

performing MD simulation. It was found that 1-butanol showed higher interaction in 2:1 menthol: lauric acid due comparing to 1-propanol and ethanol [26].

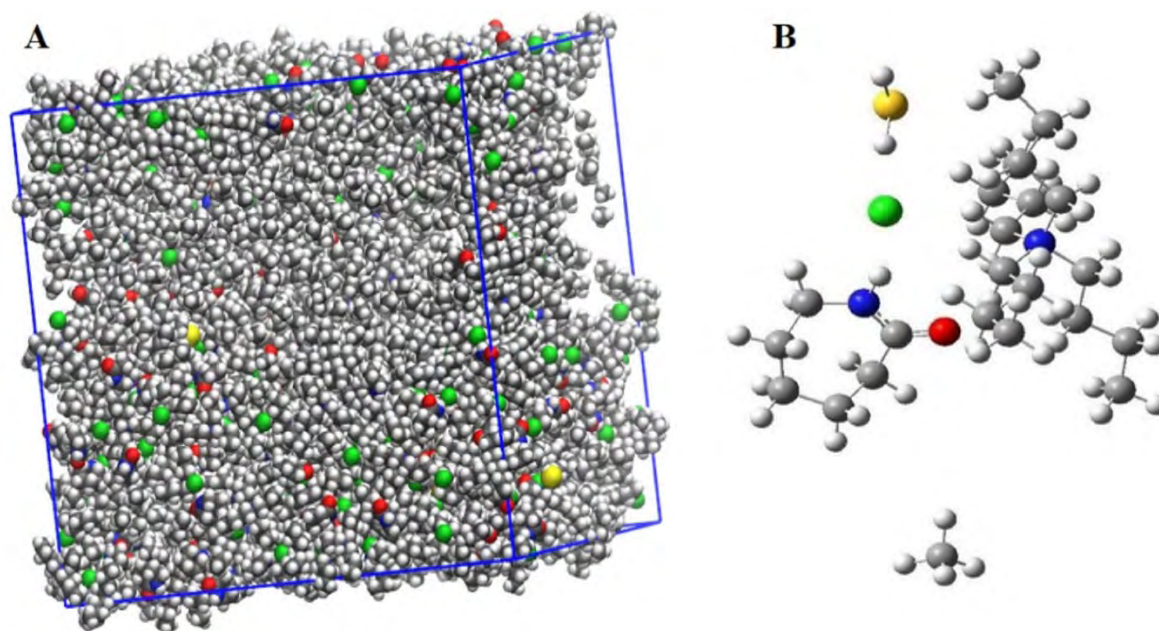


Figure 1.2: Simulation structure of (CPL/TBACl) + H₂S + CH₄ DES obtained from GROMACS. Color code – white: hydrogen; grey: carbon; blue: nitrogen; yellow: sulfur; and green: chloride [18].

Absorption and adsorption: Absorption or adsorption of small molecules by DES can be performed from the studies of MD simulation [13], [23], [31]. Alexander et al. considered two systems by using a pure DES and DES with a saturated amount of SO₂ and performed Ab initio molecular dynamics simulation. The results showed that SO₂ can be adsorbed efficiently by the eutectic mixtures of choline chloride and glycerol, urea, thiourea, malonic acid, ethylene glycol, levulinic acid. The absorption capacities vary from 1.4 – 3 mol SO₂ per mol of DES at 298 K [11]. DES can also act as a soft surface solvent by which transition metal oxides can adsorb. Rimsza et al. used 1:2 ChCl: Urea DES to make adsorption of CuO on the surface of the DES [13].

Solubility prediction by capturing molecules: DES can predict the solubility by capturing small molecules concerning the environmental issue and pharmaceuticals industry [10], [20], [21], [23]–[25], [28], [30]. Amin et al. predicted the solubility of CO₂ along with CO, CH₄, N₂, H₂ by NRTL and COSMO-RS methods using 1:2 ChCl: Urea DES. The result showed that NRTL methods predicted accurately in comparison with the COSMO-RS method [28]. QM/MD simulation technique also used by Ullah et al. for CO₂ capturing purposes using 1:2

ChCl/luvenic acid DES. The results showed that luvenic acid of DES interacts strongly with the interfacial DES-gas region which leads to slow migration to the bulk fluid region [10]. Uses of DES in the pharmaceutical industry can enhance the solubility of API due to the increase of solubility in comparison to the solubility in water. Henrik et al. examined that DES are the alternatives to the use of poorly water-soluble solvents such as PEG300, ethanol, and glycerol because DES can increase the solubility of the API ingredients. The group predicted the computational solubility by using COSMO-RS and showed good agreement with the experimental results [30].

Thermal applications: Dehury et al. investigated two novel DESs including DL-menthol+diphenyl ether as DES-1 and DL-menthol+oleyl alcohol as DES-2 and modified the DESs by dispersing hexagonal boron nanoparticles producing DES-based nanofluids. The group predicted the eutectic point of these DESs by the COSMO-SAC model and observed that these DES-based nanofluids can increase the thermo-physical properties [17].

In computational aspects, DES microstructures are studied extensively by performing simulation study and several groups investigated DES formation to explain the structural orientation, physiological properties, charge density, conductivity [19], [32-51]. For instance, Supreet et al. observed the microscopic structure of ethaline DES (1:2 Choline chloride: Ethylene glycol, ChCl: EG). The group showed the arrangement of EG species plays a crucial role in laying down the microscopic structure of DESs. **Figure 1.3** refers that the ethaline DES are formed by the interaction of hydrogen bonding with $[\text{Ch}]^+$ and EG. The EG-EG inter and intramolecular H-bonding interaction was also observed but EG-EG pairs are not much profound [32]. The group also investigated the role of hydration on the nanostructure of ethaline (1:2 Choline chloride: Ethylene glycol) DES using MD simulation. The initiation of disruption of the native structure of the DES is observed at 40 mol% of water. Then the long- and short-range intermolecular interactions between the components of pure ethaline, were destructed with the increase of dilution. At a higher hydration level, the chloride ion forms strong H-bonds with water and breaks the bridge between the choline cation and ethylene glycol. The spatial isodensity surfaces (in **Figure 1.3b**) and radial angular distribution functions suggest that the strength of H-bonding interactions among the ethylene glycol molecules is observed on increasing hydration levels. Hence, the segregation of ethylene glycol is predicted to occur in the aqueous mixtures of $[\text{Ch}]^+[\text{Cl}]^-$ at a higher hydration level. The chloride anion, which was earlier acting as a bridge between the choline cation and ethylene

glycol species in the neat ethaline, is rapidly solvated by the formation of hydrogen bonds with water molecules [42].

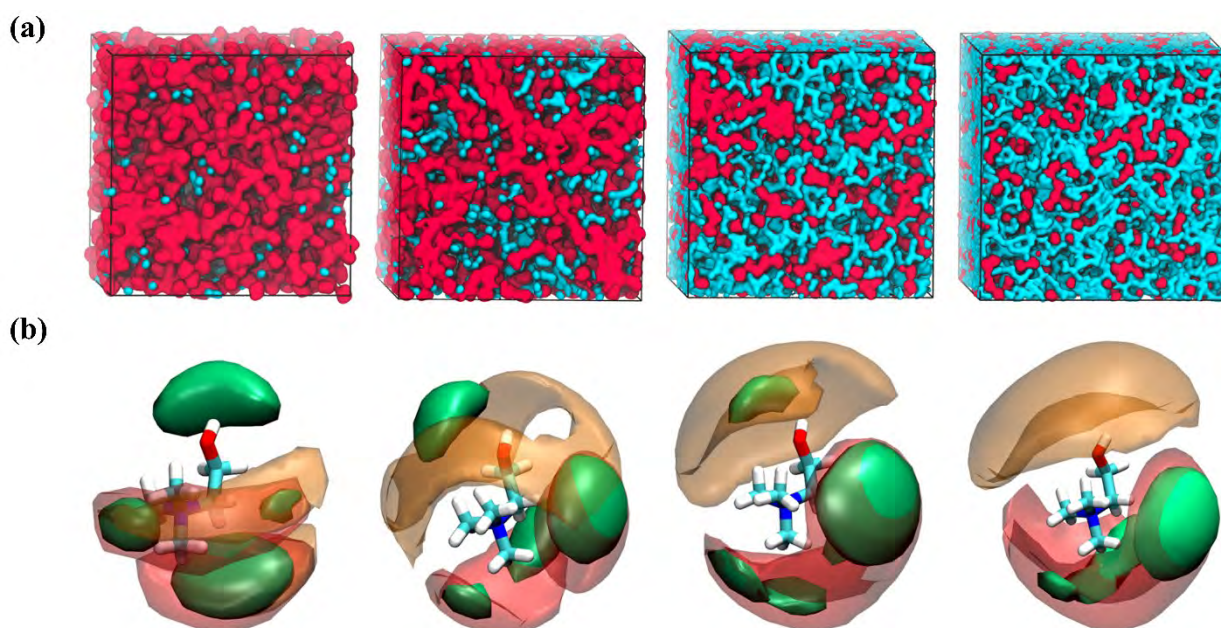


Figure 1.3: (a) Simulation snapshots of ethaline-water mixtures at equilibration describing the structural arrangement of hydrogen bond donors (ethylene glycol and water molecules) in 0.5-w, 2-w, 10-w, and 20-w ethaline-water mixtures where the cyan and red isosurfaces represent water and ethylene glycol, respectively. (b) Isodensity surfaces around the central choline cation for 0.5-w, 2-w, 10-w, and 20-w ethaline-water mixtures. Here, the transparent red isosurface indicates the water molecule, the transparent orange isosurface indicates the EG molecule, and the solid green isosurface indicates the $[Cl]^-$ [42].

Adriaan van den Bruinhors co-workers have reported the Physicochemical Properties of two Proline-based DES, GlyA:Pro (3:1, 2:1 and 1:1) and MalA:Pro (1:2 and 1:3). The MD simulations give insight at the atomistic level showing the prevail of H-bonding interaction at acid-rich compositions. Malic acid-based DESs show stronger acid-acid HB interactions than glycolic acid-based ones, possibly explaining its extreme viscosity. In addition to proline, the inter-species interactions become predominant, confirming the formation of the widely assumed HB network between the DESs constituents in the liquid phase. Proline was found to activate the inter-species HB by disrupting the acid-acid interactions. Glycolic acid was found to be equally efficient as malic acid to engage proline, possessing weaker acid-acid interactions compared to malic acid. This was also confirmed by the radial distribution functions [40].

After having the proper orientation of H-bonds between DES components from MD simulation, the quantum calculations are needed to optimize with minimum energy to obtain the proper orientation of DES components. With the help of quantum chemical methods, the proper orientations can be understood by unveiling the DES microstructure formation through molecular interaction such as hydrogen bonding. Several computational methods including the level of theory can be applied to elucidate the DES structures. MP2/6-31G*; B3LYP/6-31+G**; DFTB3 (density-functional tight-binding method); M06-2X/6-31++G(d,p); DFT-D3/6-311++G(2d,p) and (DFT)- ω B97XD/6-311G (d,p) level of computation were used in several literatures to come across the structures [40], [52-65]. For example, Ackas et al. investigated structural properties and non-bonding interactions of 1:1 dl-menthol: acetic acid system DES using (DFT)- ω B97XD/6-311G (d,p) level of theory. The group showed in **Figure 1.4** that the formation of a hydrogen bond network occurred in the O atom and O-H part of both menthol and acetic acid [63]. Wagle et al. studied non-covalent interactions, charge transfer, and thermodynamics calculations of three DESs ChCl/U, ChCl/EG, and ChCl/MA using the M06-2X/6-31++G(d,p) level of theory. The result showed the direct correlation between the melting points of the DESs and the sum of the bond orders associated with the choline-Cl⁻ interactions in the DESs [62].

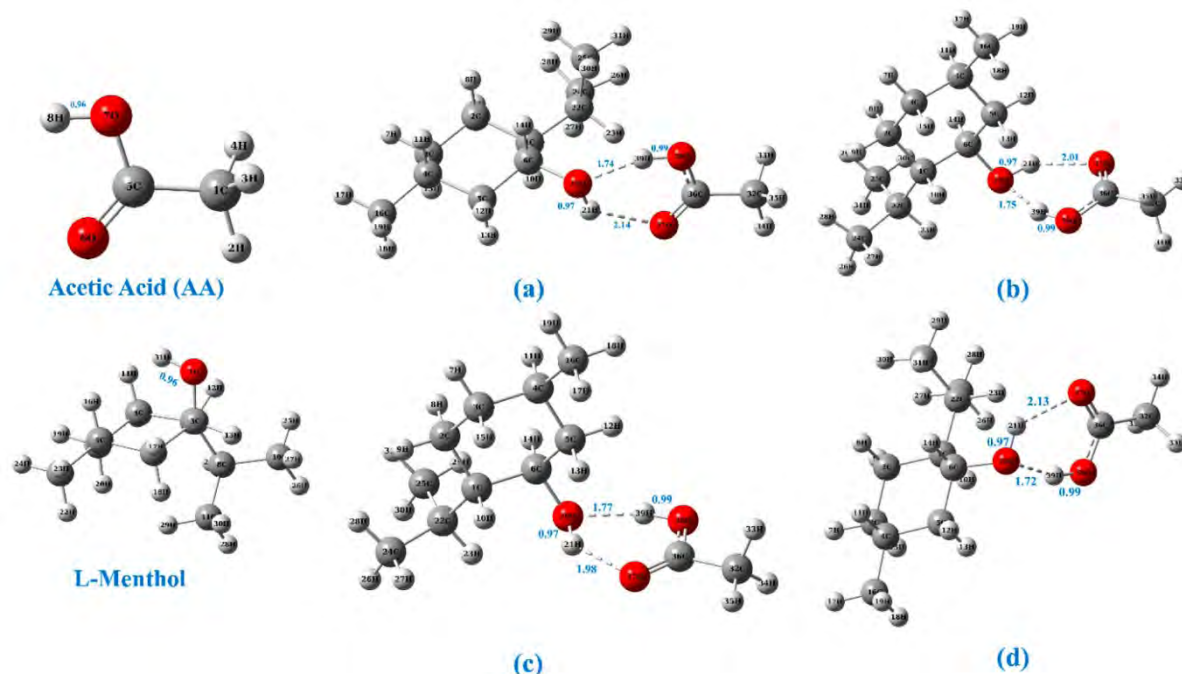


Figure 1.4: The lowest energy cluster conformers of 1:1 L-Men/AA DES are (a) conformer A, (b) conformer B, (c) conformer C, and (d) conformer D, optimized at the ω B97XD/6-311G (d,p) level of theory [63].

Saha et al. showed that the DES clusters stabilized when hydrogen bonds formed between DES components by observing the spontaneity of ΔG , ΔE , and ΔS values of the DES clusters [47]. The reason behind the formation of H-bond interaction is charge transfer between the interacting atoms because the interactions are dominated by transferring charges [47], [55], [63]. Li et al. investigated that SO_2 molecule obtained negative charge after the interaction with both of ChCl and glycerol and this resulted in the cause of SO_2 adsorption [31]. By observing NBO and CHELPG charges, Ashworth investigated that in 1:2 Choline chloride: Urea, the charge delocalization from urea to choline chloride caused molecular interaction [55]. Using NBO and CHELPG charges analyses, similar results were also explained by Saha et al. with 1:1 Choline chloride (ChCl): Acetylsalicylic acid (ASA) that the charges of Cl^- transferred to Ch^+ ion and ASA molecules which showed the dominion of H-bond interaction [47]. To characterize the DES clusters with theoretical results, IR and VCD (vibrational Circular Dichroism) spectra help to determine the presence of different functional groups [47], [63]. For example, 1:1 choline chloride (ChCl)/acetylsalicylic acid (ASA) therapeutic deep eutectic solvent (THDES) was characterized by IR. The IR peaks for $-\text{COOH}$, $-\text{COOR}$, and $-\text{OH}$ functional groups of ASA and ChCl are either broadened or disappear when the cluster conformers are formed [47]. Similarly, the formation of 1:1 L-menthol/acetic acid DES was characterized by IR spectra and it was observed that some significant IR spectra appeared in DES clusters whereas in individual forms of DES those spectra were missing [63]. In addition, VCD is another complementary tool to IR spectroscopy for chiral-based DES. Due to charge transfer and hydrogen bonding interaction, a chirality is transferred from chiral molecule to achiral molecule [66], [67]. Ackas et al. showed that in 1:1 L-menthol/acetic acid DES the chirality transferred from chiral menthol to achiral acetic acid was confirmed by VCD spectra analysis [63].

On the other hand, proteins have a significant effect on DES. Proteins are one of the most essential chemicals found in living organisms. Particularly, changes in the conformation of the protein structure are the fundamental features that regulate the activity of biological function [68]–[73]. Protein denaturation through unfolding (in **Figure 1.5**) happens when the protein loses its native structure and turns to primary structure [74], [75]. Besides, the stability of the protein conformation depends on various factors such as pH, temperature, pressure, solvents, and other chemical entities [72], [76]. Specifically, deep eutectic solvents (DES) can affect the protein stability, conformation, dynamics, folding and unfolding [77], [78], [87], [79]–[86]. Susmita Roy and co-workers studied the unfolding conditions of four proteins including single

immunoglobulin-binding domain protein G, chymotrypsin inhibitor 2, IgG-binding domain of protein L, human erythrocytic ubiquitin by MD simulation. The group showed that urea and Dimethyl sulfoxide (DMSO) solution can cause denaturation of the studied proteins. Further, the contact map analysis provides the evidence that 8M urea solution denatures the α -helix preferentially and then β -sheet. In contrast, 8M DMSO denatures β -sheet first and follows α -helix [77].

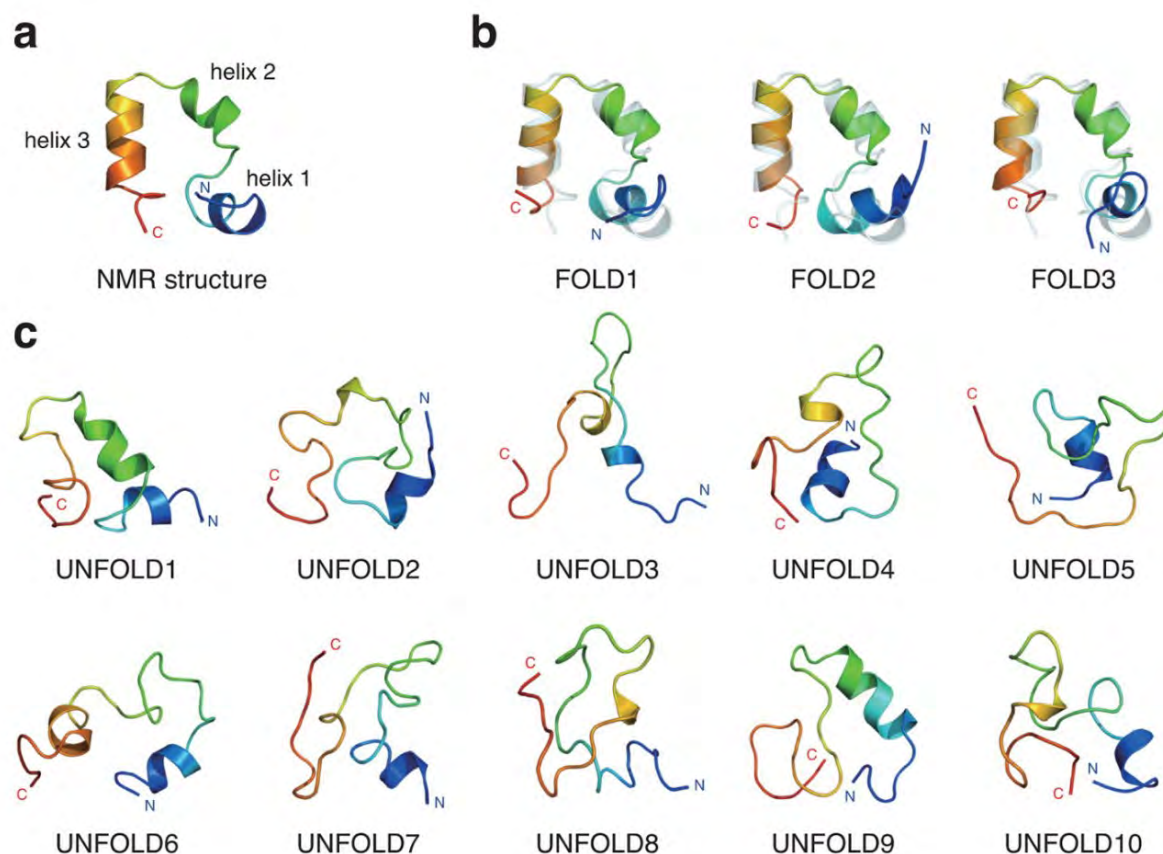


Figure 1.5: (a) Crystal structure of HP-36 (PDB: 1VII). The locations of helix 1 (residues 4–8), helix 2 (15–18), and helix 3 (23–32) are also indicated. (b) Folded conformations are FOLD1–FOLD3. (c) Unfolded conformations are UNFOLD1–UNFOLD10.

Biswajit Biswas and co-workers studied the activity and denaturation of hen egg-white lysozyme (PDB: 1AKI) by Urea: Guanidinium chloride (Urea: GdmCl) through experimental and computational methods. Simulating by MD, the group calculated spatial density distribution function (SDF) of Gdm⁺ and urea within 5Å of lysozyme and it was found that Gdm⁺ interacts with the catalytic active site with the residues of Asp52 and Glu35. These interactions are responsible to inhibit the catalytic activity of lysozyme.

However, radial distribution function (RDF) analysis gives evidence that the electrostatic interactions between Gdm^+ and the residues inhibit the interaction of the substrate with these residues. In contrast, urea does not interact with these residues, hence, no change in activity is observed in urea solution [78].

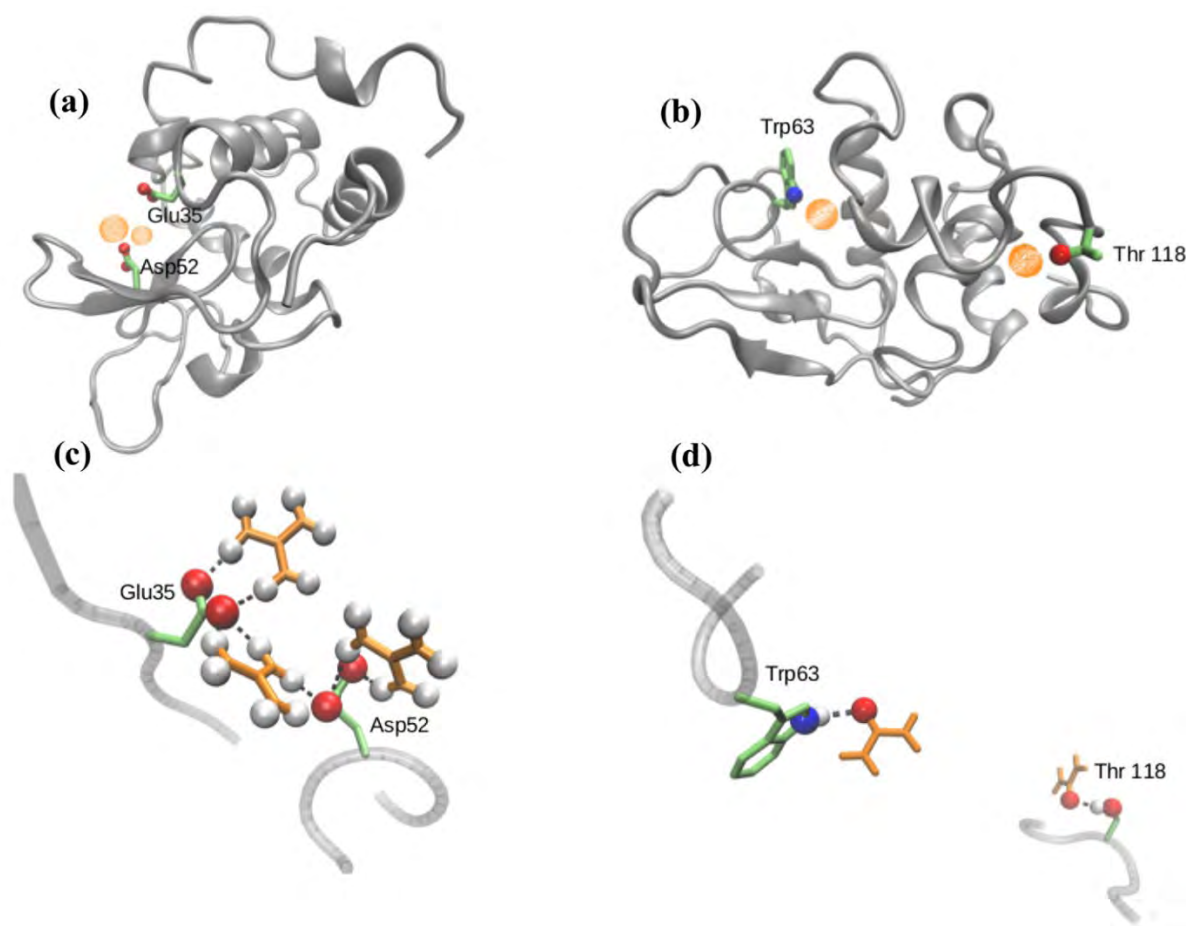


Figure 1.6: Spatial density maps of (a) Gdm^+ and (b) urea within 5 Å of the protein in 2 M denaturant solution at $T = 300$ K. Here, the protein is shown in gray, and orange dots show Gdm^+ or urea fractional occupancy. (c) Interaction of Gdm^+ with Asp52 and Glu35. (d) Interaction of urea with Trp63 and Thr118. In (a) – (d), red spheres denote oxygen, blue spheres denote nitrogen, and white spheres denote hydrogen.

Pratibha Kumari and co-workers also explored how 1:2 choline chloride: Urea DES can affect the lipase conformation. It is shown that the protein was denatured in 8M urea by a 'direct denaturation mechanism' forming hydrogen bonding by urea with the core residues. In contrast, the protein remained intact when reline solution (Choline chloride: Urea DES) was used, and in the reline solution, the urea can only interact with the surface residues of the protein. The reason behind this is the electrostatic interaction of choline and chloride ions with the surface

residues which makes the urea immobilized. Due to this immobilization of urea in reline solution, the protein enhances itself to greater stability than by the urea in 8M urea solution. However, in the 8M urea solution, high RMSD also confirms that the protein denatured completely because urea can form hydrogen bonding strongly to the core residues and larger R_g indicates that the protein is less compact. But in the reline solution, RMSD and R_g show that the protein detained to its native conformation [79].

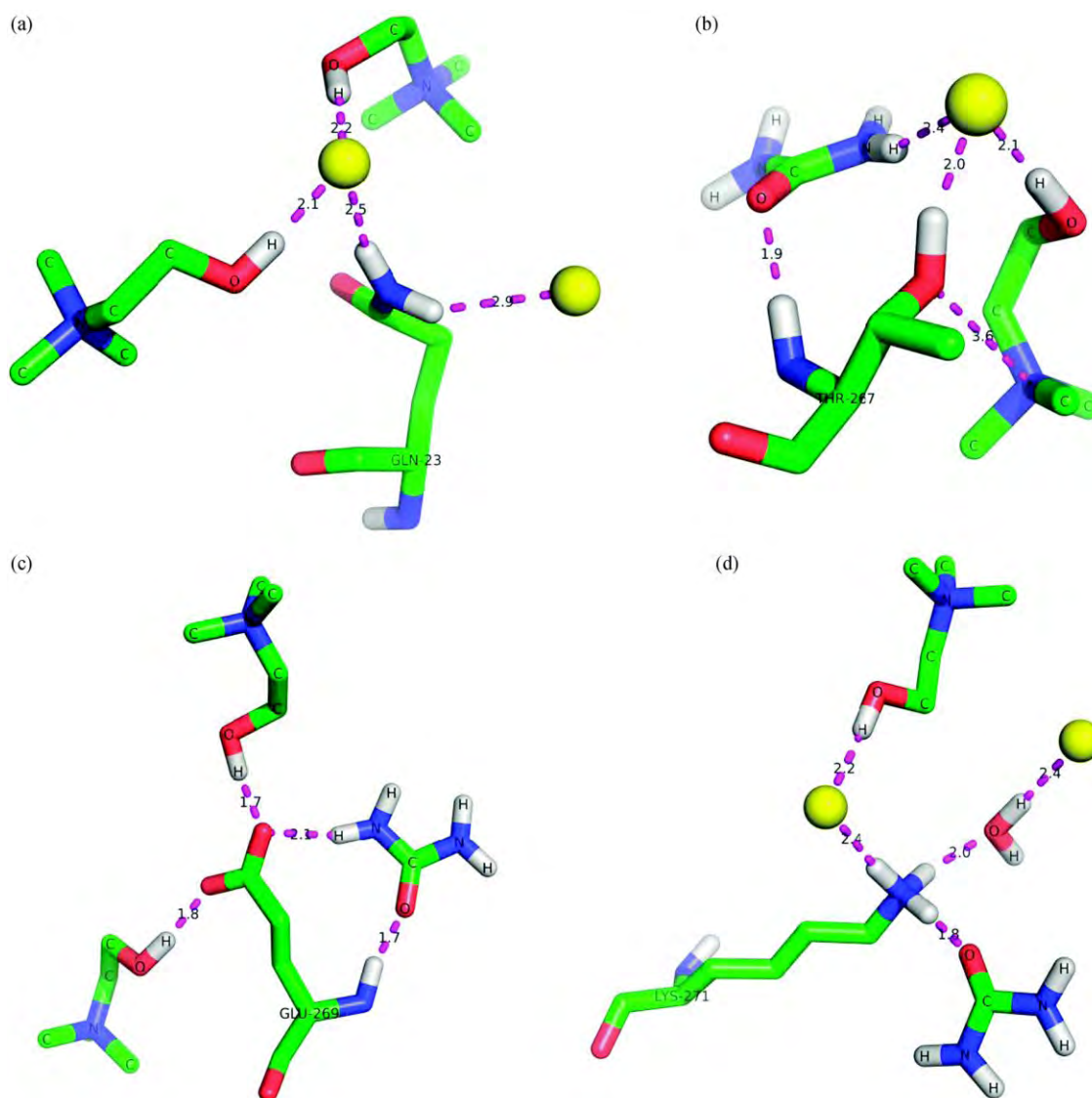


Figure 1.7: Interactions between (a) Gln23, (b) Thr267, (c) Glu269, and (d) Lys271 with urea, choline and chloride ions in Reline at 300 K.

The group also investigated the impact of reline DES and reline-water mixtures on hen egg-white lysozyme (HEWL) structure. Five systems including pure reline DES, HEWL in aqueous media, 50/50 reline/water, 75/25 reline/water media are used to describe the effect on the conformation and stability of HEWL. Applying MD simulation, it was found that 50/50

reline/water system induces the protein structure greater than that by other solvent media. The analysis of RMSD, in **Figure 1.8**, confirmed the most deviation in the protein structure than the native structure and the RMSF gave the information about the most flexibility in the 50/50 reline/water system. However, the radius of gyration (R_g) was quite opposite to RMSD which means that the protein structure is more compact in DES media. The most swollen structure was found in reline DES and the least swollen structure was observed in 50/50 reline/water media. Furthermore, the conformation of HEWL differs when solvents interact differently by H-bonding. For example, in pure reline solution, the residues of HEWL interact more with $[\text{Ch}]^+$ ions than interacting with urea. With the uptake of water molecules, HEWL-urea interaction was found more than in HEWL- $[\text{Ch}]^+$ and produce different conformations [80].

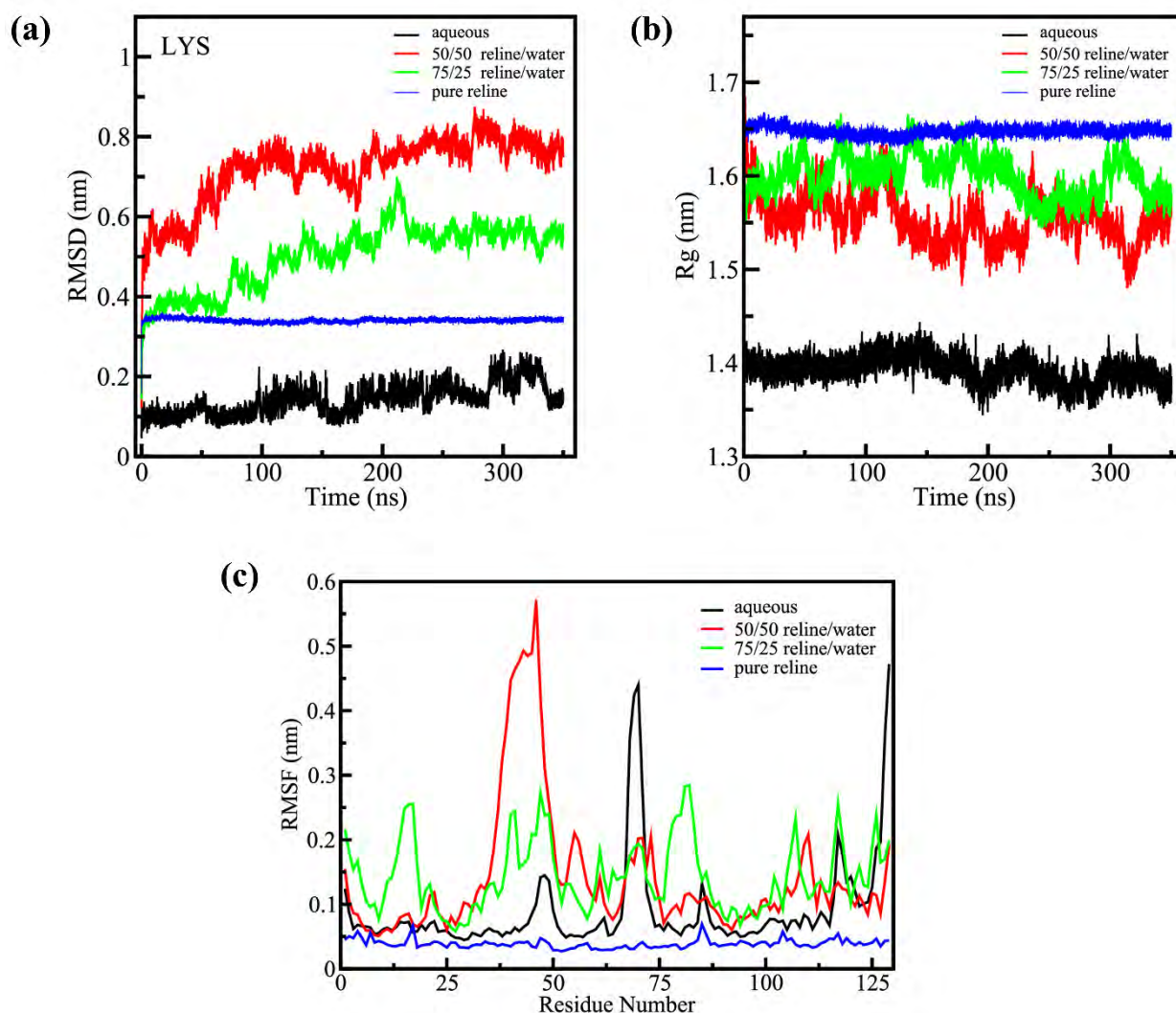


Figure 1.8: (a) RMSD of C α atoms of HEWL backbone with its crystal structure; (b) the radius of gyration of HEWL; (c) root-mean-square fluctuations of C α atoms of each residue averaged

over the last 100 ns in the presence of water, 50/50 reline/water, 75/25 reline/water, and pure reline.

Shehata et al. explored the structural conformation and dynamics of thermoalkalophilic lipases in choline chloride/urea-based DES (reline) using MD simulation. The group used the reline solution varying the hydration level. The result showed that the lipase structure introduced some fluctuations with the increase of hydration level. Although 8M urea and water solution caused the most significant loss of secondary structure of lipase, reline stabilized the whole conformation at 373 K. On the other hand, by observing very small changes of R_g and SASA, $C\alpha$ fluctuations indicated that the lipase structure was almost frozen with fluctuations lower than 1 Å at 310 K in pure reline. However, the addition of water to reline solution increases the mobility of the backbone and decreases the compactness of lipase structures at 373 K and high water contents [82]. Yves et al. investigated the molecular interaction of N, N-diethyl ammonium chloride (DAC)-based-DES with cancer cell membranes such as HeLaS3, AGS, MCF-7, and WRL-68. The group used the COSMO-RS model and performed MD simulation where the results were shown that DAC-base-DES is more toxic in comparison to the ChCl-base DES. Further, COSMO-RS analyses indicated that salt hydrophobicity which comes from possessing a longer alkyl chain has a closer relation to the studied DES toxicity and sequentially resulted in cell death [83].

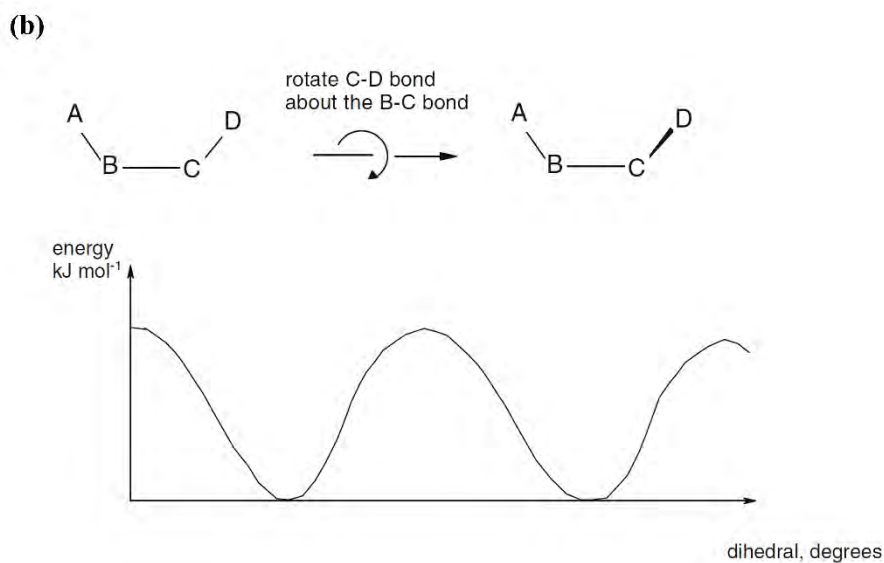
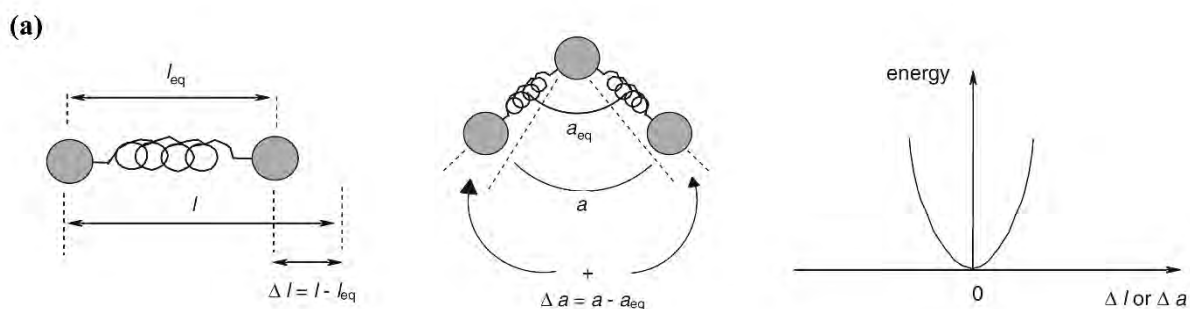
To sum up, first, the orientation, physiological properties of DES are comprehended by the analysis of microstructures obtained from MD simulation. Sequentially, the extracted structures with eutectic mixtures of DESs are computed theoretically with the interest of level of theory. Finally, with that eutectic mixtures, the effect of DES on protein structures can be studied extensively. These all consequences together can give a whole understanding of the properties and function of the usage of deep eutectic solvents.

1.2 Theoretical approach

Treatment of a molecular system by theoretical methods can be classified into two major categories based on the scale of molecular interactions between chemical compounds - *Force field methods* and *Electronic structure theory*. Methods based on force fields such as molecular dynamics, and Monte Carlo methods, Ab initio classical molecular dynamics are used to describe the interactions between molecules as a function of potentials. Force field methods are also considered as 'Molecular Mechanics (MM) method' which are based on balls and spring model where atoms (balls) are held together by bonds (springs). Molecular mechanics

CHAPTER 1

force field methods contain bonded interactions such as bond stretching, angle bending, and torsional distortion and non-bonded interactions such as electrostatic and van der Waals interactions [88]. For a given molecular system where a set of atoms is involved, once the bond lengths, angles of that molecular geometry have been known, the total energy of that system can be calculated. However, molecules with the same entities change their geometries by possessing a series of energy until the energetically lowest and stable geometry is found which is called geometry optimization [89].



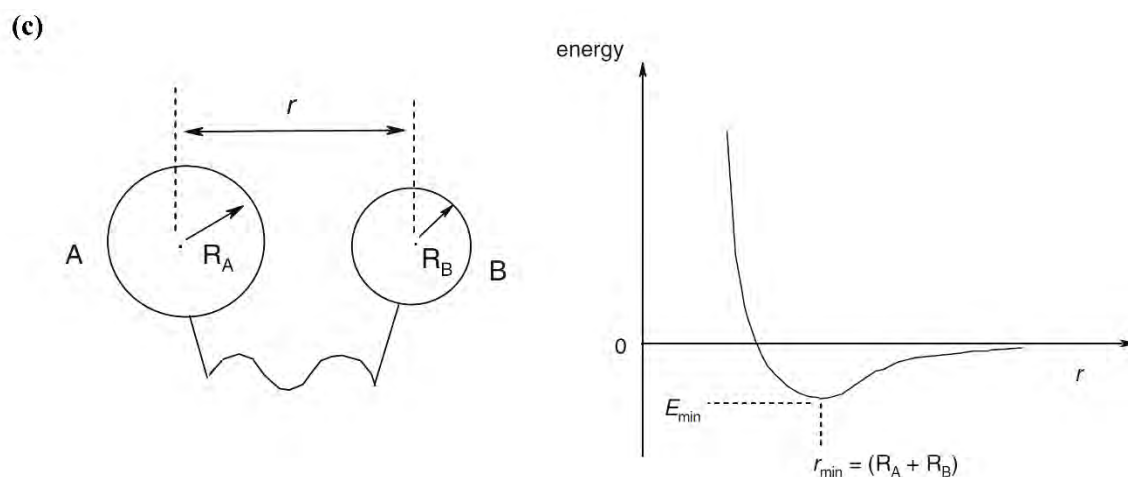


Figure 1.9: Geometry optimization by force field methods - (a) the change in energy of a molecule with the changes of bond lengths and bond angles; (b) dihedral angles (torsional angles) effect on molecular geometries and energies and (c) variation of the energy of a molecule with separation of nonbonded atoms or groups. Atoms A and B can be the same molecule (as indicated here) or the interaction can be intermolecular and the minimum energy occurs at van der Waals contact [89].

The energy expression of total energy, E_{total} from molecular mechanics is –

$$E_{total} = \sum_A^{bonds} E_A^{stretch} + \sum_A^{bond\ angles} E_A^{bend} + \sum_A^{torsional\ angles} E_A^{torsion} \\ + \sum_A^{non-bonded\ atoms} \sum_B E_{AB}^{non-bonded}$$

In this equation, the first three terms come from bonded energy and the last term comes from non-bonded energy where electrostatic, van der Waals interaction between molecules. On the other hand, electronic structure theory where electrons of a molecule are treated based on the Schrodinger equation. The energy of molecular geometry is also calculated based on the Schrodinger equation [12-14]. The mathematical expression for the Schrodinger equation is –

$$\hat{H}\psi = E\psi$$

Involving the terms of electrons and nuclei to the Schrodinger equation,

$$\hat{H}\psi = \left(\sum_i^{\text{electrons}} \frac{-\hbar^2}{2m_e} \nabla_i^2 + \sum_A^{\text{nuclei}} \frac{-\hbar^2}{2m_e} \nabla_A^2 + \sum_i^{\text{electrons}} \sum_A^{\text{nuclei}} \frac{-e^2 Z_A}{r_{iA}} + \sum_{i>j}^{\text{electrons}} \frac{e^2}{r_{ij}} + \sum_{A>B}^{\text{nuclei}} \frac{e^2 Z_A Z_B}{R_{AB}} \nabla_i^2 \right) \psi$$

Here, \hat{H} is Hamiltonian operator, ψ is the wave function. The first and second terms represent the kinetic energy of the electron and nuclei, the third term is the electrostatic interaction between the electrons and nuclei, the fourth and last terms refer to the electrostatic interaction between electrons and between nuclei, respectively [93].

The Schrodinger equation can be solved exactly when involved one electron only but for multi-electron, the Schrodinger equation cannot be solved exactly. For, the solution of a multi-electronic system, the Born-Oppenheimer approximation method is used. The Born-Oppenheimer approximation depicts that “As nuclei are heavier than electrons, electrons move faster than nuclei. Therefore the motion of the nuclei is assumed to be negligible compared to the motion of the electrons. Hence, the electronic part can be solved separately while keeping the nuclear positions fixed”.

The mathematical expression of Schrodinger equation using Born-Oppenheimer (BO) approximation –

$$\hat{H}\psi = \left(\sum_i^{\text{electrons}} \frac{-\hbar^2}{2m_e} \nabla_i^2 + \sum_i^{\text{electrons}} \sum_A^{\text{nuclei}} \frac{-e^2 Z_A}{r_{iA}} + \sum_{i>j}^{\text{electrons}} \frac{e^2}{r_{ij}} \right) \psi$$

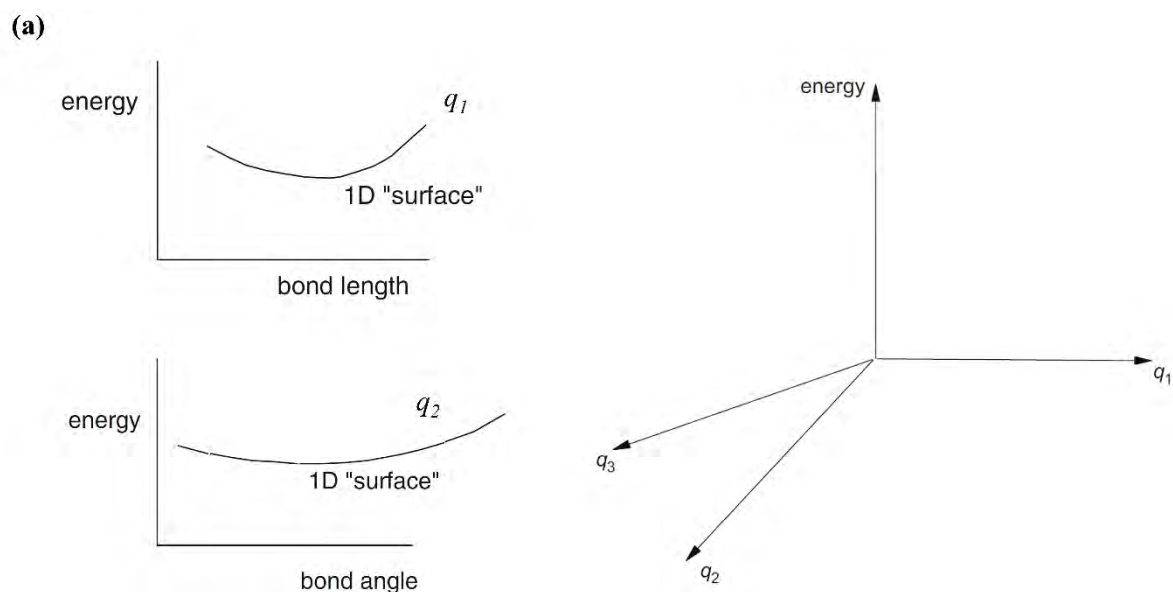
Besides, BO approximation, there are other approximations of molecular structure treatment such as Hartree-Fock approximation, LCAO approximation is further used.

1.3 Potential energy surface (PES) and global minimum energy structure

The concept of the potential energy surface (PES) was originated by Rene Marcelin (who was killed at the age of 29 in 1914 during World War I) in his dissertation. Although his work was not well-known at that time, later Rudolph Marcus acknowledged the gravity of his work when he won the Nobel Prize in 1992. However, the first potential energy surface was calculated by Eyring and Polanyi in 1931.

CHAPTER 1

The PES of a chemical reaction can be considered as a saddle-shaped region holding a transition state by connecting reactant and product. The visualization of PES while examining the changes of the direction and curvature of the reaction path is very sophisticated. To obtain a deeper look at PES, we can consider a molecule where atoms are vibrating by springs (chemical bonds). The bonds are stretching or compressing with the changes of energy and this energy is potential rather than kinetic is known as potential energy. The potential energy vs bond length plot is considered potential energy surface which is a two-dimensional surface, shown in **Figure 1.10(a)**. Incorporating the angular parameter when bond angles are involved, this PES will significantly add one more dimension. More parameters such as torsional angles, electrostatic parameters, van der Waals parameters will incorporate, the more dimension will add to the same PES called potential energy hypersurfaces. Thus, all parameters uniquely give rise to a complex PES which is beyond the imagination. In the complex PES, a molecule undergoes several stationary points and each point determines a structure that varies the energies with the changes of different parameters at the same time. By mathematically, a stationary point is



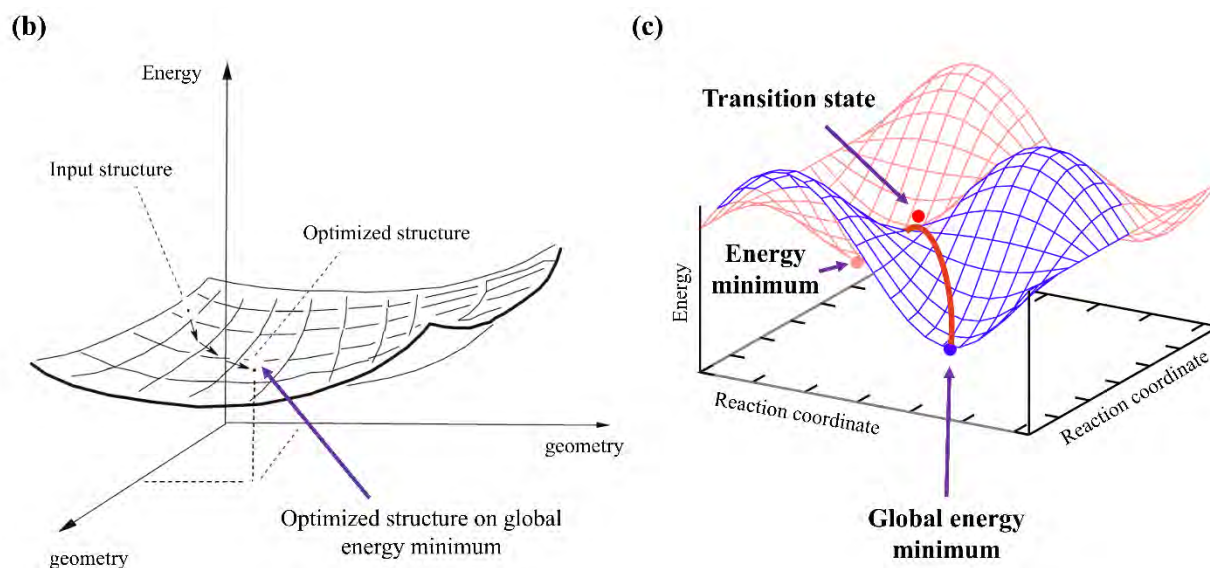


Figure 1.10: (a) Geometric parameters (such as q_1, q_2, q_3, \dots) in a cartesian coordinate system where the PES lies; (b) A potential energy surface (PES) where given input structure is turned to optimized structure and (c) The lowest energetical structure is the global energy minimum where the optimized structure is obtained [89].

the first derivative of the potential energy with respect to each geometric parameter and the first derivative of the potential energy, E is always zero.

$$\frac{\partial E}{\partial q_1} = \frac{\partial E}{\partial q_2} = \dots = 0$$

Here, q_1, q_2, \dots are the geometric parameters.

The lowest energy minimum in the whole PES is called the global minimum. The global minimum structure is the actual structure where geometric parameters such as bond length, bond angles, dihedral angles, and so on are on the optimum level. The global structure of input structures is known as optimized structure (in **Figure 1.10b and 1.10c**) and this optimized structure is the 'structure of interest' while dealing with the accuracy of the calculation. The nearby point of global minimum on the PES is called relative minimum and the lowest energy pathway that links two minima is known as intrinsic reaction coordinates (IRC) or the reaction coordinate. Molecules go from one minimum to another when the molecules get enough energy to overcome the activation barrier by passing through the transition state. The shape from one minimum to another with transition state is saddle-shaped and the transition state is itself is saddle point which lies in the center of the saddle-shaped region. The greatest usage of the PES is molecular dynamics (MD) simulation where several structures are originated by varying the

energy by changing the geometric parameters. The molecule of interest lies where the lowest energy of that molecule dominates [89].

1.4 Basis set and its classification

Basis set: A basis set is a set of mathematical functions as linear combinations which yield molecular orbitals (MOs) to represent the electronic structure of a molecule. Approximating the MOs as linear combinations of basis functions is called the LCAO (Linear Combination of Atomic Orbitals) approach. The mathematical expression of a basis set –

$$\psi_i = \sum_{\mu}^{\text{basis functions}} c_{\mu i} \phi_{\mu}$$

Here, c denotes the molecular orbital coefficients referred to as the molecular orbitals and ϕ is usually centered at the nuclear positions. The equation is termed the Linear Combination of Atomic Orbitals or LCAO approximation.

The use of the basis set is to shape or expand the MOs in wave function or Kohn-Sham density functional methods. To obtain the MOs, Slater-type and Gaussian-type functions are used to dominate the molecular system.

The mathematical expression for Slater-type orbital (STO) function is –

$$\chi_{\alpha,n,l,m}(r, \theta, \varphi) = NY_{l,m}(\theta, \varphi)r^{n-1}e^{-\alpha r}$$

And the Gaussian-type orbital (GTO) function is –

$$\chi_{\alpha,n,l,m}(x, y, z) = NY_{l,m}(\theta, \varphi)r^{n-1}e^{-\alpha r^2}$$

Here, n , l , and m denote the usual quantum numbers; α is the effective nuclear charge, and NY is the normalization constant.

Slater-type functions are used for are good approximations to atomic wave functions to obtain the accuracy of the calculation of a molecular system whereas Gaussian functions are preferred due to the better computational efficiency. The purpose of a basis set usage is to provide the best representation of the unknown molecular orbitals or electron density. Basis set usage depends on the interest of different theoretical methods and molecular properties [89].

CHAPTER 1

Classification of basis set - STO-3G Minimal basis set: This basis set is the simplest possible atomic orbital that is termed as minimal basis set. This is composed only of those functions when maintaining overall spherical symmetry. This basis set involves a single 1s function for H and He; a set of five functions (1s, 2s, 2p_x, 2p_y, 2p_z) for Li to Ne and a set of nine functions (1s, 2s, 2p_x, 2p_y, 2p_z, 3s, 3p_x, 3p_y, 3p_z) for Na to Ar and so on. The STO-3G basis set has two drawbacks – (a) all basis functions are spherical or come in sets that describe a sphere and (b) basis functions are atom centered which restricts their flexibility to describe electron distributions between nuclei. Considering these two drawbacks and the calculation of accuracy, split-valence basis, and polarization, these types of basis sets have emerged.

3-21G, 6-31G, and 6-311G Split-Valence Basis Sets: A split-valence basis set represents the core atomic orbitals by one set of functions and the valence atomic orbitals by two sets of functions. For example, a 6-31G basis set is constructed with core orbitals represented in terms of six Gaussians and valence orbitals split into three and one Gaussian component. Further, additional valence-shell splitting such as 6-311G basis set which splits the valence functions into three parts instead of two, these being written in terms of three, one, and one Gaussians, respectively.

6-31G, 6-31G**, 6-311G*, and 6-311G** Polarization Basis Sets:* These basis sets are used for the treatment of minimal basis functions that were considered as centered functions. This basis set provides d-type functions on main-group elements where the valence orbitals are of s and p-type functions are added on hydrogen. This allows the displacement of electron distribution away from the nuclear position.

cc-pVDZ, cc-pVTZ, and cc-pVQZ Augmented Basis Sets: These types of basis sets are called correlation-consistent basis sets are based on Hartree-Fock calculations. These are used in correlated models such as density functional theory (DFT), MP2 models as well as configuration interaction models. cc-pVDZ, cc-pVTZ, and cc-pVQZ are "correlation consistent polarized Valence Double, Triple and Quadruple Zeta" basis sets that are used to yield the lowest possible couple-cluster ground-state atom energy.

*6-311+G** and 6-311++G** Diffuse Basis set:* These types of basis sets incorporate the diffuse function where extra electrons in a molecule such as cation or anion are present. Here, '+' and '++' indicate the diffuse functions. Excited-state molecules can be studied with these types of basis sets.

Besides, there are different types of basis sets such as Karlsruhe basis set (def2-SVP, def2-SVPD, def2-TZVP, def2-TZVPD, and so on); plane-wave basis sets; real-space basis sets. These may be used as the interest for the treatment of molecular calculations [11, 16].

1.5 Electronic structure theory

Wave functional theory: Wave functional theory yields molecular properties considering the accuracy and computational cost that are dependent on the level of theory. Electron correlation, the size of basis sets are responsible for the accuracy of calculated molecular properties. The very first wave functional theory is *Hartree-Fock (HF) theory*. In HF, each electron interacts only with the average electrostatic field with all other electrons. One of the drawbacks of HF wave function usage is that HF considers the repulsion between the same spin electrons but not Coulombic repulsion between negative charges. To solve the electron-electron interaction, electron correlation treatments involving antisymmetry of the wave function, coulombic repulsion, and static correlation arising from the degeneracy of *electronic correlation* are important. In correlation methods, several methods such as Møller–Plesset (MP) perturbation theory, coupled-cluster (CC) methods are used. In Møller–Plesset (MP) perturbation theory, the simplest method is the MP2 model which is known as an improved HF method. MP2 typically overshoots correlation effects such as overestimating $\pi - \pi$ interactions and overbinding molecules. This method also explains hydrogen bonding well. On the other hand, the coupled-cluster (CC) method provides the exact solution of the Schrodinger equation when all excitations are included. For example, CCSD increases the accuracy when considered single excitations and recovers 90-95% of the correlation energy. This method is feasible for the elements of the first two periods when a large system of atoms involves in a clustering format. The benchmark of the coupled-cluster method is the DLPNO-CCSD(T) method which is robust for the treatment of the electronic structure [90].

Density functional theory: Density functional theory (DFT) is based on the Hohenberg and Kohn theorems which define that the ground-state properties on an atom or molecule are determined by the electron probability density function or electron density or charge density and designated by $p(x,y,z)$. In the Kohn-Sham formalism, the ground-state electronic energy E , is written as a sum of the kinetic energy, E_T , the electron-nucleus interaction energy E_V , the Coulomb energy E_J , and the exchange/correlation energy E_{XC} .

$$E = E_T + E_V + E_J + E_{XC}$$

Except for E_T , all components depend on the total electron density, $\rho(r)$.

$$\rho(r) = 2 \sum_i^{\text{orbitals}} |\psi_i(r)|^2$$

Here, ψ_i are the so-called Kohn-Sham orbitals and the summation is carried out over pairs of electrons.

The density defines a molecular system completely because the integral of the density indicates the number of electrons, the cusps in the density define the position of the nuclei and the heights of the cusps define the corresponding nuclear charges. The electron density is the square of the wave function, integrated over N-1 electron coordinates and each spin density only depends on the three spatial coordinates and is independent of the number of electrons. The main purpose of DFT methods is to design functionals connecting the electron density with the energy to calculate the molecular geometries and the energies of molecules. The advantages of using the DFT calculation are that the electron density function is measurable, intuitively comprehensive, and mathematically more tractable. DFT models are well-defined and produce unique results. Various methods are available such as LSDA, B3LYP, CAM-B3LYP, B3PW91, PBEPBE, ω B97XD to optimize the molecular structure [13–15].

1.6 Problem statement and present approach

The main intention to use deep eutectic solvents is to reduce the usage and production of hazardous substances for chemical processes. In the pharmaceutical industry, most of the used organic solvents are detrimental, toxic, and environmentally unfriendly. Therefore, their use poses risks to human health and the environment. Scientists continue to use greener solvents that are capable to replace the conventional toxic volatile organic compounds. This issue rises when it becomes difficult to acquire more sustainable greener solvents that are alternative to toxic chemicals with desired chemical and physical properties [95]. In most cases, ensuring the availability of greener solvents to replace the non-green solvents is problematic. To ensure the sustainability of greener solvents, high basicity-low polarity, low basicity-low polarity, high basicity-high polarity, and low basicity-high polarity need to be considered [96]. Recently, most research works are concentrated on deep eutectic solvents (DES) because DES is non-volatile, non-toxic, and environmentally friendly which can minimize the usage of volatile and toxic chemicals [8], [97]. Paiva et al. mentioned the natural deep eutectic solvents (made of plant metabolites such as ammonium salts, sugars, and organic acids) as next-generation

solvents which have renewable sources [96]. On the other hand, DES is also used as alternative usages of ionic liquids (ILs) because ILs are toxic and expensive. DES is considered as superior green solvents compared to ILs. To unravel how DES components interact with each other at the molecular level in respect to molecular interaction, the computational technique is a must. The most common DES is choline chloride: urea in 1:2 molar ratio which has extensive studies. Valentina Migliorati and co-workers studied the DES formulation for 1:2 choline chloride: urea DES to identify the impact of cation in DES formulation. The group showed that the presence of a hydroxyl group on the cation which allows the formation of strong cation-anion hydrogen bonds gives rise to a different three-dimensional arrangement of DES components. Strong hydrogen bond interactions between chloride ions and urea molecules are found in both systems and the results show that these interactions are even more favorable, suggesting that the formation of anion-urea hydrogen bonds cannot be the only factor at the origin of the large melting point depression observed in DES [38].

However, most researches are concentrated on choline chloride: urea like hydrophilic DES which limits the solvents utilization to polar environments. Due to the scarcity of greener hydrophobic DES solvents, most scientists still resort to toxic organic chemicals and this is the major drawback to the call for environmental sustainability. This curiosity in searching for non-polar or hydrophobic DES can lead to an alternative solution to the usage of toxic and volatile chemicals. Dannie et al. mentioned that amino acid-based DES such as arginine, proline, and glutamic acid are good examples of hydrophobic DES [98]. To obtain the DES structural formation by computational methods can be one of the ways to minimize the wastage and cost of using chemicals. The computational method specifically density functional methods can lead to the understanding of structural entities of DES microstructure formation. To correlate the theoretical results with experimental results, dispersion force combined with the DFT method is also important to obtain the DES formation. Zhu et al. used the DFT-D3/6-311++G(2d,p) level of computation which assisted a good explanation formation of hydrogen bond between quaternary ammonium salt and HBD (Hydrogen Bond Donor) [65]. The chemical insight into the hydrogen bonding network and the spontaneity of DES clusters can be confirmed by the calculation of ΔG (change in Gibb's free energy), ΔE (change in electronic energy), and ΔS (change in entropy) values [47], [63].

In this study, proline-based DES such as L-Proline: Urea and D-Proline: Urea in 1:1 molar ratio will be investigated with computational technique and this computational work is yet to explore [99]. Another major application to select proline-based DES is to analyze the protein folding

to reveal the protein conformation because proline is an alpha-helix breaker and most protein residues dominate hydrophobicity. It is yet to know how the protein behaves in the proline-based DES environment. This can also lead to the application in the usage of solvents such as the replacement of organic solvents in the pharmaceutical industry.

Objectives:

The main objective of this study is to design new DES proline-based deep eutectic solvents which are capable of replacing volatile organic compounds and cost-effective and greener solvents also. The purpose of this work is to reveal the structural formation and spectroscopic features of 1:1 L-Proline: Urea and 1:1 D-Proline: Urea DESs by computational DFT method and further their interaction with the residues alpha-lactalbumin protein by employing molecular dynamics (MD) simulations.

- I. To generate the 1:1 L-Proline: Urea and 1:1 D-Proline: Urea cluster conformers of DES employing B3LYP-D3/6-311+G(d,p) level of theory in the gas phase by employing density functional theory (DFT).
- II. To investigate the IR, VCD spectral features of 1:1 L-Proline: Urea and 1:1 D-Proline: Urea clusters from individual components.
- III. To analyze the charge transfer from individual to 1:1 L-Proline: Urea and 1:1 D-Proline: Urea DES cluster conformers.
- IV. To reveal the changes of conformation, secondary structural elements (α -helix, β -sheet, β -turn, coil, 3_{10} helix) of alpha-lactalbumin in five different solvents such as L-Proline DES, 20% water-DES, 40% water-DES, D-Proline DES, and physiological solution by performing 500 ns MD simulation.
- V. To analyze the structural changes of alpha-lactalbumin by the root mean square deviation (RMSD), the radius of gyration (R_g), solvent accessible surface area (SASA), and root mean square fluctuations (RMSF).
- VI. To find out the non-bonding interactions of DES components with the residues of the protein.

CHAPTER 2

COMPUTATIONAL METHODOLOGY

“Those who are not shocked when they first come across quantum theory cannot possibly have understood it.” — Niels Bohr

2.1 Preparation of Deep Eutectic Solvent (DES) components

Initially, L-Proline, D-Proline, and urea structures were prepared as DES components using the Gaussian software package [100]. These structures were optimized at the pm6 (parameterized model 06) level of theory in the gas phase for molecular dynamics (MD) simulation. The gas-phase optimized structures are given in **Figure 2.1**

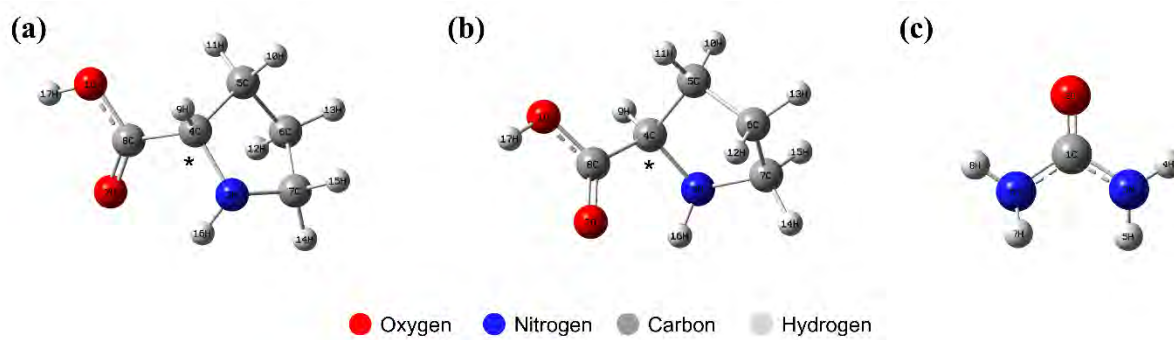


Figure 2.1: Optimized structures of (a) L-Proline, (b) D-Proline, (c) Urea in the gas phase calculated at pm6 level of theory. The asterisk (*) sign indicates the chiral center.

2.2 Molecular Dynamics (MD) Simulation of DES components

2.2.1 Required number of molecules of L-Proline and Urea for MD simulation

The optimized structures were used to perform molecular dynamics (MD) simulation to generate the spontaneous DES clusters of 1:1 Proline: Urea (for both L-Proline and D-Proline). Considering the L-Proline first, 50, 100, 150, 200, and 250 pairs of L-Proline and urea were taken so that the 1:1 ratios were retained. The required number of molecules for these pairs of L-Proline and urea are given in **Table 2**. The MD simulation for these ratios was performed for 50 ns in the gas phase at 298 K. For gas-phase parameterization, the pH and Na^+Cl^- salt concentration were not considered.

SI No.	L-Proline: Urea	No. of L-Proline molecules	No. of Urea molecules
1	50:50	50	50
2	100:100	100	100
3	150:150	150	150
4	200:200	200	200
5	250:250	250	250

Table 2: Required number of molecules of L-Proline and urea for 50, 100, 150, 200, and 250 pairs for MD simulation in the gas phase.

2.2.2 YASARA Dynamics tool for MD simulation of 1:1 L-Proline: Urea DES

To simulate the L-Proline and urea mixtures in the gas phase, a simulation box with $50 \text{ \AA} \times 50 \text{ \AA} \times 50 \text{ \AA}$ dimension was employed in a cubic cell where periodic boundary condition was considered. During the whole simulation, the AMBER14 force field was applied within 8 \AA cut-off radius for short-range van der Waals and Coulomb interaction, and the particle-mesh Ewald (PME) method was employed to compute the long-range interactions [63]. The whole gas-phase simulation proceeded with the NVT ensemble. As the simulation progressed to 50 ns, each structure is generated at every 0.1 ns (100 picoseconds). So, a total of 500 simulation snapshots (structures) were generated in that 50 ns, and the best pairs of 1:1 L-Proline: Urea were isolated by the analysis of 50 ns simulation snapshots.

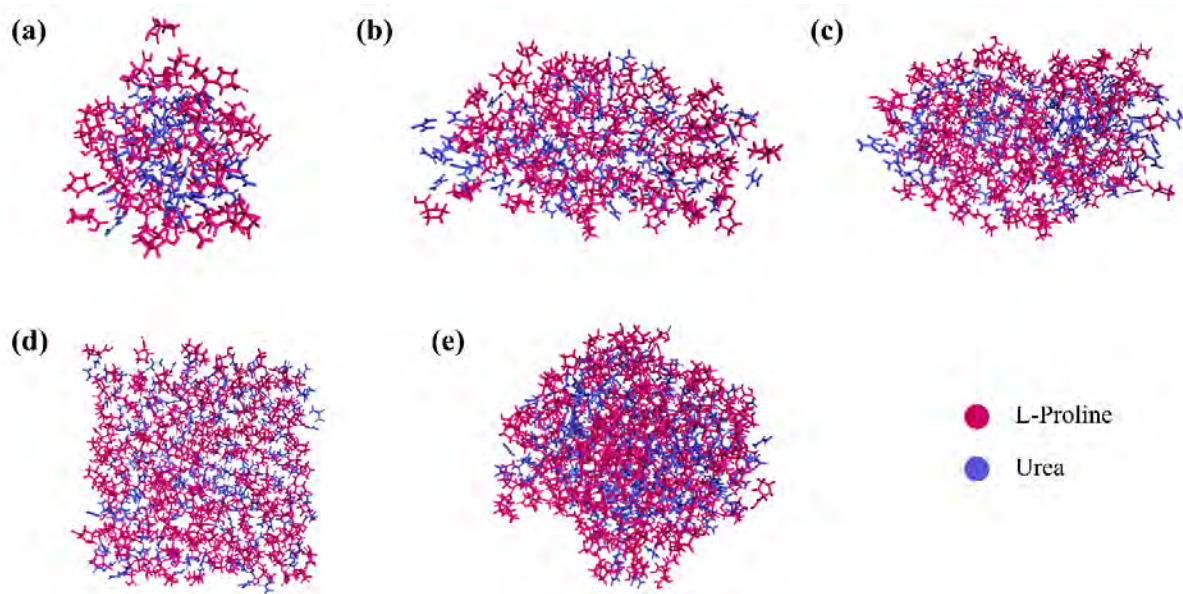


Figure 2.2: 50 ns simulation snapshot (structure) at (a) 50:50, (b) 100:100, (c) 150:150, (d) 200:200 and (e) 250:250 ratios obtained from MD simulation in the gas phase.

The 50 ns simulation snapshots from all pairs were analyzed by BIOVIA Discovery Studio software to find out the best pair non-bonding interaction which finally, lead to the final isolation of the 1:1 L-Proline: Urea cluster conformers.

2.3 Analyses of MD simulation results of DES components

2.3.1 Analyses of 50 ns L-Proline and urea DES micro-structures

Analyses of 50 ns simulation isolated structures showed that 200 pairs of L-Proline and urea give the most possible hydrogen bonding interactions, shown in **Figure 2.3**

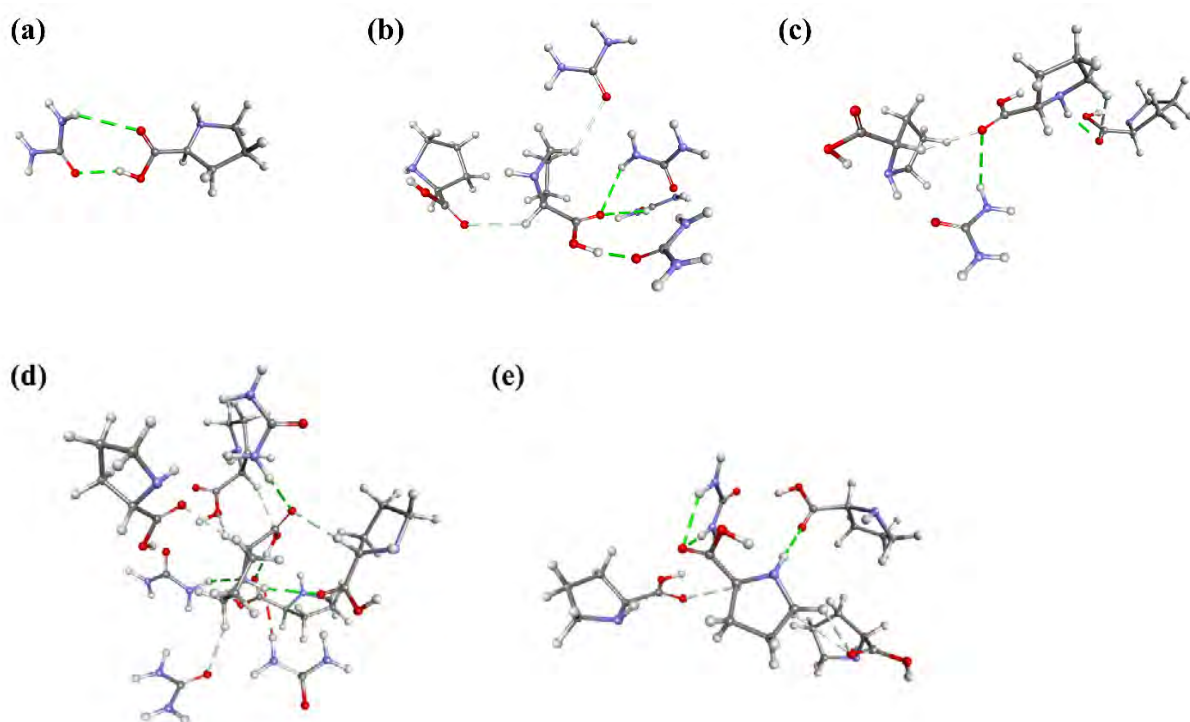


Figure 2.3: 50 ns simulation structures of (a) 50:50, (b) 100:100, (c) 150:150, (d) 200:200 and (e) 250:250 ratios of L-Proline: Urea in the gas phase obtained from molecular dynamics (MD) simulation showed hydrogen bond interactions.

2.3.2 Non-bonding interaction of DES components

By analyzing the non-bonding interactions of 500 structures from each pair, only 1:1 L-Proline: Urea clusters were isolated. These clusters that were obtained from all pairs, were tabulated in **Table 3(a – e)**.

CHAPTER 2

(a)

50:50 Ratio			
Time (ns)	$\text{CO}_{\text{L-Pro}} \dots \text{NH}_{\text{Urea}}$	$\text{OH}_{\text{L-Pro}} \dots \text{CO}_{\text{Urea}}$	$\text{OH}_{\text{L-Pro}} \dots \text{NH}_{\text{Urea}}$
4.2	2.72	1.75	-
5.5	-	-	1.83
7.2	-	1.78	-
14.9	2.11	1.78	-
15.8	2.49	1.88	-
16.0	1.96	1.87	-
16.2	1.83	1.59	-
19.1	2.59	1.7	-

(b)

100:100 Ratio		
Time (ns)	$\text{CO}_{\text{L-Pro}} \dots \text{NH}_{\text{Urea}}$	$\text{OH}_{\text{L-Pro}} \dots \text{CO}_{\text{Urea}}$
1.7	1.71	1.73
3.9	2.32	1.85
6.7	1.89	1.62
8.2	2.05	1.8
8.8	2.15	1.73
9.0	1.71	1.73
9.4	2.08	1.75
9.5	2.32	1.68
9.7	1.92	1.72
26.4	2.02	1.61
27.5	1.85	1.8
27.6	2.5	1.74
28	2	1.69
30.4	2.12	1.76
32.7	2.85	1.76
32.8	1.89	1.86

(c)

150:150 Ratio		
Time (ns)	$\text{CO}_{\text{L-Pro}} \dots \text{NH}_{\text{Urea}}$	$\text{NH}_{\text{L-Pro}} \dots \text{CO}_{\text{Urea}}$
39.4	2.42	2.61
44.2	2.45	2.96

(d)

200:200 Ratio				
Time (ns)	$\text{CO}_{\text{L-Pro}} \dots \text{NH}_{\text{Urea}}$	$\text{OH}_{\text{L-Pro}} \dots \text{CO}_{\text{Urea}}$	$\text{NH}_{\text{L-Pro}} \dots \text{NH}_{\text{Urea}}$	$\text{NH}_{\text{L-Pro}} \dots \text{CO}_{\text{Urea}}$
0.3 ns	2.08	1.69	-	-

2.7 ns	-	1.72	-	-
2.8 ns	2.37	-	-	-
3.5 ns	-	1.76	-	-
20.5 ns	-	2.75	2.16	-
20.6 ns	-	2.81, 2.70	-	-
39.1 ns	-	-	2.56	-
39.2 ns	-	-	1.93	-
40.8 ns	-	1.92	-	1.92
42.2 ns	2.15	-	-	-
48.5 ns	-	-	-	1.97

(e)

250:250 Ratio	
Time (ns)	CO _{L-Pro} NH _{Urea}
39.4	2.42
44.2	2.45

Table 3: H-bond distances of (a) 50, (b) 100, (c) 150, (d) 200 and (e) 250 pairs of L-Proline and urea of 1:1 L-Proline: Urea DES cluster conformers.

2.3.3 Selection of the best pair and isolation of 1:1 L-Proline: Urea DES clusters

Based on the 50 ns analyzed structures from **Figure 2.3** and the hydrogen bonding of isolated clusters from **Table 3(a – e)**, it is observed that the 200:200 ratio of L-Proline: Urea form the highest numbers of hydrogen bond interactions which can generate all possible 1:1 L-Proline: Urea cluster conformers in the gas phase.

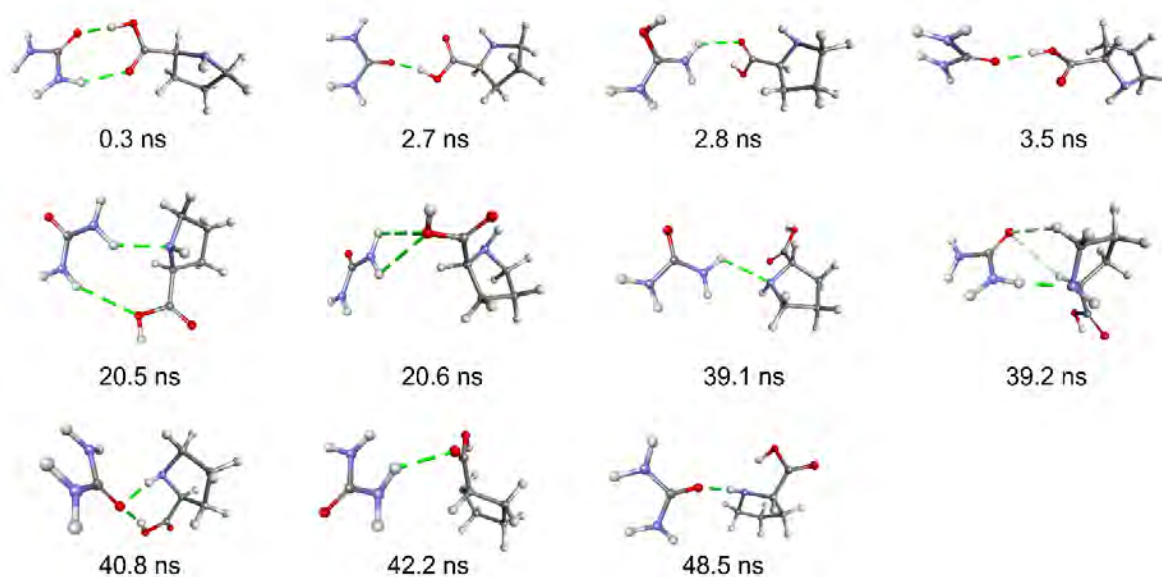


Figure 2.4: A total of 11 clusters of 1:1 L-Proline: Urea DES were isolated from 200:200 ratio in the gas phase.

The gas-phase 1:1 L-Proline: Urea clusters are given in **Figure 2.4**. From the 200:200 ratio, a total of 11 clusters of 1:1 L-Proline: Urea conformers were obtained using the BIOVIA Discovery Studio software package.

2.3.4 Finalization of the best structures from 1:1 L-Proline: Urea DES clusters

To acquire the best structures, only the equilibrated structures at 30 – 50 ns were considered and the 11 clusters were reduced to 5 clusters from equilibration (30 – 50 ns) which were finalized by single-point energy, SPE, shown in **Figure 2.5**

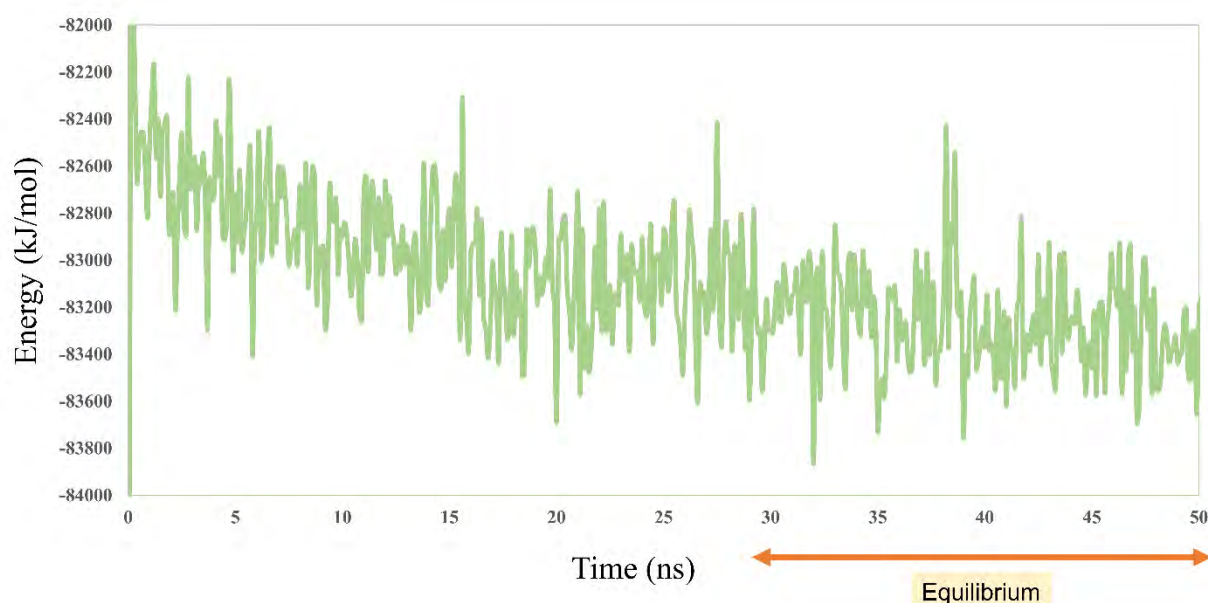


Figure 2.5: Total 50 ns Energy (kJ/mol) vs Time (ns) plot of 200:200 of L-Proline: Urea obtained from the analysis of MD simulation results which shows equilibrium at 30 – 50 ns.

Based on single-point energy (SPE) calculations (**Figure 2.6**), only three clusters that are the most energetically stable were finalized from those equilibrated (30 – 50 ns) structures. These structures were isolated and taken further for final quantum calculation. From the quantum calculation, the molecular orientation, molecular geometries, hydrogen bonding interaction, spectral signatures were obtained to understand a complete feature of 1:1 L-Proline: Urea and 1:1 D-Proline: Urea DES formation.

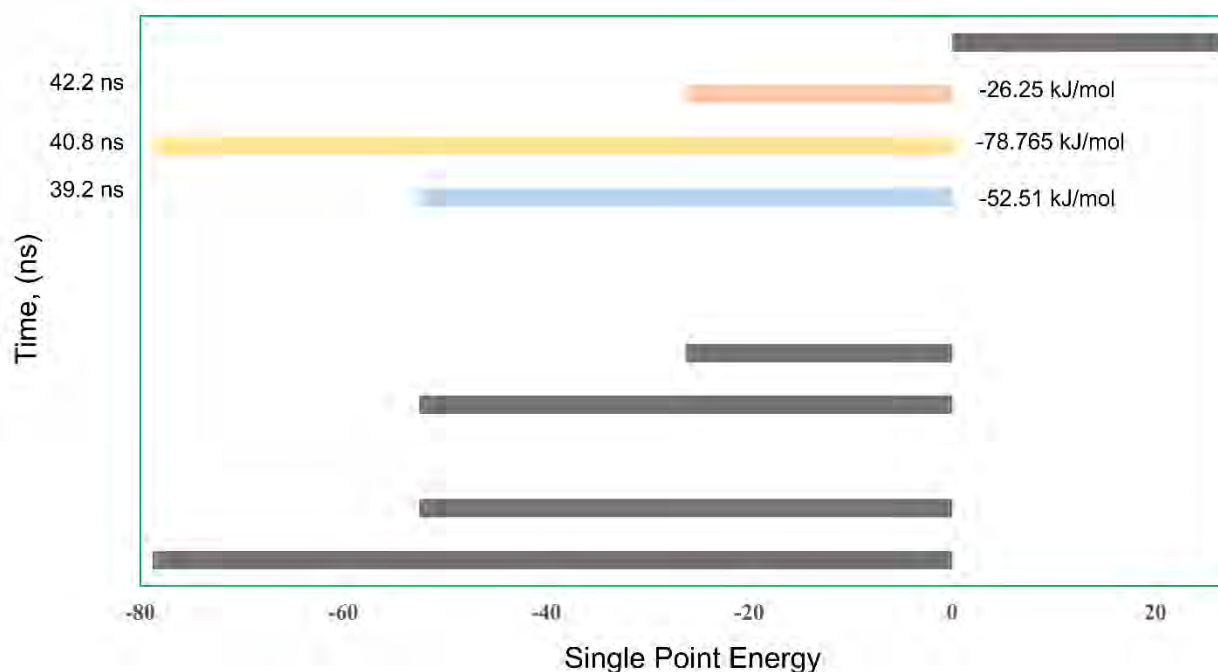


Figure 2.6: Single point (SP) energy calculation of 11 clusters of 1:1 L-Proline: Urea clusters and the chosen three clusters at 39.2, 40.8 and 42.2 ns were highlighted after reaching equilibrium at 30 – 50 ns.

2.3.5 Quantum mechanical calculation of the final three structures of 1:1 L-Proline: Urea DES clusters

The finalized three clusters namely L1, L2, and L3 were further optimized at the B3LYP-D3/6-311+G(d,p) level of theory in the gas phase. Here, B3LYP (Becke 3-Parameter, Lee, Yang, and Parr) is a functional that is applied to resolve the exchanged correlation and dynamic electron correlation which is used to express the exchange energy and to simulate the spectra successfully and the dispersion-corrected functional (D3) is employed to calculate the long-range dispersive interaction [101]. IR and VCD spectra were also calculated at the same level of theory. Further, the thermochemistry, the molecular electrostatic potential charges, HOMO-LUMO energies, and NBO charges were calculated. These analyses will confirm the 1:1 L-Proline: Urea and 1:1 D-Proline: Urea DES formation, the structural orientation of DES clusters, hydrogen bonding interaction, freezing point depression between L-Proline and urea in 1:1 L-Proline: Urea DES clusters as well as D-Proline and urea in 1:1 D-Proline: Urea clusters.

Type	Keyword	Explanations
Method	B3LYP	DFT method
	D3	Calculation of dispersion force
Basis set	6-311	Calculation of hydrogen bonding
	+	Diffusion functional addition
	d, p	Addition of d and p functional

Table 4: Explanation of theoretical method, B3LYP-D3/6-311+G(d,p) level of theory that was used for studied DES.

2.4 MD simulation of 1:1 D-Proline: Urea DES of 200 pairs

In the case of 1:1 D-Proline: Urea clusters, D-Proline of 200 pair with urea were additionally used for MD simulation and a similar procedure as the 1:1 L-Proline: Urea DES system was followed from cluster isolation to quantum mechanical calculations.

SI No.	D-Proline: Urea	No. of D-Proline molecules	No. of Urea molecules
1	200:200	200	200

Table 5: Required number of molecules of D-Proline and urea of 200 pairs of 1:1 D-Proline: Urea for MD simulation in the gas phase.

In this case of D-Proline and urea pairs, the gas phase parameterization of MD simulation protocol was also applied according to 200 pairs of L-Proline DES and urea. 500 simulation structures were generated during the 50 ns simulation run.

2.5 Analyses of 200 pairs of D-Proline: Urea DES

2.5.1 Analysis of 50 ns 1:1 D-Proline: Urea DES micro-structures

Observing the final simulation snapshot at 50 ns of 1:1 D-Proline: Urea clusters through non-bonding interaction (**Figure 2.7**), the highest number of hydrogen bonding interactions can be visualized.

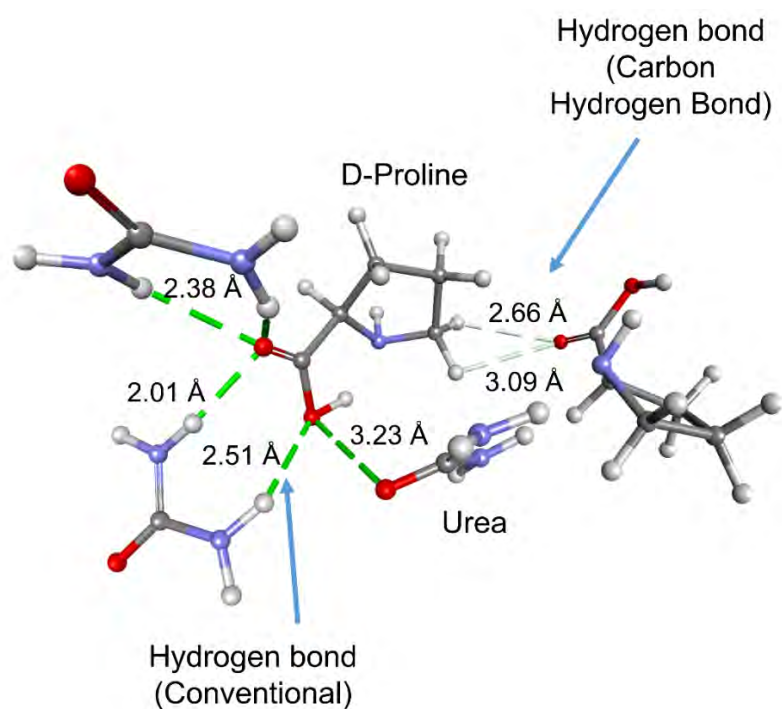
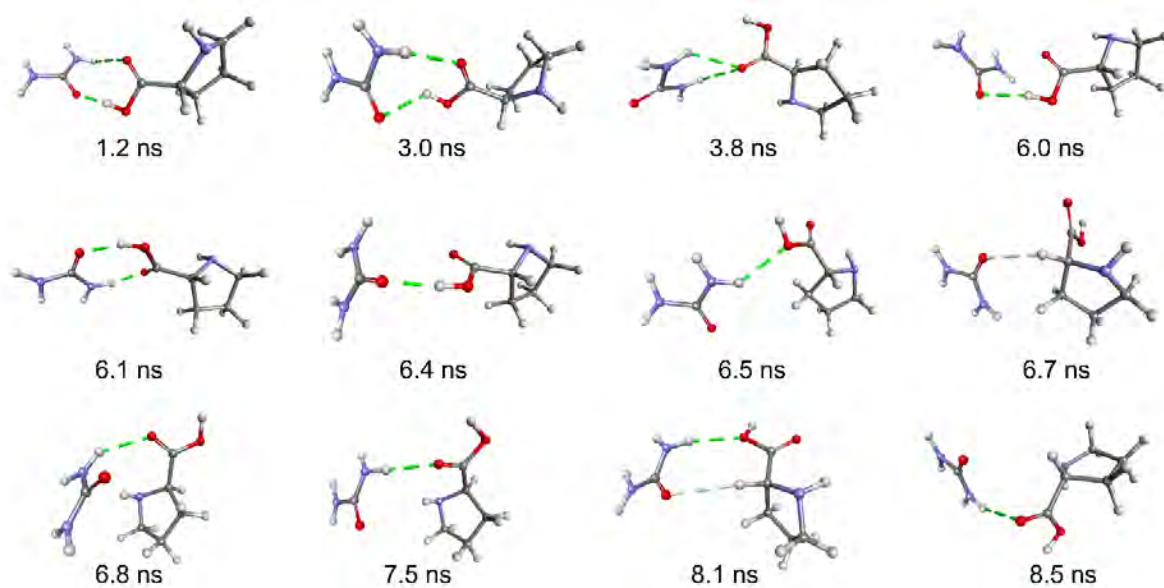
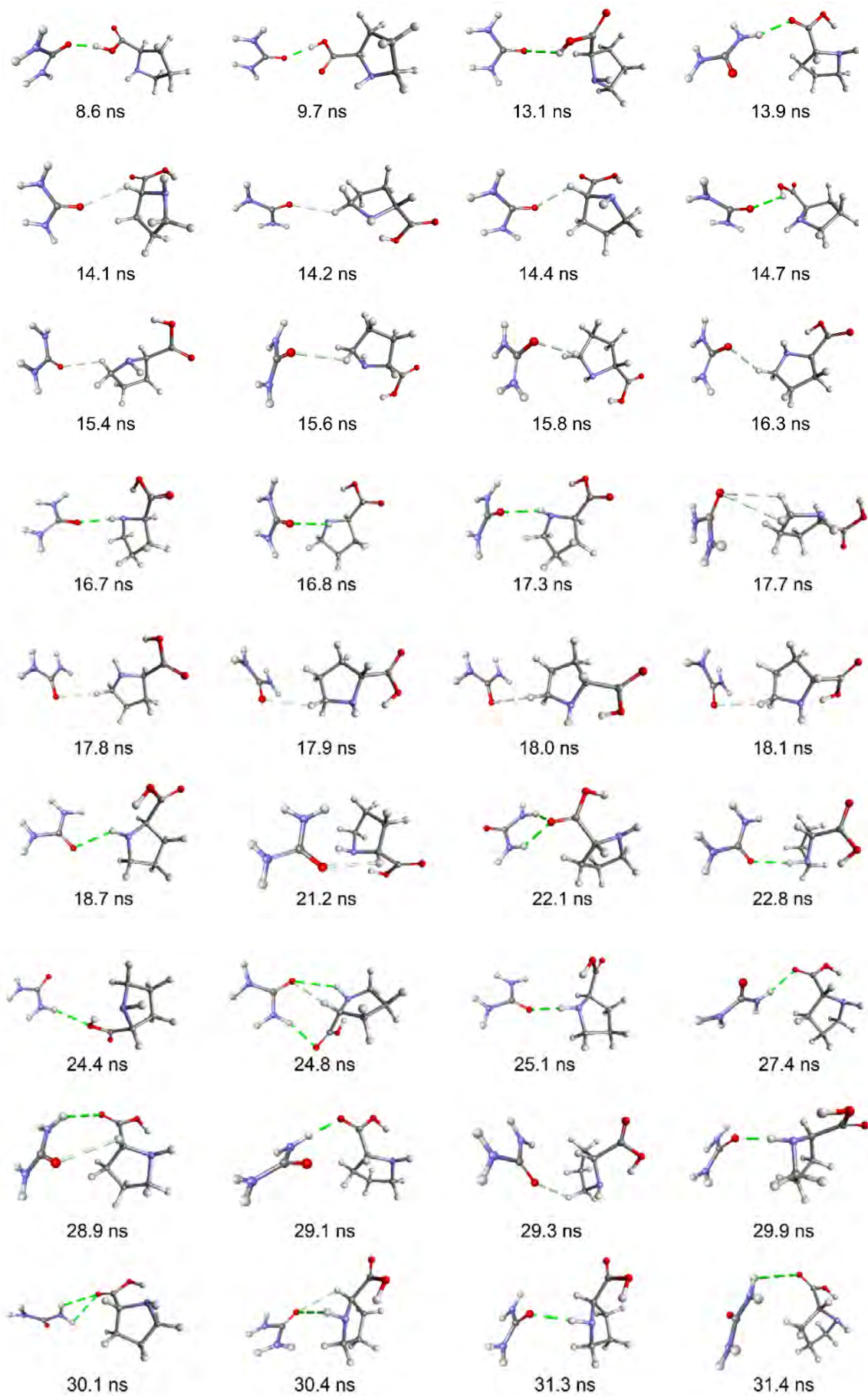


Figure 2.7: 50 ns simulation structure of 200:200 of L-Proline: Urea in the gas phase obtained from molecular dynamics (MD) simulation.

2.5.2 Non-bonding interaction of 1:1 D-Proline: Urea DES clusters

The non-bonding interactions of 500 structures from 200 pairs of D-Proline and urea were analyzed and the 1:1 D-Proline: Urea clusters were isolated. For the case of D-Proline, a total of 58 clusters of 1:1 D-Proline: Urea were observed. The figure of total 58 clusters of 1:1 D-Proline: Urea is given in **Figure 2.8**





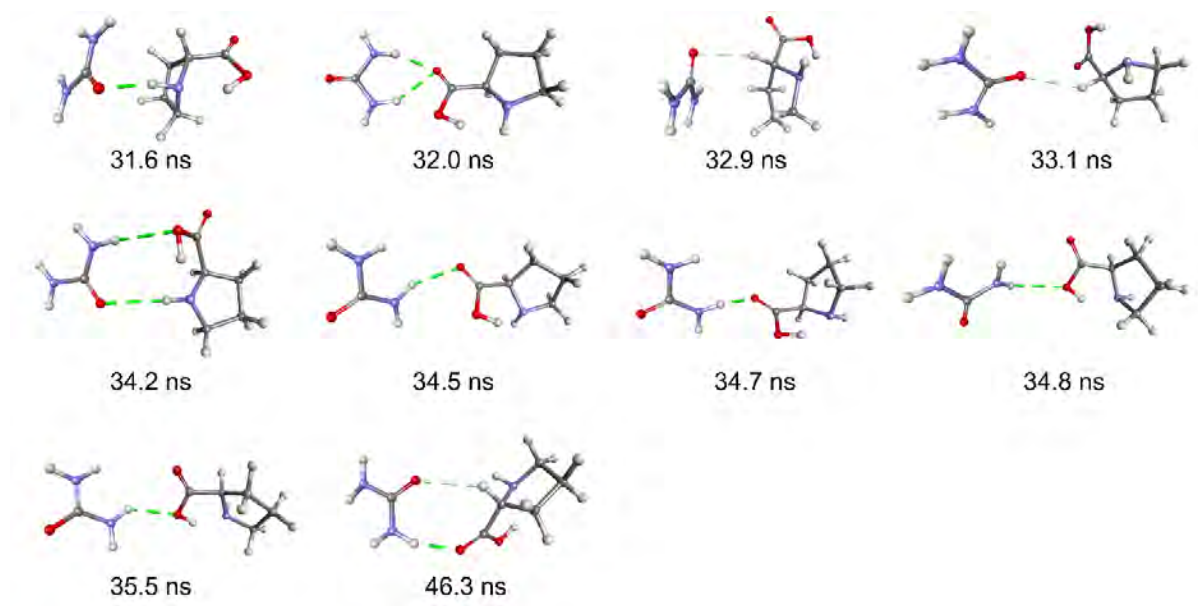


Figure 2.8: Total 58 clusters of 1:1 D-Proline: Urea DES were isolated from 200:200 ratio in the gas phase.

2.5.3 Finalization of the best structures from 1:1 D-Proline: Urea DES clusters

To obtain the best structures from 58 clusters, only the equilibrated structures at 30 – 50 ns were considered and the 58 clusters were reduced to 14 clusters from equilibration which were finalized by single-point energy (in **Figure 2.9**)

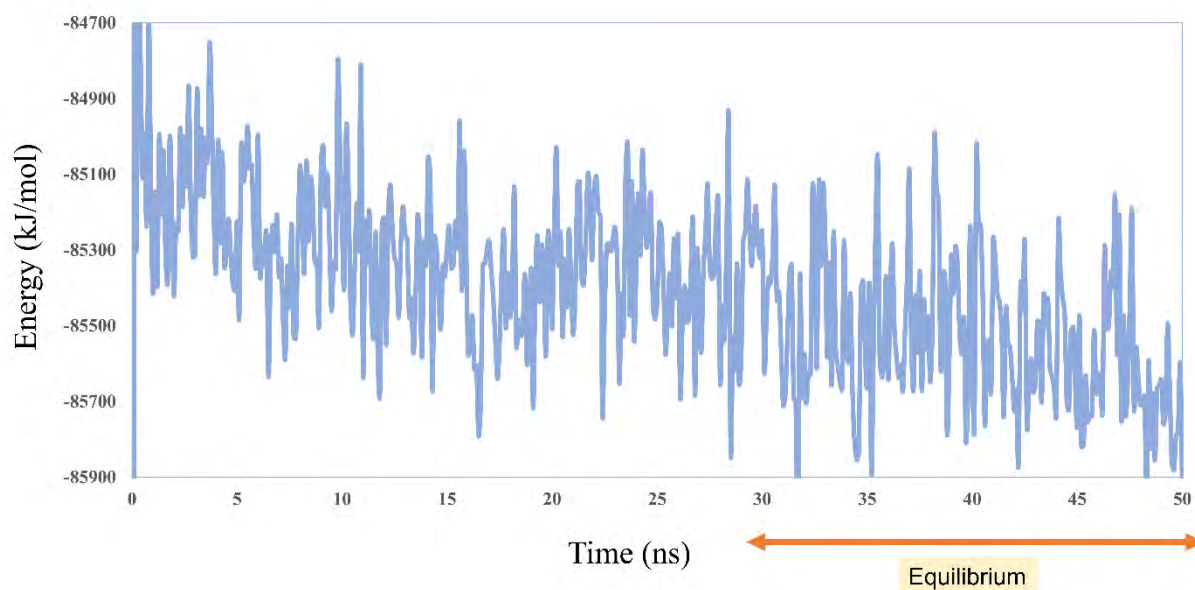


Figure 2.9: Total 50 ns Energy (kJ/mol) vs Time (ns) plot of 200:200 of D-Proline: Urea obtained from the analysis of MD simulation results which shows equilibrium at 30 – 50 ns.

Based on single-point energy (SPE) calculations, only three clusters that are the most energetically stable were finalized from those equilibrated (30 – 50 ns) and isolated structures.

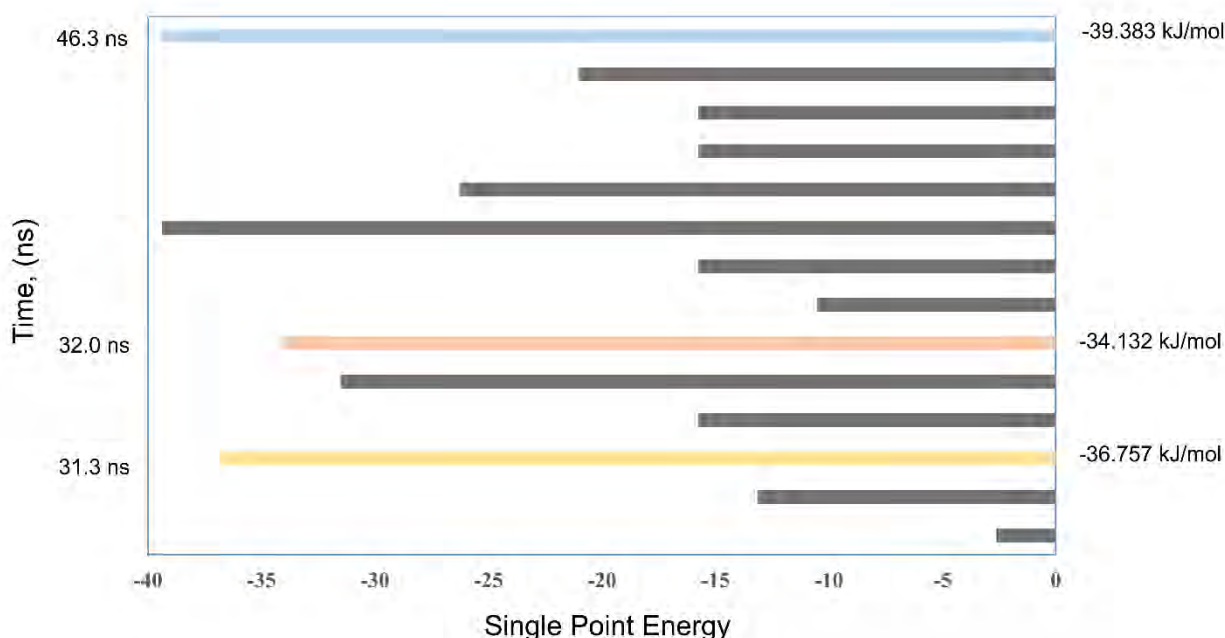


Figure 2.10: Single point (SP) energy calculation of 14 clusters of 1:1 D-Proline: Urea clusters and the three clusters at 31.3, 32.0 and 46.3 ns were highlighted and finalized after reaching equilibrium at 30 – 50 ns.

2.5.4 Quantum calculation of final three structures of 1:1 D-Proline: Urea DES clusters

The final three cluster conformers namely D1, D2, and D3 of 1:1 D-Proline: Urea were obtained which were optimized at the B3LYP-D3/6-311+g(d,p) level of theory. These 3 clusters were also optimized and then IR, VCD, and NBO charge calculations were performed at the same level of theory. The scaling factor 0.98 was used for all IR spectra [102], [103]. All the quantum calculations were performed using the Gaussian09 software program [100]. With the aid of IR and VCD spectral signatures, the DES formation was studied by examining the characteristic functional groups. By performing frequency analyses of 1:1 L-Proline: Urea and 1:1 D-Proline: Urea clusters, the absence of imaginary frequency was confirmed in the optimized structures, which are at minima on the potential energy surface (PES).

2.6 Protein preparation

To understand the effect of DES on protein, the alpha-lactalbumin protein (PDB ID: 1hfx) was selected for MD simulation. The protein was downloaded from the protein data bank (PDB) and the SwissPDB software package was used to minimize the energy of the protein.



Figure 2.11: Crystal structure of alpha-lactalbumin (PDB ID: 1hfx, resolution 1.90Å) obtained from protein data bank (<https://www.rcsb.org/structure/1hfx>). The different colors indicate the different domains of the protein.

2.7 YASARA Dynamics tool for protein MD simulation in DES solvents

Five different DES systems including L-Proline DES, 20% water-DES, 40% water-DES, D-Proline DES, and physiological solution were employed to perform MD simulations of the selected protein. The required number of L-Proline, urea, D-Proline, and water molecules for DES-protein MD simulation are given in **Table 6**.

Sl No.	No of Alpha-lactalbumin molecule	L-Proline molecules	Urea molecules	Water molecules	Description
1	1	200	200	3	Pure L Proline-Urea DES (where 0.15 – 0.3% moisture)
2	1	200	200	486	20% water uptake
3	1	200	200	1296	40% water uptake
4	1	0	0	3583	100% water uptake with 0.9% Na ⁺ Cl ⁻ salt

Table 6: The required number of molecules of L-Proline, urea, D-Proline, and water molecules for DES-protein MD simulation.

2.8 Parameters for protein MD simulation in DES solvents

The whole MD simulation runs for DES-protein were proceeded for 500ns. During the protein-DES simulation run, a few Na^+ and Cl^- were added by default for cell neutralization so that no charge can interrupt the simulation run. For only physiological solutions, 0.9% Na^+Cl^- were added into the DES-protein simulation. For all MD simulations, the YASARA dynamics program was used where the AMBER14 force field was applied. A molecular cut-off radius of 8.0 Å was applied for short-range van der Waals and Coulomb interaction and the particle-mesh Ewald (PME) method was employed to compute the long-range interactions. During the whole simulations, a cubic cell was considered where periodic boundary condition was applied with $50\text{Å} \times 50\text{Å} \times 50\text{Å}$ cell dimension. The temperature of 298K was considered using the NVT ensemble. All snapshots were saved at every 100ps with a 1.25fs time step.

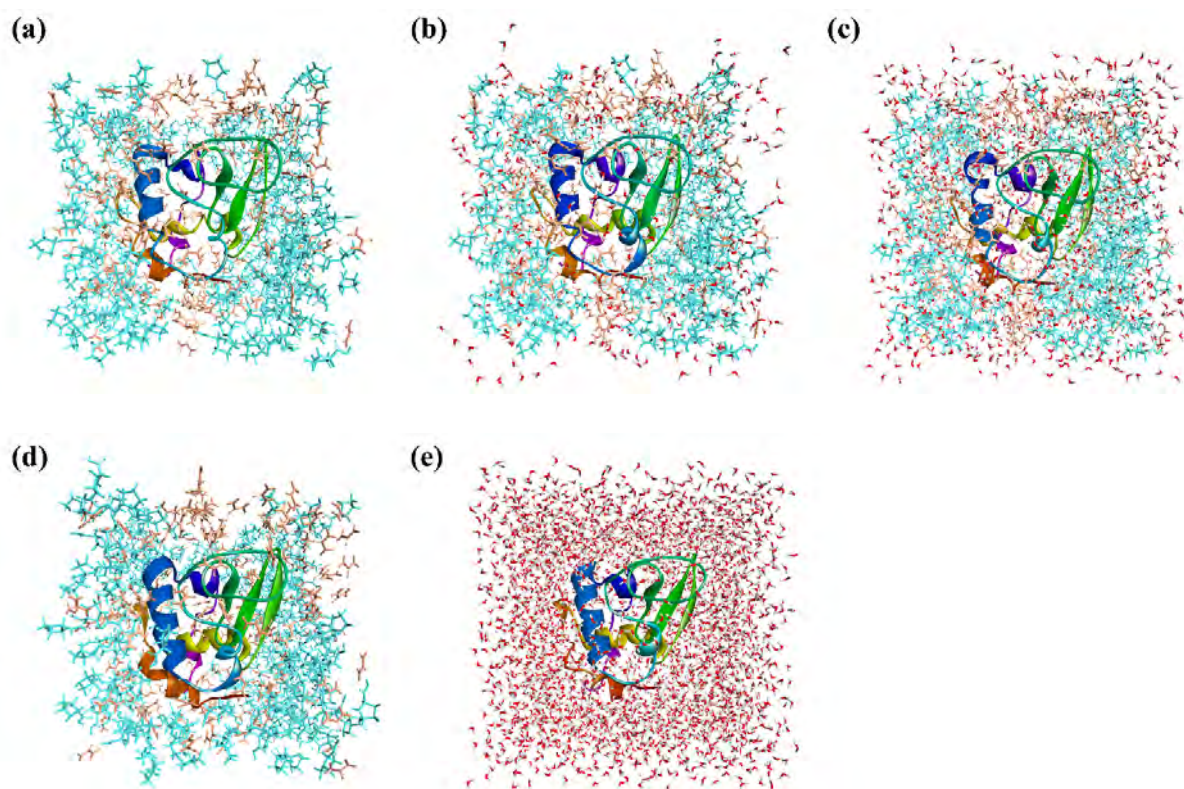


Figure 2.12: Initial simulation soup of Alpha-lactalbumin in (a) L-Proline DES, (b) 20% water-DES, and (c) 40% water-DES (d) D-Proline DES and (e) Physiological solution where the magenta color indicates the L-Proline and orange color indicates the urea molecules.

CHAPTER 3

RESULTS AND DISCUSSION

“Everything in the future is a wave, everything in the past is a particle” - William Lawrence Bragg

3.1 Quantum calculation of 1:1 L-Proline: Urea and 1:1 D-Proline: Urea cluster conformers

3.1.1 Structural geometry and hydrogen bond analysis by DFT calculation

Employing density functional theory (DFT), the isolated final three clusters of 1:1 L-Proline: Urea and 1:1 D-Proline: Urea are optimized at B3LYP-D3/6-311+G(d,p) level of theory in the gas phase. The gas-phase clusters are given in **Figure 3.1**

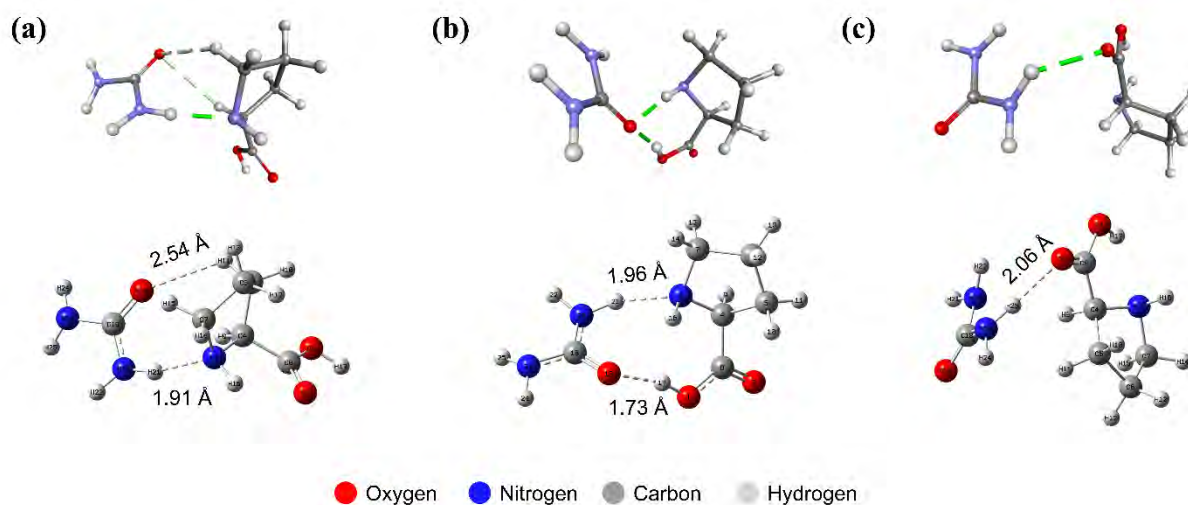


Figure 3.1: Optimized structures of (a) L1, (b) L2 and (c) L3 cluster conformers of 1:1 L-Proline: Urea DES calculated at B3LYP-D3/6-311+g(d,p) level of theory. The dotted bonds indicate the hydrogen bonding interactions.

During DES formation, the structural orientations are one of the pivotal features to understand the eutectic nature, and the physical properties are determined by molecular interactions. In this study, the most susceptible regions to form H-bonds are –COOH and –NH moieties of Proline and C=O and –NH₂ moieties of urea by which the DES cluster formations are understood. In 1:1 L-Proline: Urea clusters, the hydrogen bonds, NH_{L-Pro} ... HN_{Urea}, CO_{Urea} ...

CHAPTER 3

$\text{HC}_{\text{L-Pro}}$, $\text{OH}_{\text{L-Pro}}$... OC_{Urea} and CO_{Urea} ... $\text{HN}_{\text{L-Pro}}$ are responsible for DES formation. The list of H-bond distances of 1:1 L-Proline: Urea clusters are provided in **Table 7**. The range 1.73 – 2.54 Å of H-bond distances are found in L1, L2, and L3 clusters. It is observed that these three clusters form strong hydrogen bonding interactions when the DESs are formed. For example, the hydrogen bond distances, $\text{NH}_{\text{L-Pro}}$... HN_{Urea} , $\text{OH}_{\text{L-Pro}}$... OC_{Urea} in the L1 cluster are 1.91 and 2.54 Å respectively.

In terms of 1:1 D-Proline: Urea clusters (**Figure 3.2**), the hydrogen bonds are found a bit longer ranging from 2.05 to 2.36 Å (**Table 7**) compared to that of 1:1 L-Proline: Urea clusters.

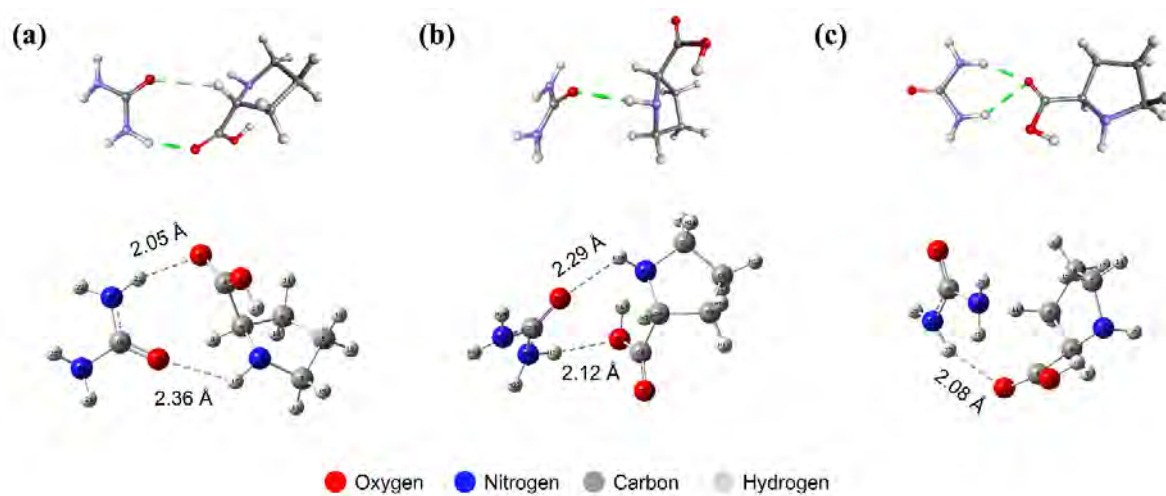


Figure 3.2: Optimized structures of (a) D1, (b) D2 and (c) D3 cluster conformers of 1:1 D-Proline: Urea DES calculated at B3LYP-D3/6-311+g(d,p) level of theory. The dotted bonds indicate the hydrogen bonding interactions.

Assignment	1:1 L-Proline: Urea DES			1:1 D-Proline: Urea DES		
	L1	L2	L3	D1	D2	D3
H-Bond distances						
N3 ... H21	1.91	1.96	-	-	-	-
O19 ... H11	2.54	-	-	-	-	-
O19 ... H17	-	1.73	-	-	-	-
O2 ... H25	-	-	2.05	-	-	2.08
O1 ... H21	-	-	-	-	2.12	-
O2 ... H21	-	-	-	2.05	-	-
O19 ... H16	-	-	-	2.36	2.29	-

Table 7: Selected H-bond distances of 1:1 L-Proline: Urea and 1:1 D-Proline: Urea DES calculated at D3-B3LYP/6-311+G (d,p) level of theory.

This indicates that during 1:1 D-Proline: Urea DESs formation, D-Proline, and urea interact weakly compared to that of 1:1 L-Proline: Urea DES clusters. However, by analyzing the H-bonds, O ... H and N ... H give the major contributions in interaction in all the DES clusters. Overall, the hydrogen bonding interactions indicate the proper formation of 1:1 L-Proline: Urea and 1:1 D-Proline: Urea DESs.

3.1.2 Thermochemistry calculation

Thermodynamic properties such as changes in Gibbs free energy (ΔG), electronic energy (ΔE), and enthalpy (ΔH) give evidence of DES formation [63], [104]. The thermochemical values of all clusters are obtained by the following equation: $\Delta X_{DES} = X_{DES} - X_{L-/D-Proline} - X_{Urea}$, where X is Gibbs free energy (G), either electronic energy (E) or enthalpy (H). The corresponding data of energies is given in **Table 8**.

(a)

1:1 L-Proline: Urea DES				
Cluster Conformers	Δ Gibb's Free Energy (kJ/mol)	Δ Enthalpy (kJ/mol)	Δ Electronic Energy (kJ/mol)	K_{eq}
L1	-41.69	-44.58	-43.42	2.01054373E+07
L2	-32.45	-35.45	-32.97	4.83723429E+05
L3	-19.26	-20.46	-17.98	2.36619651E+03

(b)

1:1 D-Proline: Urea DES				
Cluster Conformers	Δ Gibb's Free Energy (kJ/mol)	Δ Enthalpy (kJ/mol)	Δ Electronic Energy (kJ/mol)	K_{eq}
D1	-8.52	-52.17	-49.69	3.11270692E+01
D2	-7.76	-52.58	-50.09	2.29192377E+01
D3	-0.82	-46.78	-44.30	1.39161118E+00

Table 8: Change in Gibbs Free Energies, Enthalpies, and Electronic Energies of (a) 1:1 L-Proline: Urea and (b) 1:1 D-Proline: Urea DES calculated at D3-B3LYP/6-311+G (d,p) level of theory.

Table 8 shows that a low change in Gibbs free energy, electronic energy, and enthalpy are observed when 1:1 L-Proline: Urea and 1:1 D-Proline: Urea DESs are formed. Moreover, the results indicate that these DES cluster conformers are more stable compared to the pure components in the gas phase. The corresponding Gibbs free energy (ΔG), electronic energy (ΔE), and enthalpy (ΔH) change of most stable cluster L1 from 1:1 L-Proline: Urea are -41.69, -44.58 and -43.42 kJ/mol and D2 from 1:1 D-Proline: Urea are -8.52, -52.17 and -49.69 kJ/mol. However, the negative values of ΔG , ΔE , and ΔH indicate that the formation of all DES clusters is spontaneous in the gas phase.

3.1.2 Molecular electrostatic potential (MEP) mapping surface, HOMO-LUMO and NBO charge analysis

Electrostatic potential maps denoted by colors, provide the insight of reactive surface to explain the charge distribution in DES clusters [105], [106]. **Figure 3.3** depicts that the red region indicates the negative electrostatic potential (mostly O, N atoms) which means to have the greater electron density, and the blue region indicating the positive electrostatic potential (hydrogen atoms) shows the least electron density.

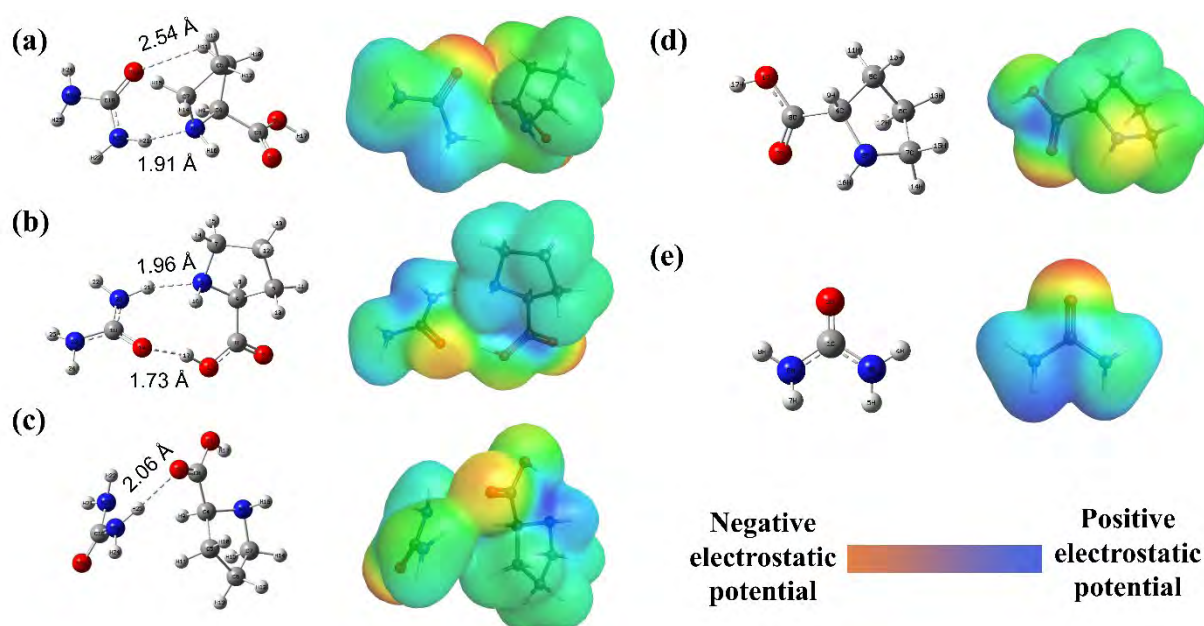


Figure 3.3: Molecular electrostatic potential (MEP) surface of (a) L1, (b) L2, (c) L3 cluster, (d) L-Proline and (e) Urea calculated at B3LYP-D3/6-311+g(d,p) level of theory highlighting

the regions to interact through hydrogen bonding. The red region is the negative electrostatic potential and the blue region is the positive electrostatic potential.

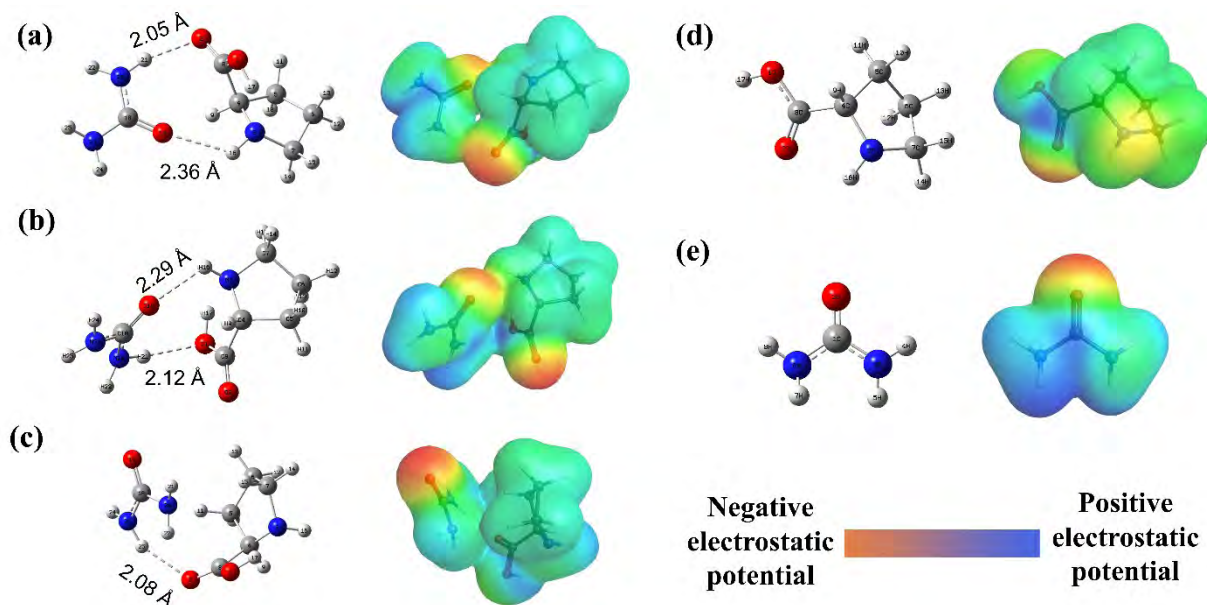


Figure 3.4: Electrostatic potential (ESP) surface map of (a) D1, (b) D2, (c) D3 cluster, (d) D-Proline and (e) Urea calculated at B3LYP-D3/6-311+g(d,p) level of theory highlighting the regions to interact through hydrogen bonding. The red region is the negative electrostatic potential and the blue region is the positive electrostatic potential.

In L-Proline and D-Proline DES clusters, the opposite charges are shown in two different color regions in MEP surfaces being either negative or positive. MEP surfaces (**Figure 3.4**) show that the H-bonds between Proline and urea are occurred in the opposite charges due to attractive forces. To comprehend the stability of DES clusters, the HOMO and LUMO energies were calculated. The HOMO-LUMO energies are the indicators to determine the chemical interactions which give information about the stability and reactivity of DES structures [107]. The HOMO is considered as the highest occupied of electrons whereas LUMO is considered to have no electrons. The HOMO-LUMO energy gap (ΔE) determines the stability between DES components [47], [107].

From **Figure 3.5 and 3.6**, the overall electron cloud shifting is observed between Proline and urea in 1:1 L-Proline: Urea and 1:1 D-Proline: Urea clusters respectively. The contribution of HOMO frontier orbital compositions is found higher in L-Proline of L1 and L2 cluster and the urea of L3 cluster and the vice versa scenario is observed for LUMO orbital compositions.

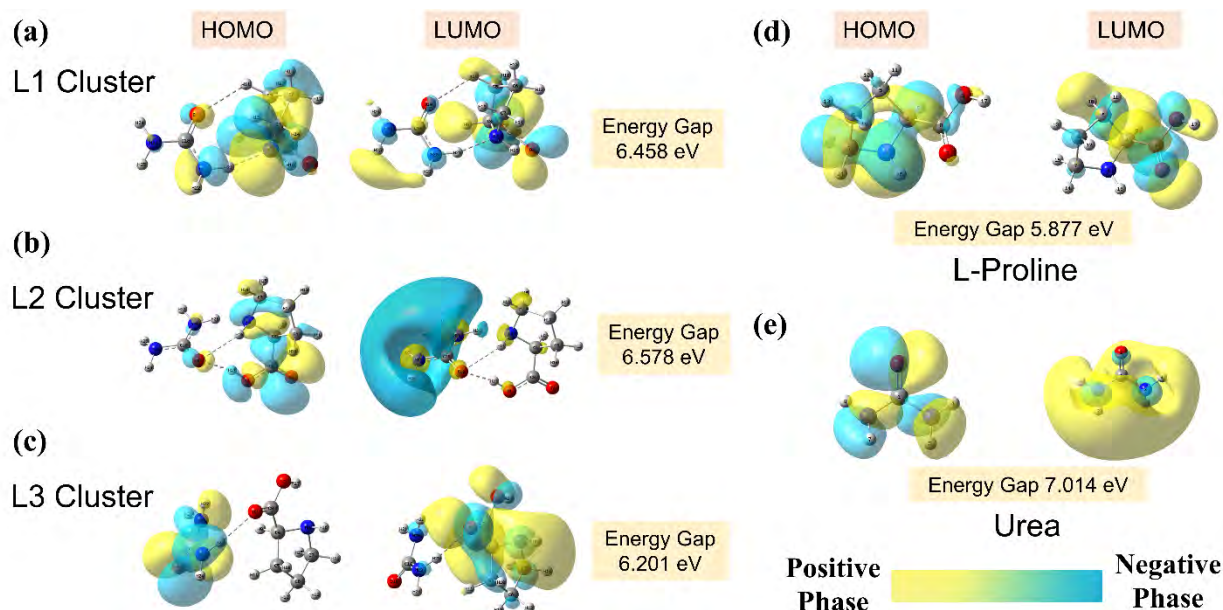


Figure 3.5: Frontier molecular orbitals (HOMO-LUMO) with an energy gap of (a) L1, (b) L2, (c) L3 cluster, (d) L-Proline, and (e) Urea calculated at B3LYP-D3/6-311+g(d,p) level of theory. The yellow regions indicate the positive isosurfaces and the blue regions indicate the negative isosurfaces.

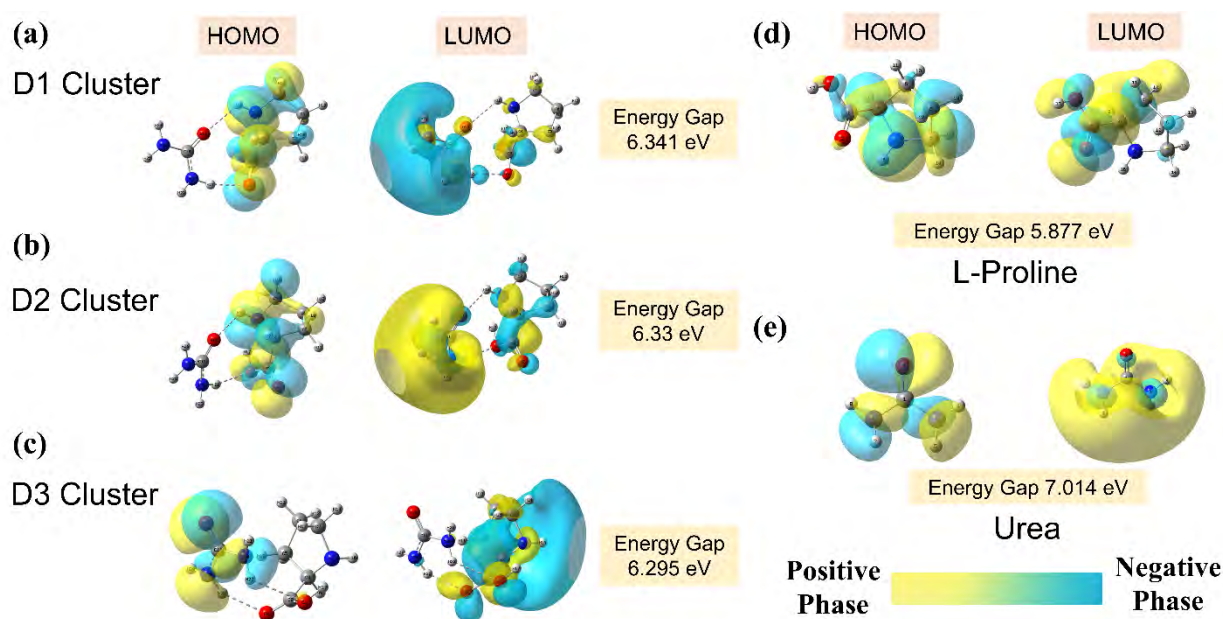


Figure 3.6: Frontier molecular orbitals (HOMO-LUMO) with an energy gap of (a) D1, (b) D2, (c) D3 cluster, (d) D-Proline, and (e) Urea calculated at B3LYP-D3/6-311+g(d,p) level of theory. The yellow regions indicate the positive isosurfaces and the blue regions indicate the negative isosurfaces.

CHAPTER 3

Similar cases are also noticed for 1:1 D-Proline: Urea clusters. However, as the HOMO-LUMO energies do not give well-satisfactory explanations, hence, NBO charge analyses were carried out to visualize the atom to atom charge delocalization. This delocalization of charges between interacting atoms in DES clusters gives the actual reason for the depression of the freezing point of DESs [8]. **Table 9** shows that the interacting atoms with high electronegativity show the decrease of charges and the less electronegative atoms show the increase of charges in 1:1 L-Proline: Urea DES clusters compared to the pure components.

(a)

1:1 L-Proline: Urea DES							
Clusters Conformers	N3 _(Pro)	H11 _(Pro)	H17 _(Pro)	O2 _(Pro)	O19 _(U)	H21 _(U)	H25 _(U)
L1	-0.719	0.234	-	-	-0.693	0.432	-
L2	-0.723	-	0.508	-	-0.728	0.435	-
L3	-	-	-	-0.620	-	-	0.413
L-Proline	-0.686	0.218	0.486	-0.611	-	-	-
Urea	-	-	-	-	-0.647	0.396	0.378

(b)

1:1 D-Proline: Urea DES							
Clusters	O1 _(Pro)	O2 _(Pro)	H16 _(Pro)	O19 _(U)	H21 _(U)	H22 _(U)	H25 _(U)
D1	-	-0.647	0.403	-0.709	0.402	-	-
D2	-0.720	-	0.408	-0.707	0.417	-	-
D3	-0.687	-0.639	-	-	-	0.391	0.413
D-Proline	-0.693	-0.611	0.377	-	-	-	-
Urea	-	-	-	-0.647	0.396	0.378	0.378

Table 9: NBO Charges of (a) L1, L2, and L3 clusters of 1:1 L-Proline: Urea DES (b) D1, D2, and D3 clusters of 1:1 D-Proline: Urea DES calculated at B3LYP-D3/6-311+g(d,p) level of theory. (N3_(Pro) = N3 atom of Proline in 1:1 L-Proline: Urea DES).

CHAPTER 3

For example, the charge of the N3_{L-Proline} atom is reduced from L-Proline (-0.686) to L1 (-0.719) and L2 (-0.723) clusters respectively. Similar cases were also observed in 1:1 D-Proline: Urea clusters. This delocalization of NBO charges strongly suggests that during the formation of hydrogen bonding in studied DES clusters, the charge transfers occur.

3.1.3 Calculated IR spectra analysis

The calculated IR and VCD spectra of urea (Not VCD active), L-Proline, D-Proline, 3 clusters of 1:1 L-Proline: Urea, and 3 clusters of 1:1 D-Proline: Urea in the gas phase are given in **Table 10** and **11**.

Type	Frequency (cm ⁻¹)					Percentage of peak shift (%)		
	Urea	L-Proline	L1	L2	L3	L1	L2	L3
N – C – N sym. str.	932.69	-	953.92 ^a	976.44 ^a	935.55 ^a	-2.27	-4.69	-0.31
N – C – N asym. str.	1376.51	-	1406.48 ^a	1443.29 ^a	1381.77 ^a	-2.18	-4.85	-0.38
C = O str.	1750.68	1764.33	1726.13 ^a 1758.03 ^b	1696.88 ^a 1760.87 ^b	1735.35 ^a 1779.44 ^b	1.40 0.36	3.07 0.20	0.88 -0.86
C* – H str.	-	2966.21	3003.95 ^b	2974.99 ^b	2952.22 ^b	-1.27	-0.30	0.47
(NH _{Pro} ...) N – H str.	-	-	3155.26 ^a	3196.99 ^a	-	-	-	-
(CO _{Pro} ...) N – H str.	-	-	-	-	3452.86 ^a	-	-	-
N – H str.	-	3475.11	3436.66 ^b	3391.04 ^b	3374.72 ^b	1.11	2.42	2.89
C – N – C sym. str.	-	-	930.06 ^b	962.09 ^b	955.45 ^b	-	-	-
C – N – C asym. Str.	-	1101.28	1080.55 ^b	1081.02 ^b	1089.56 ^b	1.88	1.84	1.06
O – H str.	-	3683.86	3685.80	3307.33	3546.88	-0.05	10.22	3.72

Where, a = Urea; b = L-Proline; The asterisk sign (*) indicates the chiral center; Asym. str. = asymmetric stretching; Sym. str. = symmetric stretching.

Table 10: Calculated vibrational frequencies of the major functional groups of 1:1 L-Proline: Urea DES cluster conformers and their relative wavenumber changes (%) in the DES with respect to urea and L-Proline.

Type	Frequency (cm ⁻¹)					Percentage of peak shift (%)		
	Urea	D-Proline	D1	D2	D3	D1	D2	D3
N – C – N sym. str.	932.69	-	953.10 ^a	953.86 ^a	938.13 ^a	-2.19	-2.27	-0.58
N – C – N asym. str.	1376.51	-	1402.10 ^a	1397.52 ^a	1381.17 ^a	-1.86	-1.53	-0.34
C = O str.	1750.68	1764.33	1717.87 ^a 1766.18 ^b	1720.43 ^a 1795.81 ^b	1731.46 ^a 1776.01 ^b	1.87 -0.10	1.73 -1.78	1.10 -0.66
C* – H str.	-	2966.21	3026.68 ^b	3020.39 ^b	2998.83 ^b	-2.04	-1.83	-1.10
(CO _{Pro} ...) H – N str.	-	-	3443.92 ^a	-	3466.17 ^a	-	-	-
(OH _{Pro} ...) H – N str.	-	-	-	3461.29 ^a	-	-	-	-
N – H str.	-	3475.11	3484.95 ^b	3492.68 ^b	3470.44 ^b	-0.28	-0.51	0.13
C – N – C sym. str.	-	-	945.61 ^b	951.97 ^b	911.75 ^b	-	-	-
C – N – C asym. Str.	-	1101.28	1098.51 ^b	1100.50 ^b	1077.41	0.25	0.07	2.17
O – H str.	-	3683.86	3250.18	3144.01	3274.07	11.77	14.65	11.12

Where, a = Urea; b = L-Proline; The asterisk sign (*) indicates the chiral center; Asym. str. = asymmetric stretching; Sym. str. = symmetric stretching.

Table 11: Calculated vibrational frequencies of the major functional groups of 1:1 D-Proline: Urea DES cluster conformers and their relative wavenumber changes (%) in the DES with respect to urea and D-Proline.

For L-Proline DESs, the three cluster conformers show characteristic IR spectra. The corresponding IR spectra are given in **Figure 3.7**. In the 1500 – 4000 cm⁻¹ region, the major hydrogen bonds, NH_{L-Pro} ... H(21) – N(20)_{Urea}, CO_{L-Pro} ... H(25) – N(23)_{Urea} and OH_{L-Pro} ... O(19) – C(18)_{Urea} are responsible to DES formation. By analyzing IR data, the most prominent new peak for – H(21) – N(20)_{Urea} stretching for L1 and L2 clusters appear at 3155.26 and 3196.99 cm⁻¹ respectively. In the L3 cluster, this peak is absent due to a change in the orientation of interaction, and instead, – H(25) – N(23)_{Urea} peak appears newly at 3452.86 cm⁻¹. Another evidence for DES formation is the close presence of dual IR peaks of C = O stretching (ranging from 1696.88 to 1779.44 cm⁻¹) in L-Proline DES clusters. These three clusters show shifts of 1.40%, 3.07% and 0.88% respectively from urea and 0.36%, 0.20% and -0.86% respectively from L-Proline. Besides, O(1) – H(17) stretching is located at 3685.80,

3307.33, and 3546.88 cm^{-1} respectively, interestingly, the L2 cluster is shifted to 10.22% from L-Proline

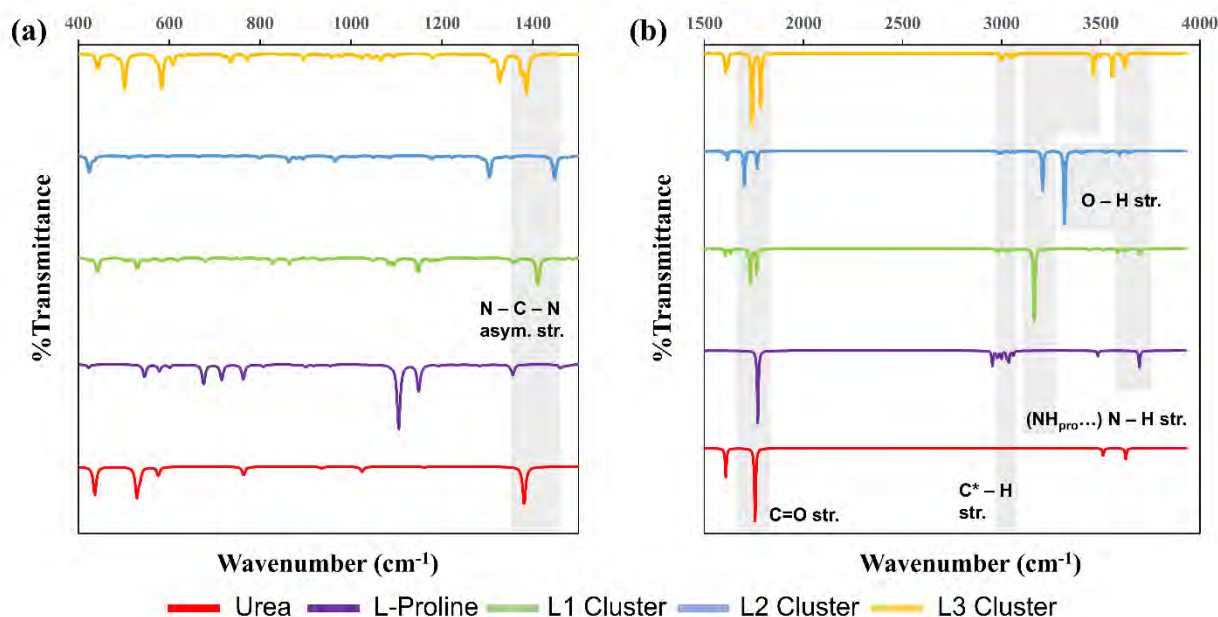


Figure 3.7: Calculated IR spectra of urea, L-Proline, L1, L2, and L3 clusters at (a) Low-wavenumber region and (b) High-wavenumber region at B3LYP-D3/6-311+G(d, p) level of theory in the gas phase.

which denotes that a strong interaction is present over that stretching vibration mode. In 400 – 1500 cm^{-1} region, the N – C – N_{Urea} asymmetric stretching vibrations (ranging 1381.77 – 1443.29 cm^{-1}) for L-Proline clusters show peak shifts of -2.18%, -4.85% and -0.38% from urea. In addition, C – N – C_{L-Pro} asymmetric stretching vibrations of L-Proline DES clusters are located in the region of 1080.55 – 1089.56 cm^{-1} with peak shifts of 1.88%, 1.84%, and 1.06% from L-Proline. Similar cases in IR spectra and peak shifts have been found in 1:1 D-Proline: Urea cluster conformers have given in **Figure 3.8**

Here also, the characteristic H-bonds in D-Proline DES clusters, CO_{D-Pro} ... H(21) – N(20)_{Urea}, NH_{D-Pro} ... O(19) – C(18)_{Urea}, OH_{D-Pro} ... H(21) – N(20)_{Urea} and CO_{D-Pro} ... H(25) – N(23)_{Urea} are observed. Due to change in interaction orientation, for example, the new appearance peak, – H(21) – N(20)_{Urea} stretching vibrations in D1 and D3 are located in 3443.92 and 3466.17 cm^{-1} respectively and the – H(21) – N(20)_{Urea} stretching in D2 is located at 3461.29 cm^{-1} . Again, O(1) – H(17) stretching vibrations in D-Proline DES clusters are found in the range of 3144.01 – 3274.07 cm^{-1} with peak shifts of 11.77%, 14.65%, and 11.12% respectively and these peak shifts indicate the presence of H-bond interaction in D-Proline DES clusters.

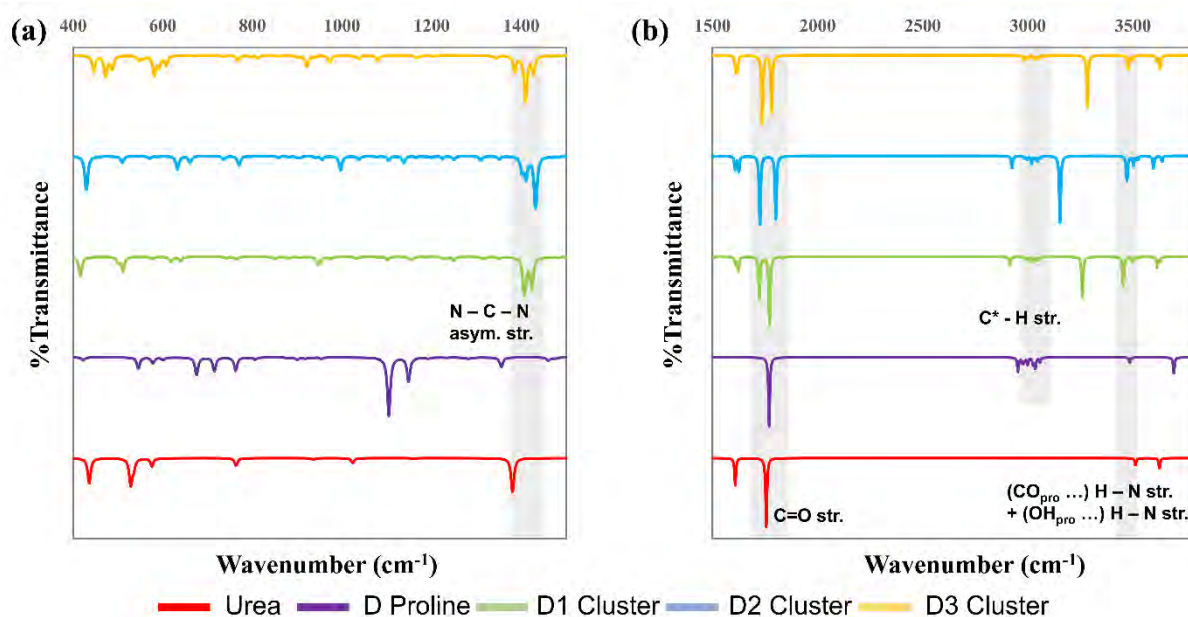


Figure 3.8: Calculated IR spectra of urea, D-Proline, D1, D2, and D3 clusters at (a) Low-wavenumber region and (b) High-wavenumber region at B3LYP-D3/6-311+G(d, p) level of theory in the gas phase.

3.1.4 Calculated VCD spectra analysis

Table 12 describes the VCD rotational strength of L-Proline DES and D-Proline DES clusters.

Type	L1 Cluster			L2 Cluster			L3 Cluster		
	Frequency (cm ⁻¹)	IR	VCD rot. strength × 10 ⁻⁴⁴ esu ² cm ²	Frequency	IR	VCD rot. strength × 10 ⁻⁴⁰ esu ² cm ²	Frequency	IR	VCD rot. strength × 10 ⁻⁴⁰ esu ² cm ²
N – C – N sym. str.	953.92 ^a	13.349	13.309	976.44 ^a	8.729	-13.425	935.55 ^a	11.543	14.538
N – C – N asym. str.	1406.48 ^a	318.683	-9.865	1443.29 ^a	392.508	80.337	1381.77 ^a	232.875	-209.893
C = O str.	1726.13 ^a	442.196	-	1696.88 ^a	584.521	-25.663	1735.35 ^a	492.552	22.509
	1758.03 ^b	308.618	70.135 82.198	1760.87 ^b	310.752	-37.274	1779.44 ^b	351.611	-68.911
C* – H str.	3003.95 ^b	7.505	-7.345	2974.99 ^b	8.558	13.910	2952.22 ^b	2.612	0.007
(NH _{Pro} ...) H – N str.	3155.26 ^a	907.736	-	3196.99 ^a	682.090	389.382	-	-	-
(CO _{Pro} ...) N – H str.	-	-	-	-	-	-	3452.86 ^a	152.629	-134.618
N – H str.	3436.66 ^b	25.403	-0.003	3391.04 ^b	43.547	-34.937	3374.72 ^b	0.788	-3.448
C – N – C	930.06 ^b	25.641	-	962.09 ^b	93.146	-83.409	955.45 ^b	26.268	36.419

sym. str.									
C – N – C asym. Str.	1080.55 ^b	73.173	-24.497	1081.02 ^b	27.183	34.942	1089.56 ^b	17.644	-0.826
O – H str.	3685.80	75.841	1.032	3307.33	1303.311	473.870	3546.88	157.599	42.436

Table 12: Calculated IR and VCD intensities of the characteristic functional groups of L1, L2, and L3 clusters of 1:1 L-Proline: Urea DES

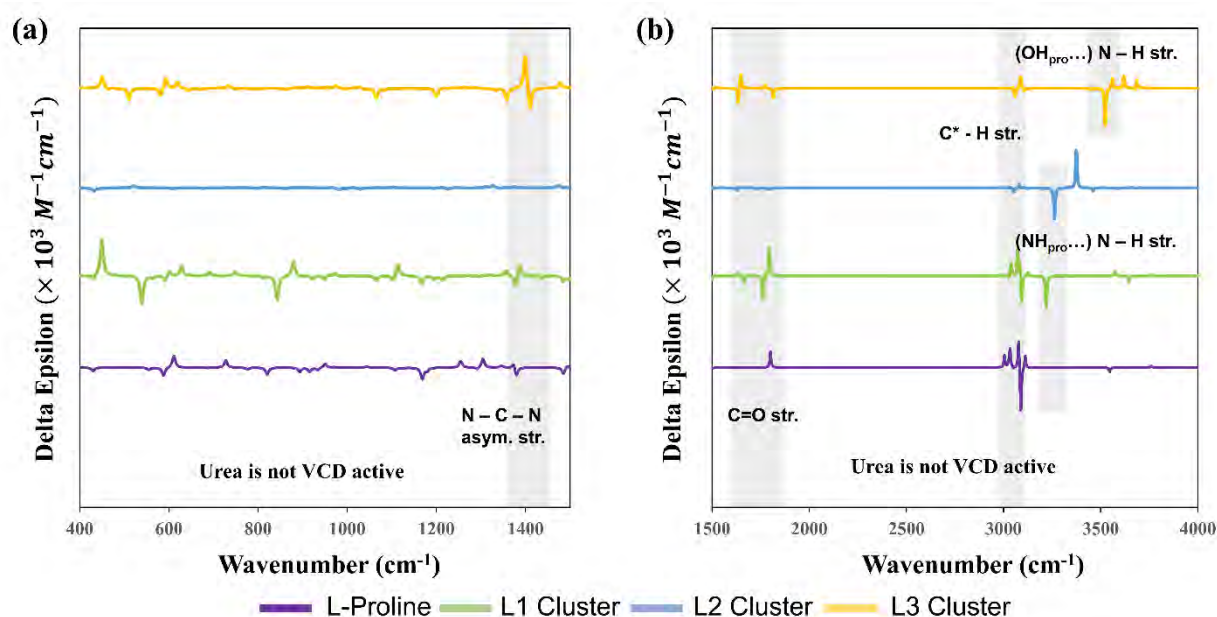


Figure 3.9: Calculated vibrational circular dichroism (VCD) spectra of L-Proline, L1, L2, and L3 clusters at (a) Low-wavenumber region and (b) High-wavenumber region at B3LYP-D3/6-311+G(d, p) level of theory in the gas phase.

The 1500 – 4000 cm^{-1} region shows marked rotational strength of important vibration modes. In the L1 cluster, $-\text{H}(21) - \text{N}(20)_{\text{Urea}}$ stretching shows VCD rotational strength of $-51.613 \times 10^{-44} \text{esu}^2\text{cm}^2$ with corresponding to its IR intensity of 907.735. The L2 cluster with the same stretching vibration produces intense VCD with negative rotational strength of $-389.382 \times 10^{-44} \text{esu}^2\text{cm}^2$. A similar case is also found for $-\text{H}(25) - \text{N}(23)_{\text{Urea}}$ stretching having rotational strength of $-134.618 \times 10^{-44} \text{esu}^2\text{cm}^2$. The VCD rotational signal for $\text{O}(1) - \text{H}(17)$ stretching for L1, L2, and L3 is 1.032, 473.870, and 42.436 respectively in the region of 3307 – 3685.80 cm^{-1} . It is noticed that the L2 cluster produces a very intense rotational signal due to having strong hydrogen bonding interaction between L-Proline and urea. In terms of D1, the $\text{N} - \text{C} - \text{N}_{\text{Urea}}$ asymmetric stretching (located at 1402.10 cm^{-1}) shows intense VCD having negative rotational strength of $-135.689 \times 10^{-44} \text{esu}^2\text{cm}^2$. However, the same vibration mode for D2 and

CHAPTER 3

D3 produce intense positive VCD rotational strength of $350.667 \times 10^{-44} \text{ esu}^2\text{cm}^2$ and $136.843 \times 10^{-44} \text{ esu}^2\text{cm}^2$ respectively. The reason to change from negative to positive rotational strength is due to the difference in structural orientation and interaction as well as the opposite angle between vibrational electric and magnetic dipole moment transition vectors. Besides, these rotational signals are located easier corresponding to their IR intensity of 101.408 and 104.741 respectively.

Type	D1 Cluster			D2 Cluster			D3 Cluster		
	Frequency (cm ⁻¹)	IR	VCD rot. strength $\times 10^{-44} \text{ esu}^2 \text{ cm}^2$	Frequency (cm ⁻¹)	IR	VCD rot. strength $\times 10^{-40} \text{ esu}^2 \text{ cm}^2$	Frequency (cm ⁻¹)	IR	VCD rot. strength $\times 10^{-40} \text{ esu}^2 \text{ cm}^2$
N – C – N sym. str.	953.10 ^a	8.748	5.863	953.86 ^a	16.124	41.163	938.13 ^a	8.819	12.284
N – C – N asym. str.	1402.10 ^a	273.283	-135.689	1397.52 ^a	101.408	350.667	1381.17 ^a	104.741	136.843
C = O str.	1717.87 ^a 1766.18 ^b	392.919 615.7150	-170.095 364.563	1720.43 ^a 1795.81 ^b	478.709 438.249	-156.188 248.066	1731.46 ^a 1776.01 ^b	474.673 381.848	6.040 32.318
C* – H str.	3026.68 ^b	11.070	-22.520	3020.39 ^b	8.209	-10.106	2998.83 ^b	7.858	0.515
(CO _{Pro} ...) H – N str.	3443.92 ^a	261.905	-32.350	-	-	-	3466.17 ^a	96.370	-56.685
(OH _{Pro} ...) H – N str.	-	-	-	3461.29 ^a	171.389	90.155	-	-	-
N – H str.	3484.95 ^b	48.009	15.587	3492.68 ^b	61.943	13.042	3470.44 ^b	4.810	4.420
C – N – C sym. str.	945.61 ^b	72.834	96.033	951.97 ^b	7.484	35.464	911.75 ^b	7.616	-28.731
C – N – C asym. Str.	1098.51 ^b	28.817	-2.819	1100.50 ^b	30.423	-43.207	1077.41	36.867	-6.998
O – H str.	3250.18	372.266	210.980	3144.01	457.520	106.198	3274.07	359.349	-35.995

Table 13: Calculated IR and VCD intensities of the characteristic functional groups of D1, D2, and D3 of 1:1 D-Proline: Urea DES.

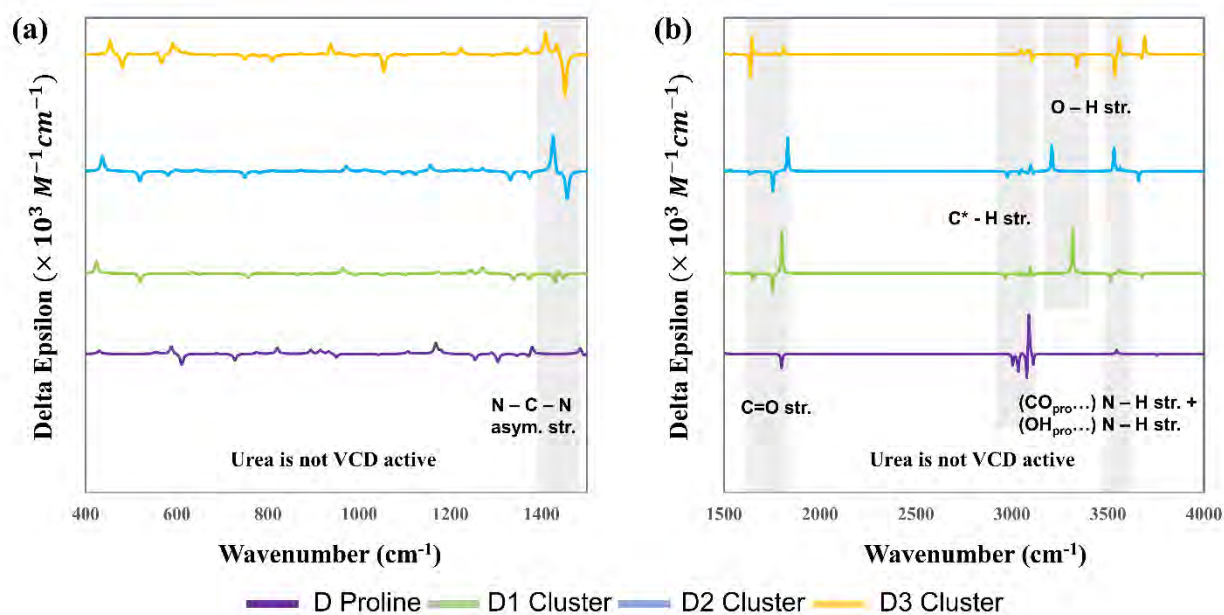


Figure 3.10: Calculated vibrational circular dichroism (VCD) spectra of D-Proline, D1, D2, and D3 clusters at (a) Low-wavenumber region and (b) High-wavenumber region at B3LYP-D3/6-311+G(d, p) level of theory in the gas phase.

3.2 MD simulation results of alpha-lactalbumin protein in the presence of DES solvents

3.2.1 Impact on the backbone structure of alpha-lactalbumin

To comprehend the structural changes of alpha-lactalbumin in the presence of different DES solvents, the root mean square deviation (RMSD) was calculated. L-Proline: Urea DES, 20% water-L Proline: Urea e DES, 40% water- L Proline: Urea DES, D-Proline: Urea DES and physiological solutions were applied as DES solvent system. **Figure 3.11** shows the variations in RMSD of $C\alpha$ -atoms of alpha-lactalbumin in these DES solvents.

Figure 3.11 depicts that the RMSD values of alpha-lactalbumin in L-Proline: Urea DES solvent are in the range of 0.38 – 1.92 Å and the average value is 1.58 Å. This RMSD noticeably increases when 20% and 40% water solvents were used in L-Proline: Urea DES system which suggests that the protein is destabilized in the hydrated L-Proline: Urea DES solvent system. The most deviation in protein structure is observed in the 20% water-L Proline: Urea DES system and the corresponding RMSD value is in the range of 0.32 – 3.40 Å. It is noticed that the RMSD of protein structure fluctuates from the initial run to 320 ns but after 320 ns the protein structure gets deviated most to 500 ns. This indicates that the protein structure

destabilizes greater after 320 ns. In 40% water-DES system, the RMSD values are found less with an average of 2.06 Å compared to the RMSD in 20% water-DES system (average 2.23 Å). In here also, similar RMS deviation as 20% water-DES is noticed after 410 ns.

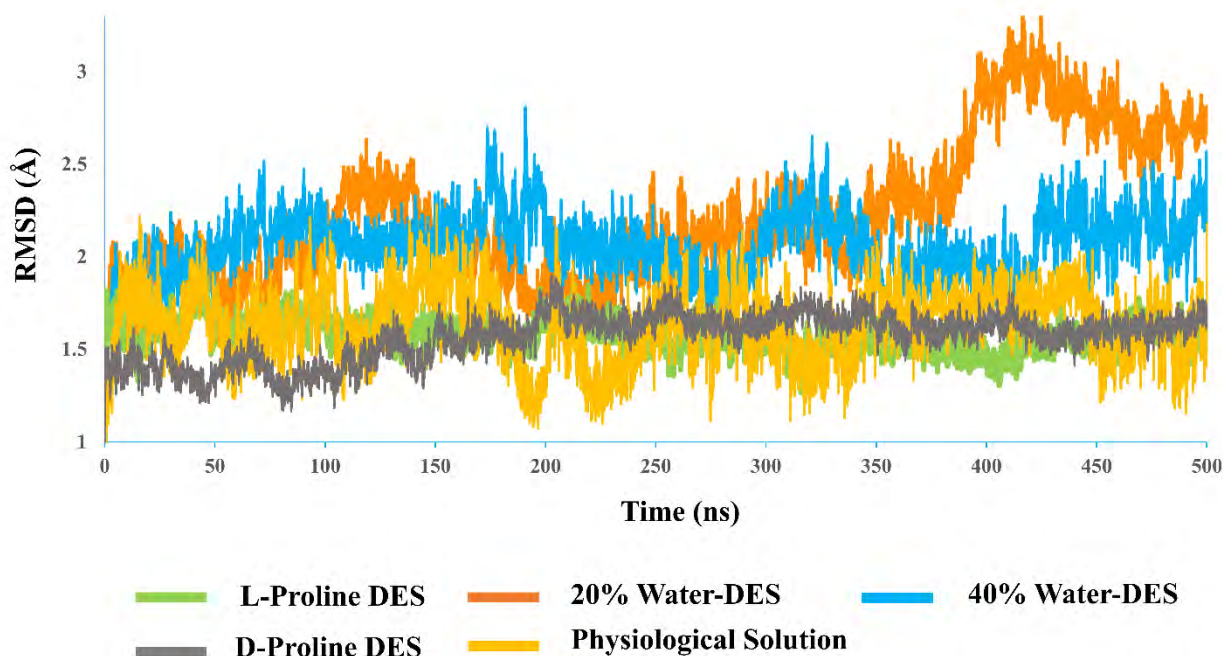


Figure 3.11: Analysis of 500ns simulation data for alpha-lactalbumin by Root mean square deviation (RMSD) values for C- α atom in Proline-based DES solvents.

The lowest deviation in RMSD is noticed in studied DES solvents. This suggests that the protein structure tends to be less destabilized in the pure DES solvents compared to other studied systems. However, there is no observable significance in RMSD in D-Proline: Urea DES and physiological solution. Besides, the protein structure seems no remarkable deviation in RMSD between D-Proline: Urea DES and L-Proline: Urea DES system. In L-Proline: Urea and D-Proline: Urea DES, the protein structure shows the least deviation in RMSD compared to the water-DES system and this indicates that the Proline-based DESs are viscous and the protein can remain stable due to the viscous nature of DES solvent throughout the 500 ns simulation.

3.2.2 Effect on the compactness of alpha-lactalbumin

The compactness of alpha-lactalbumin is measured by radius of gyration (R_g) which suggests that the protein is expanded or compacted with respect to its degree of freedom over a certain period of simulation. **Figure 3.12** depicts the changes in the radius of gyration of alpha-lactalbumin in L-Proline: Urea DES, 20% water-L Proline: Urea DES, 40% water- L Proline:

Urea DES, D-Proline: Urea DES, and physiological solution. From **Figure 3.12**, it can be seen that in L-Proline: Urea DES, the R_g value (average 14.68 Å) is less compared to the R_g in 20% and 40% water-L Proline: Urea DES solvent systems. This indicates that the protein structure remains more compact in L-Proline: Urea DES compared to the hydrated L-Proline: Urea DES system and with the presence of 20% and 40% water in L-Proline: Urea DES, the protein maintains swollen structure. The most swollen structure is observed in 20% water-L Proline: Urea DES system and the R_g values (ranging 14.26 – 15.18 Å) fluctuate over the whole simulation. In 20% water-L Proline: Urea DES system, the R_g value increases steeply after 320 ns which signifies that the protein structure swells the most after 320 ns.

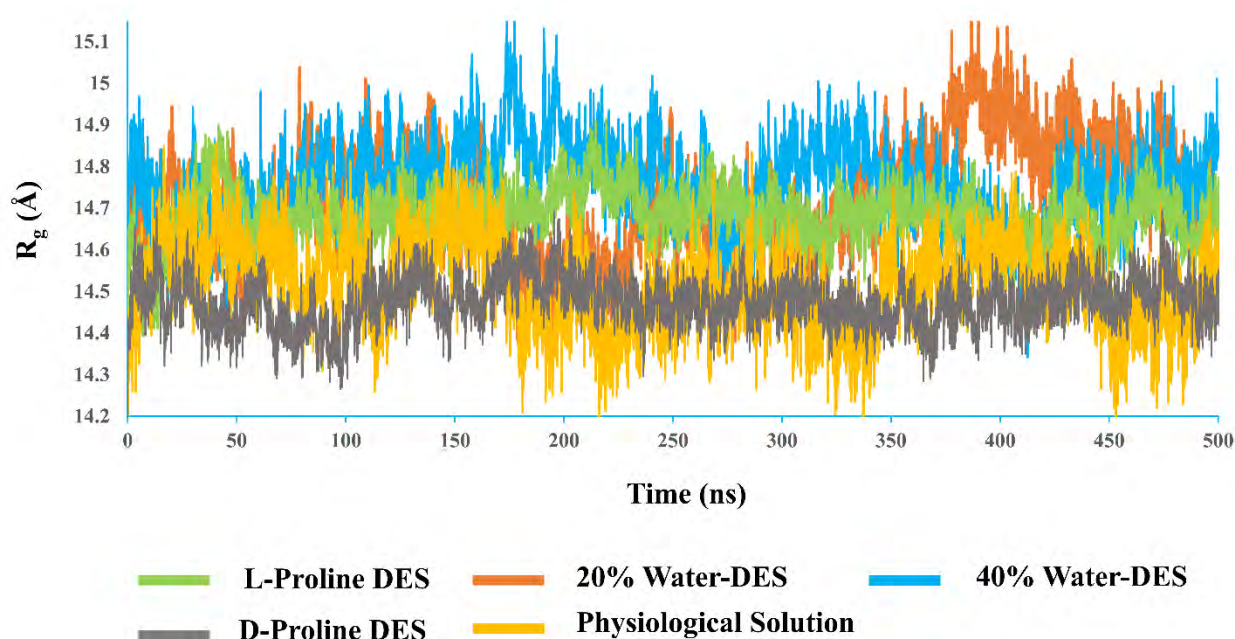


Figure 3.12: Analysis of 500ns simulation for alpha-lactalbumin by Radius of gyration (R_g) in Proline-based DES solvents.

In 40% water-L Proline: Urea DES system, the R_g (ranging 14.34 – 15.16 Å) is found less fluctuating, indicating that the protein swells less compared to that in 20% water-DES system. Besides, the protein structure is found to have similar compactness in D-Proline: Urea DES and physiological solution. In terms of RMSD and R_g , the protein shows a similar deviation. This notifies that the highest RMSD in 20% water-DES system gives the least compact protein structure.

3.2.3 Variation of the solvent-accessible surface area of alpha-lactalbumin

The variation in the solvent-accessible surface area (SASA) of alpha-lactalbumin in L-Proline: Urea DES, 20% water-L Proline: Urea DES, 40% water- L Proline: Urea DES, D-Proline: Urea DES and the physiological solution is given in **Figure 3.13**. Similar to RMSD and R_g , the highest value in SASA is observed in the 20% water-L Proline: Urea DES complex (average 6758.42 Å²). This suggests that the protein structure becomes swollen most due to covering a higher surface area in the presence of 20% water in L-Proline: Urea DES solvents. This prospect also complies with the value of RMSD and R_g . Besides, in the 40% water-DES system, the average value of SASA is 6608.24 Å² which is closer to the SASA of the L-Proline: Urea DES system (average 6636.86 Å²). A similar case is also found in D-Proline: Urea DES (average 6327.54 Å²) and physiological solution (average 6397.25 Å²).

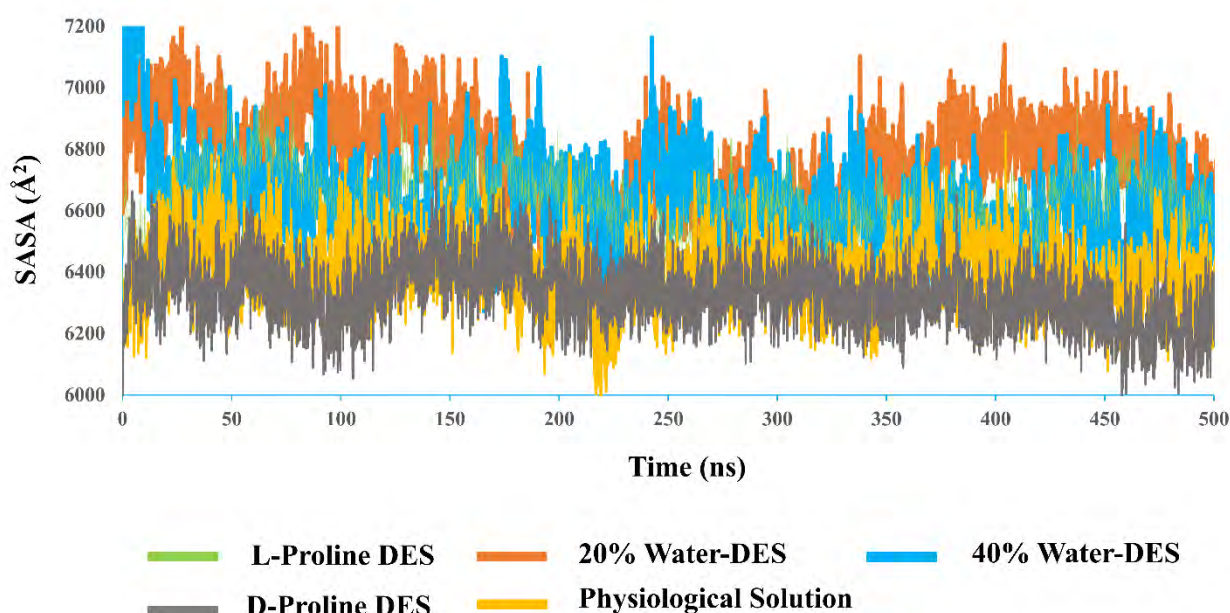


Figure 3.13: Analysis of 500ns simulation for alpha-lactalbumin by solvent accessible surface area (SASA) in Proline-based DES solvents.

Now, to understand the change in polar (Hydrophilic) and apolar (Hydrophobic) area of the protein structure at 500 ns of alpha-lactalbumin in the studied DES solvent systems, the GetArea server was used [108]–[110]. As can be seen in **Table 14** and **Figure 3.14**, the apolar surface area of alpha-lactalbumin is higher than the polar surface area. Ongoing from L-Proline: Urea DES to physiological solutions, there is seen an increasing trend of polar surface areas and vice versa for the apolar areas. The total surface area in L-Proline: Urea DES is found

CHAPTER 3

at 7411.96 Å². In 20% water-L Proline: Urea DES system, the total surface area of protein structure was the highest and the corresponding value is 7506.99 Å².

DES	Total Area (Å ²)	Polar Area (Å ²)	Apolar Area (Å ²)	% of polar area	% of apolar area
L-Proline: Urea DES	7411.96	2722.21	4689.75	36.73	63.27
20% water-L Proline: Urea DES	7506.99	2910.26	4596.73	38.77	61.23
40% water-L Proline: Urea DES	7444.66	2868.08	4576.58	38.53	61.47
D-Proline:Urea DES	7038.46	2809.19	4229.27	39.91	60.09
Physiological solution	7429.19	3170.76	4258.43	42.68	57.32

Table 14: Polar and apolar surface area of 500 ns simulation structure of alpha-lactalbumin in L-Proline: Urea DES, 20% water-L Proline: Urea DES, 40% water-L Proline: Urea DES, D-Proline: Urea DES, and physiological solution.

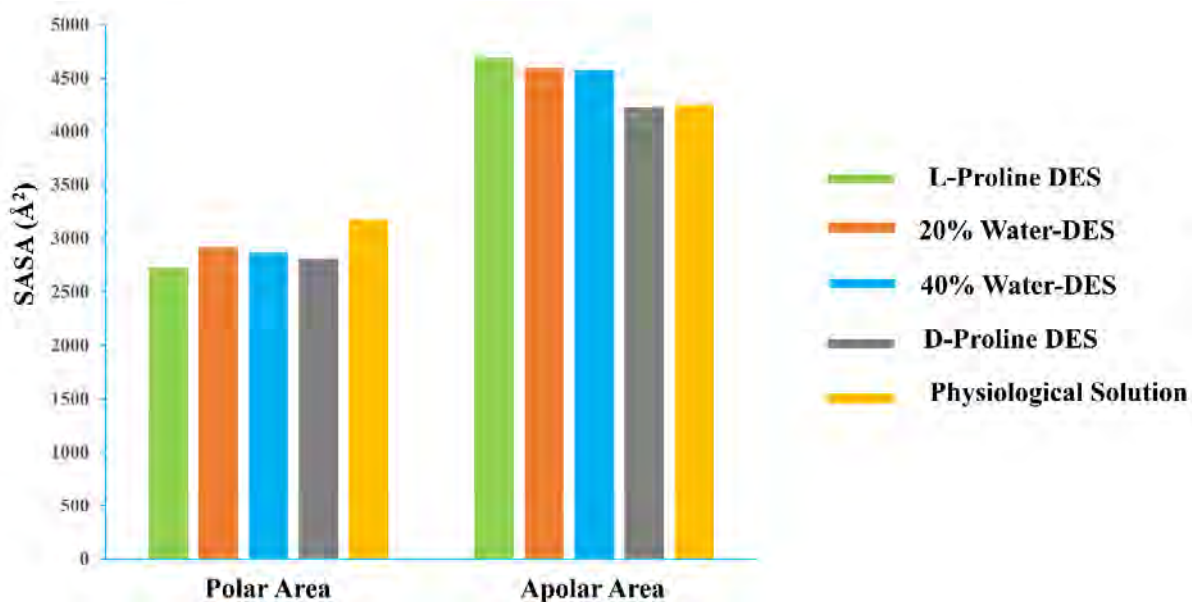


Figure 3.14: Polar (Hydrophilic) and apolar (Hydrophobic) surface area of 500 ns simulation structure of alpha-lactalbumin in Proline-based DES solvents.

An increment in the hydrophilic surface by 2.04% is observed in 20% water-L Proline: Urea DES compared to L-Proline: Urea DES. The reason to have this is that the hydrogen bonding

interaction of water molecules increases the polar surface. Simultaneously, there is a decrease at the same amount of percentage in the same water-DES system, seen in the hydrophobic surface where water molecules maintain the self-diffusion [111]–[114]. In the absence of DES system such as and physiological solution, the polar surface area increased at a higher percentage compared to the other DES solvent system.

3.2.4 Impact on the flexibility of alpha-lactalbumin

The root mean square fluctuations (RMSF) assist to describe the flexibility of the protein structure. **Figure 3.15** depicts the RMS fluctuations of $C\alpha$ -atoms for individual residues of alpha-lactalbumin in L-Proline: Urea DES, 20% water-L Proline: Urea DES, 40% water-L Proline: Urea DES, D-Proline: Urea DES, and physiological solution.

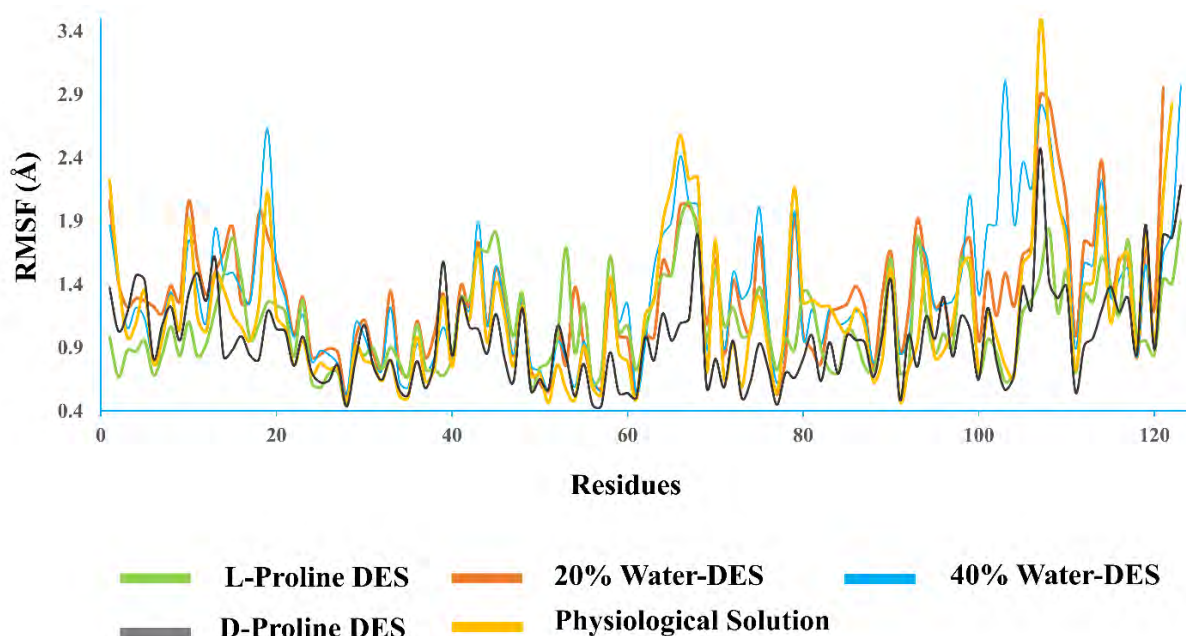


Figure 3.15: Analysis of 500ns simulation for alpha-lactalbumin by root mean square fluctuations (RMSF) in Proline-based DES solvents.

From **Figure 3.15**, it is observed that the RMSF values of the protein are found less in L-Proline: Urea and D-Proline: Urea DES solvents. The corresponding RMSF values are found in the range 0.45 – 2.05 Å in L-Proline: Urea DES and 0.44 – 2.47 Å in D-Proline: Urea DES throughout the whole simulation run. These lower RMSF values suggest that the protein structure is rigid in these pure DES solvents. Introducing 20% and 40% water contents in L-Proline: Urea DES, the protein structure is noticed to fluctuate. In the 20% water-DES system, there have been seen noticeable changes in the major portion of residues in the protein. 31.71%

amino acid residues of the total protein structure are found higher in RMSF values in 20% water-DES solvents. **Figure 3.16** depicts that the RMSF values in the residues of Leu8 – Ser9, Asp14 – Leu15, Asp20 – Thr22, His32 – Tyr36, Asp84 – Asp87, Leu110 – Cys111, and Cys120 – Glu121 are higher which alludes to the flexible nature of the alpha-lactalbumin. Further, in the 40% water-DES system, only 19.51% residues of the protein fluctuate during the whole simulation. Overall, the 20% water-DES system reflects a more flexible nature of the protein compared to the 40% water-DES system. Moreover, these results also comply with the RMSD and R_g of the protein. Besides, the RMSF value in the physiological solution is less in comparison with the water-DES system.

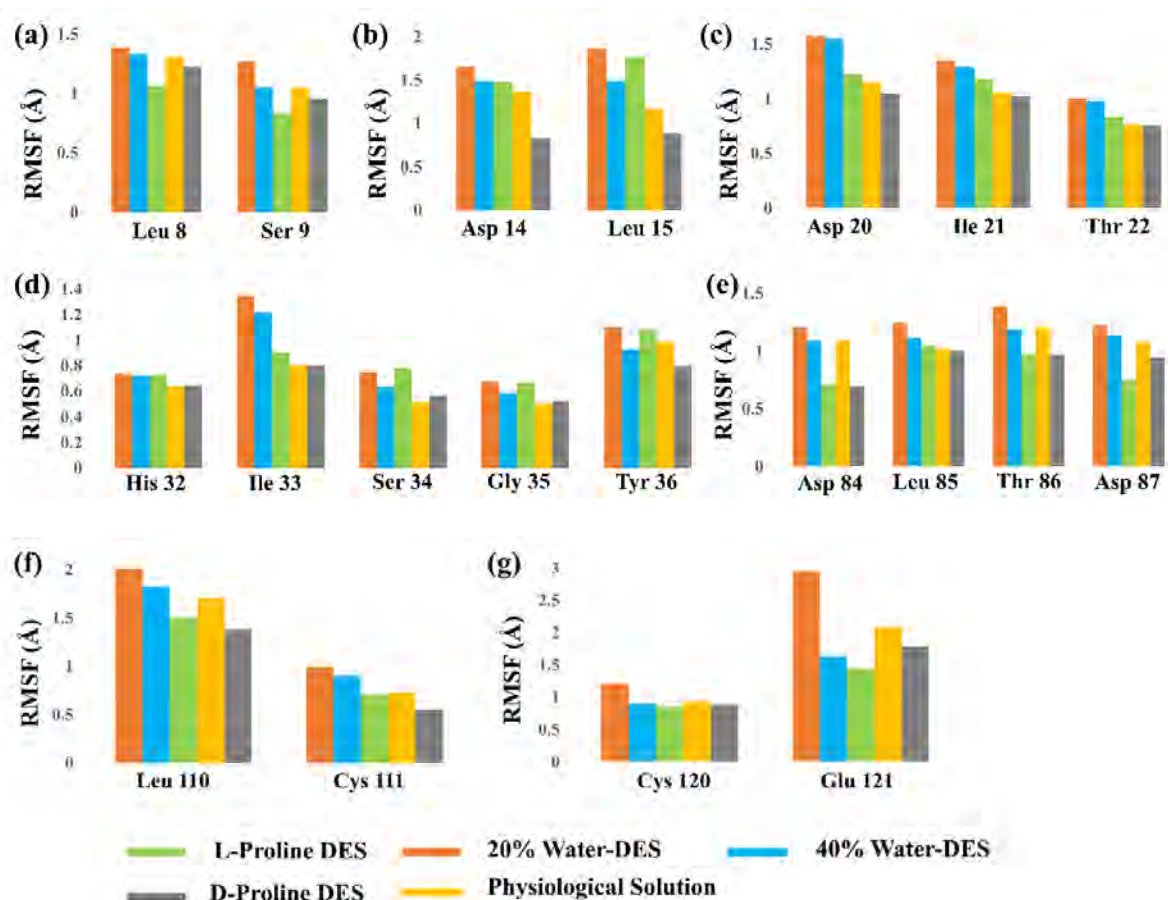


Figure 3.16: RMS fluctuation of residues (a) Leu8 – Ser9, (b) Asp14 – Leu15, (c) Asp20 – Thr22, (d) His32 – Tyr36, (e) Asp84 – Asp87, (f) Leu110 – Cys111 and (g) Cys120 – Glu121 of alpha-lactalbumin over the simulation of 500 ns.

3.2.5 Changes in the secondary structure of alpha-lactalbumin

Conformation and secondary structural elemental changes: The changes in the conformation of alpha-lactalbumin can be monitored by observing the changes of secondary structures which

affect the stability and function of the protein. **Figure 3.17** describes the conformational changes of alpha-lactalbumin in L-Proline: Urea DES, 20% water-L Proline: Urea DES, 40% water-L Proline: Urea DES, D-Proline: Urea DES, and physiological solution.

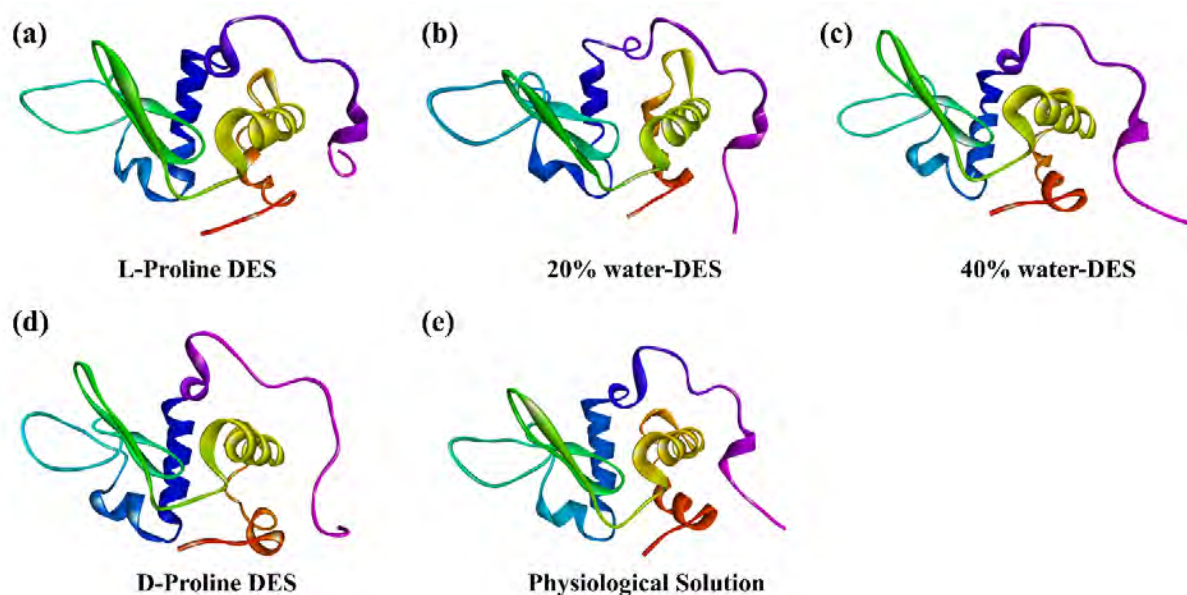


Figure 3.17: Conformational changes of alpha-lactalbumin in L-Proline: Urea DES, 20% water-L Proline: Urea DES, 40% water-L Proline: Urea DES, D-Proline: Urea DES, and physiological solution.

Further, **Figure 3.18** describes the superimposed structure also shows the structural changes of all conformers in different domains. The superimposed structures show the structural deviation of the residues of several domains of the studied protein.

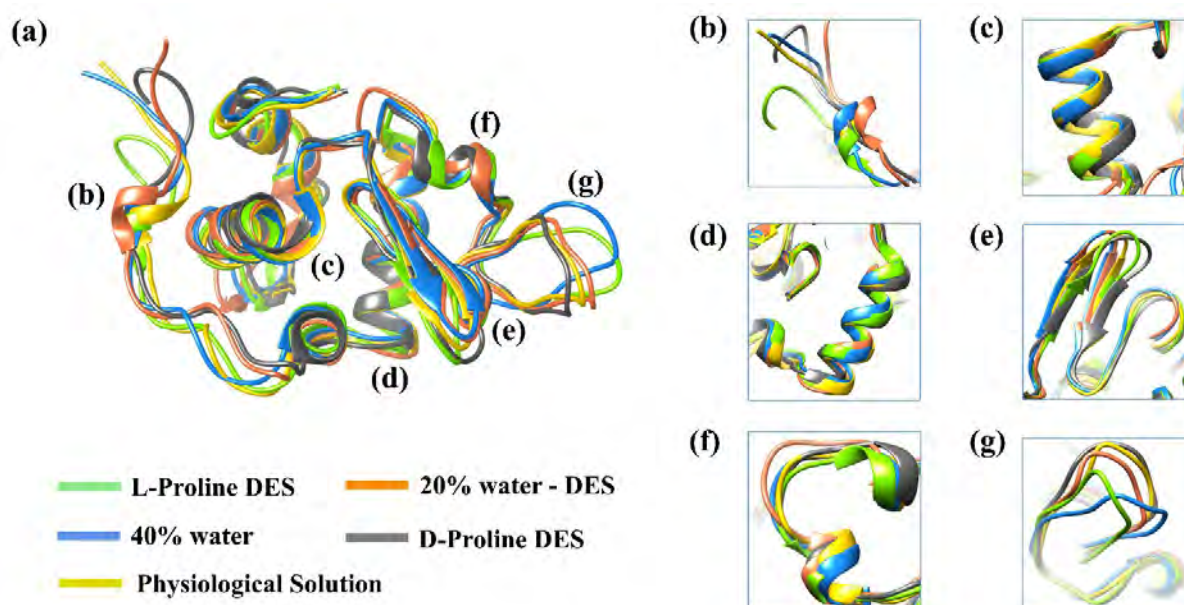


Figure 3.18: Superimposed structure of alpha-lactalbumin in L-Proline: Urea DES, 20% water-L Proline: Urea DES, 40% water-L Proline: Urea DES, D-Proline: Urea DES and physiological solution show the structural changes in different domains.

Helix transition: The analysis of secondary elements of the protein in **Table 15** and **Figure 3.19** show that the major percentage of changes in α -Helix, 3_{10} -Helix, turns and coils are responsible for the conformational changes in L-Proline DES and their hydrated solvents. During conformation changes, helix transitions were also noticed in L-Proline: Urea DES, 20% water-L Proline: Urea DES, 40% water-L Proline: Urea DES, D-Proline: Urea DES, and physiological solution. The corresponding figure is given in **Figure 3.19b** which shows the helix transition in dotted lines. For example, the residues Asn71 – Ile75 form coil shape in L-Proline: Urea DES while the 20% water-DES solution turns these residues to 3_{10} -Helix.

In 40% water-DES solution, these residues show α -Helix formation. On the other hand, the residues Leu85 – Lys99 reduce the α -Helix formation in 20% water-L Proline: Urea DES solvents compared to that in L-Proline: Urea DES, 40% water-L Proline: Urea DES, D-Proline: Urea DES, and physiological solution. This indicates that these residues are highly flexible compared to the other solvent systems which also agrees with the RMSF values (in **Figure 3.15**).

Secondary Structural Contents	(%) of L-Proline DES	(%) of D-Proline DES	(%) of 20% Water	(%) of 40% Water	(%) of Physiological Solution
Helix	29.26	26.01	25.2	31.71	37.4
Sheet	8.13	6.5	8.13	8.13	8.13
Bridge	3.25	3.25	3.25	3.25	3.25
Turn	41.46	30.08	32.52	25.2	30.89
Coil	13.01	26.02	21.14	21.14	17.89
3_{10} helix	4.88	8.94	9.76	10.57	2.44

Table 15: Percentage of secondary structure contents (α -Helix, β -Sheet, β -Bridge, Turn, Coil, and 3_{10} -Helix) of alpha-lactalbumin in L-Proline: Urea DES, 20% water-L Proline: Urea DES, 40% water-L Proline: Urea DES, D-Proline: Urea DES, and physiological solution at 500ns.

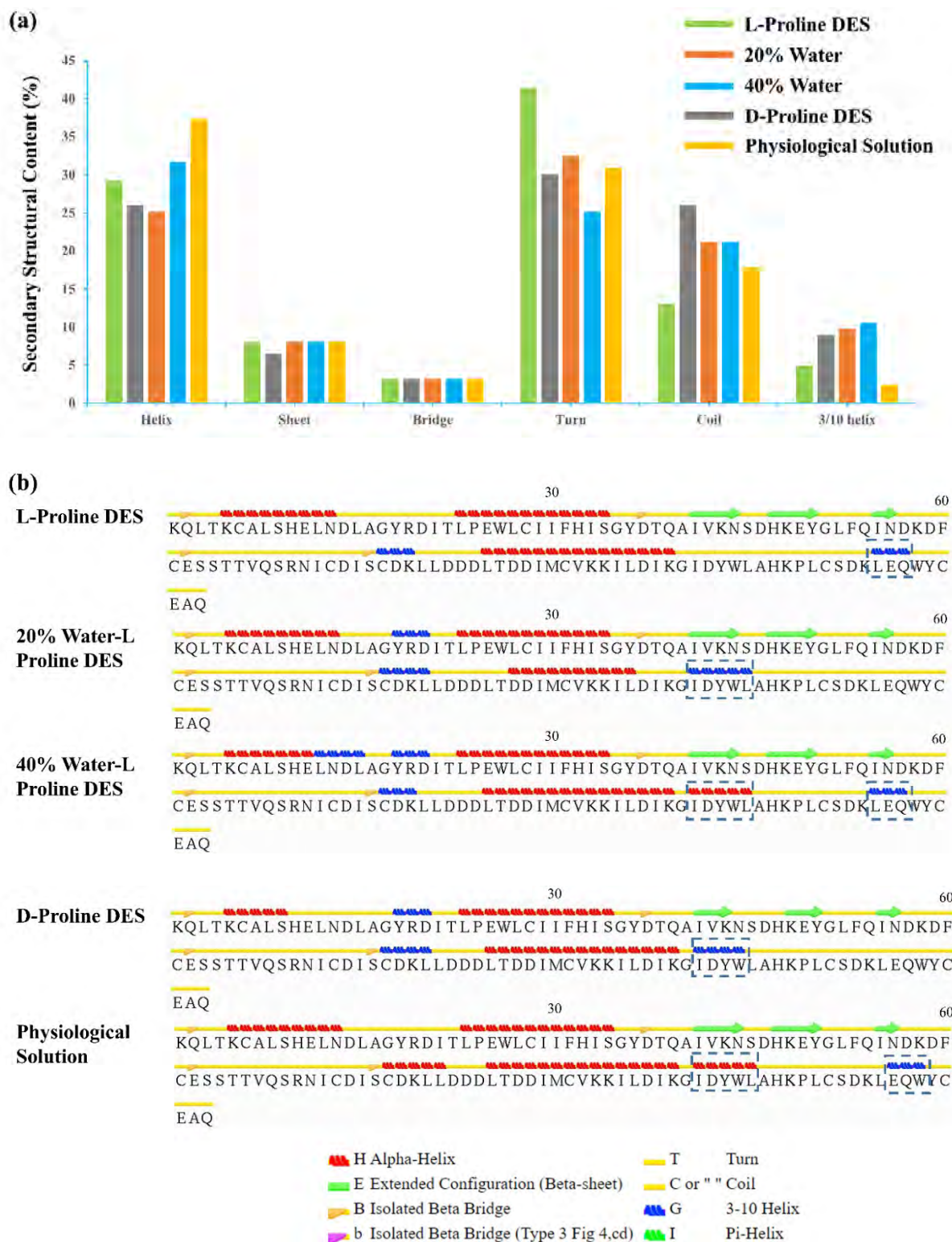


Figure 3.19: Analysis of (a) Percentage of secondary structure contents and (b) Visual changes of alpha-lactalbumin in L-Proline: Urea DES, 20% water-L Proline: Urea DES, 40% water-L Proline: Urea DES, D-Proline: Urea DES, and physiological solution at 500ns.

No changes are observed in β -Sheet and β -Bridge of the protein that can affect the whole conformer in DES and water-DES solvents. For example, the α -Helix content (29.26%) in 20% water-L Proline: Urea DES is less compared to that in pure L-Proline: Urea DES. When introducing 40% water in L-Proline: Urea DES, the α -Helix contents went higher to 31.71%. This indicates that in 20% water-DES system the α -Helix tends to get denatured while in 40% water-DES system the α -Helix is reformed. Simultaneously, the 3_{10} -Helix contents grow higher in the water-DES system compared to that in L-Proline: Urea DES system. In terms of turns, the turns of amino acid residues were reduced from 41.46% to 32.52% and 35.2% when 20% and 40% water were introduced respectively in the L-Proline: Urea DES system. However, the increasing trend of coils formation from L-Proline DES to water-L Proline: Urea DES indicates that in hydrated DES solvents the protein structure is denatured.

Molecular interaction between the residues of protein and DES components: Hydrogen bonding interaction between DES components and the residues of protein gives insight into how DES components interact with the residues of alpha-lactalbumin. **Figure 3.20** shows that the DES components, urea, and L-proline interact with the amino acid residues of alpha-lactalbumin. It is probed that urea-residues interactions are higher compared to L-proline. The reason is due to having a greater polarity of urea compared to L-Proline which leads to a higher number of interactions with urea. Similar scenarios are also found in the case of D-Proline.

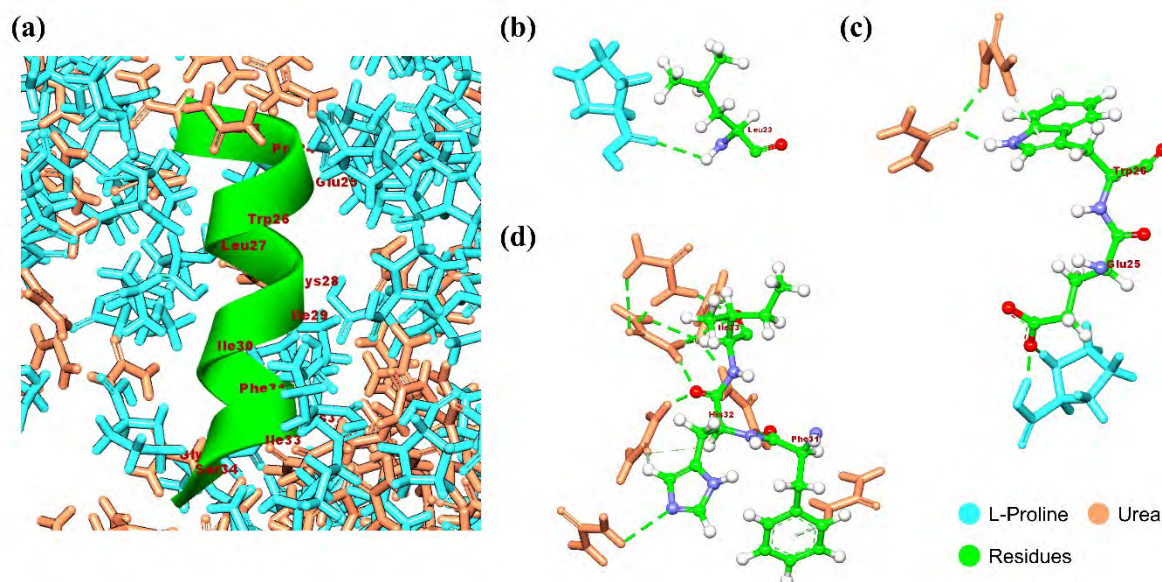


Figure 3.20: Interaction between the residues of protein and DES components showing that H-bonds dominate the residues by the urea and L-Proline.

The role of water in the interaction between water and DES component: Incorporating the water into the DES-protein environment, there are seen significant changes to the DES microstructures as well as the residues of the protein. The addition of 20% and 40% water into the DES-protein environment causes a substantial change to DES structures as well as the interaction between DES and the residues of the protein. The corresponding figures of 20% water and 40% water uptakes are given in **Figure 3.21** and **Figure 3.22**.

It is seen that in 20% water addition, the water molecules insert between DES components. **Figure 3.21** shows that water molecules form a hydrogen bonding between urea and L-Proline as a bridge by producing *urea-water-proline* or *urea-proline-water*. In this complex formation through water, L-Proline interacts more with residues while urea interacts with the residues in the absence of water. This indicates that in 20% water-DES formations start to cleave and the urea molecules tend to interact more with water because of having high polarity index. This complex structure of DES makes the whole protein unstable.

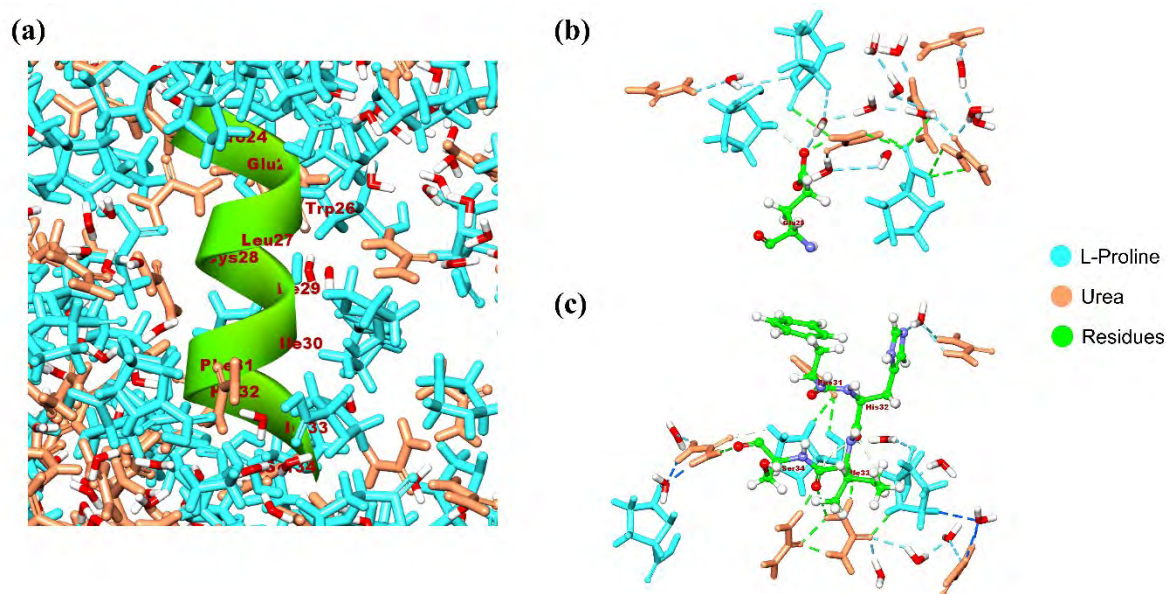


Figure 3.21: Interaction between the residues of protein and DES components with the presence of 20% water showing that *urea-water-proline* or *urea-proline-water* dominate the residues of the protein.

The simulation data of protein-DES complex, RMSD, R_g , SASA also agree that with the presence of 20% water, RMSD shows the higher fluctuation of protein, R_g indicates less compactness of the protein as well as the higher accessible surface of the protein by SASA. On the other hand, in 40% water, the DES formations cleave and a bunch of water molecules or water clusters produce *urea-(water)_{cluster}-proline* or *urea-proline-(water)_{cluster}*. The total

breakdown of DES microstructure paves to the road that in 40% water, the DES turns to the solution rather retained DES properties. This 40% water solution into L-Proline: Urea DES makes the protein relatively stable compared to that in 20% water-DES. **Figure 3.22** describes the interaction between the residues of protein and DES components with the presence of 40% water showing that *urea-(water)_{cluster}-proline* or *urea-proline-(water)_{cluster}* dominate the residues of protein and makes the whole stable in comparison to that in 20% water DES complex system.

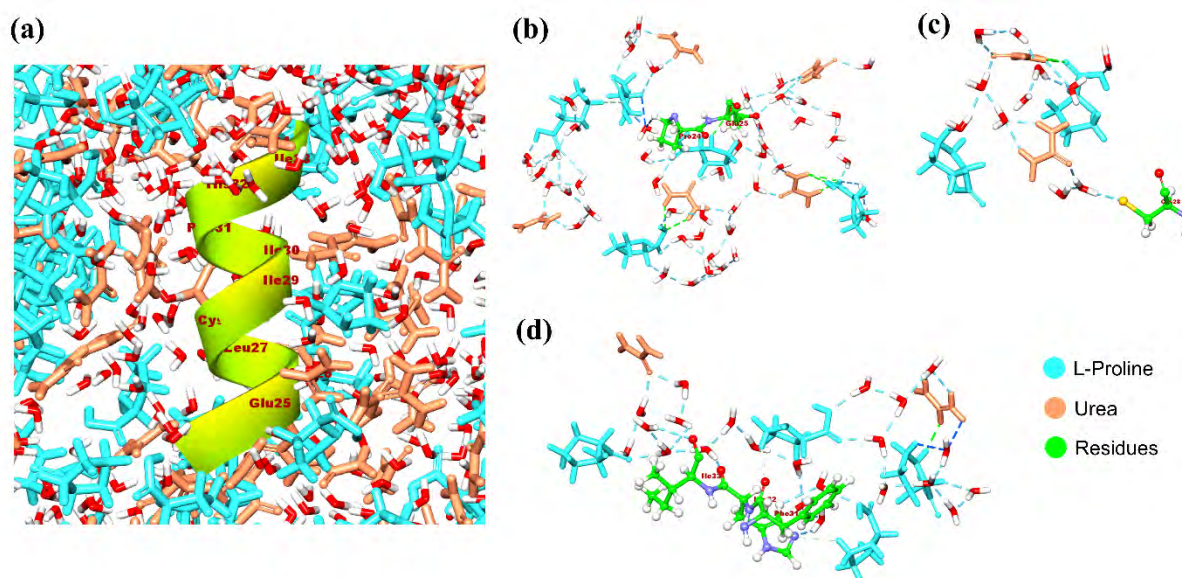


Figure 3.22: Interaction between the residues of protein and DES components with the presence of 40% water showing that *urea-(water)_{cluster}-proline* or *urea-proline-(water)_{cluster}* dominate the residues of the protein.

CHAPTER 4

CONCLUSIONS AND FUTURE ASPECTS

“Above all, don't fear difficult moments. The best comes from them.” – Rita Levi-Montalcini

4.1 Conclusion

The computational approaches by MD simulations and quantum calculations elucidate the proline-based DESs – 1:1 L-Proline: Urea and 1:1 D-Proline: Urea and the interaction of the alpha-lactalbumin protein with the studied DESs. The H-bonding interactions responsible for the formation of studied DESs are identified in L-/D-Proline and urea are $\text{NH}_{\text{L-Pro}} \dots \text{HN}_{\text{Urea}}$, $\text{CO}_{\text{Urea}} \dots \text{HC}_{\text{L-Pro}}$, $\text{OH}_{\text{L-Pro}} \dots \text{OC}_{\text{Urea}}$, and $\text{CO}_{\text{Urea}} \dots \text{HN}_{\text{L-Pro}}$. The spontaneity of the DES formation has been confirmed with the study of Gibbs free energy (ΔG), electronic energy (ΔE), and enthalpy (ΔH) changes. The characteristic spectra of studied DES cluster conformers have been established by the calculated IR and VCD signatures. Besides, the marvelous changes of conformation in alpha-lactalbumin protein have been obtained by the analyses of RMSD, R_g , SASA, and RMSF. As observed in the studied DES environments, the protein remains stable while uptake of percentages of water into those DES environments denature the protein. The reason to have denatured protein in water-DES environments is encountered by the analyses of molecular interaction between residues of protein and the water-DES components. The insights of the study can give a future direction to study the newly emerging research areas, such as amino acid-based DES and DES–protein interactions also.

4.2 Future aspects of this research

Though this work demonstrates to design the proline-based DES in a 1:1 molar ratio, there needs tremendous workouts for other molar ratios such as 1:2 L-/D-Proline: Urea or 1:3 L-/D-Proline: Urea or 1:4 L-/D-Proline: Urea and so on. Because only choosing a 1:1 molar ratio does not describe the whole nature of DES properties in real-life solutions, hence, the higher ratios can be studied for future aspects. Besides, the structural orientation, physiochemical properties of those newly thought molar ratio DESs need to be discovered which may lead to a new insight about H-bonding interaction, charge transfer calculation. However, the studies on the impact of DES on protein are very few, so, the effect on protein can be studied extensively. DES-protein interaction also needs to figure out for further prospects. This may lead to the replacements of organic solvents into the laboratory workout, pharmaceutical industries as daily activities.

REFERENCES

References:

- [1] R. A. Sheldon, "The E factor 25 years on: the rise of green chemistry and sustainability," *Green Chem.*, vol. 19, no. 1, pp. 18–43, 2017.
- [2] A. P. Abbott, G. Capper, D. L. Davies, R. K. Rasheed, and V. Tambyrajah, "Novel solvent properties of choline chloride/urea mixtures Electronic supplementary information (ESI) available: spectroscopic data. See <http://www.rsc.org/suppdata/cc/b2/b210714g/>," *Chem. Commun.*, no. 1, pp. 70–71, Dec. 2003.
- [3] B. B. Hansen *et al.*, "Deep Eutectic Solvents: A Review of Fundamentals and Applications," *Chem. Rev.*, vol. 121, no. 3, pp. 1232–1285, Feb. 2021.
- [4] E. L. Smith, A. P. Abbott, and K. S. Ryder, "Deep Eutectic Solvents (DESs) and Their Applications," *Chem. Rev.*, vol. 114, no. 21, pp. 11060–11082, Nov. 2014.
- [5] M. S. Rahman, R. Roy, B. Jadhav, M. N. Hossain, M. A. Halim, and D. E. Raynie, "Formulation, structure, and applications of therapeutic and amino acid-based deep eutectic solvents: An overview," *J. Mol. Liq.*, vol. 321, p. 114745, Jan. 2021.
- [6] X. Li and K. H. Row, "Development of deep eutectic solvents applied in extraction and separation," *J. Sep. Sci.*, vol. 39, no. 18, pp. 3505–3520, Sep. 2016.
- [7] D. Carriazo, M. C. Serrano, M. C. Gutiérrez, M. L. Ferrer, and F. del Monte, "Deep-eutectic solvents playing multiple roles in the synthesis of polymers and related materials," *Chem. Soc. Rev.*, vol. 41, no. 14, p. 4996, 2012.
- [8] A. Paiva, R. Craveiro, I. Aroso, M. Martins, R. L. Reis, and A. R. C. Duarte, "Natural Deep Eutectic Solvents – Solvents for the 21st Century," *ACS Sustain. Chem. Eng.*, vol. 2, no. 5, pp. 1063–1071, May 2014.
- [9] Q. Zhang, K. De Oliveira Vigier, S. Royer, and F. Jérôme, "Deep eutectic solvents: syntheses, properties and applications," *Chem. Soc. Rev.*, vol. 41, no. 21, p. 7108, 2012.
- [10] R. Ullah *et al.*, "A detailed study of cholinium chloride and levulinic acid deep eutectic solvent system for CO₂ capture via experimental and molecular simulation approaches," *Phys. Chem. Chem. Phys.*, vol. 17, no. 32, pp. 20941–20960, 2015.
- [11] A. Korotkevich, D. S. Firaha, A. A. H. Padua, and B. Kirchner, "Ab initio molecular dynamics simulations of SO₂ solvation in choline chloride/glycerol deep eutectic solvent," *Fluid Phase Equilib.*, vol. 448, pp. 59–68, 2017.
- [12] Y. Song, S. Chen, F. Luo, and L. Sun, "Absorption of Toluene Using Deep Eutectic Solvents: Quantum Chemical Calculations and Experimental Investigation," *Ind. Eng. Chem. Res.*, vol. 59, no. 52, pp. 22605–22618, 2020.
- [13] J. M. Rimsza and L. R. Corrales, "Adsorption complexes of copper and copper oxide in the deep eutectic solvent 2:1 urea-choline chloride," *Comput. Theor. Chem.*, vol. 987, pp. 57–61, 2012.
- [14] B. Ozturk and M. Gonzalez-Miquel, "Alkanediol-based deep eutectic solvents for isolation of terpenoids from citrus essential oil: Experimental evaluation and COSMO-RS studies," *Sep. Purif. Technol.*, vol. 227, no. June, p. 115707, 2019.
- [15] T. Jeliński and P. Cysewski, "Application of a computational model of natural deep

REFERENCES

- eutectic solvents utilizing the COSMO-RS approach for screening of solvents with high solubility of rutin,” *J. Mol. Model.*, vol. 24, no. 7, pp. 1–17, 2018.
- [16] M. Larriba *et al.*, “Choline Chloride-Based Deep Eutectic Solvents in the Dearomatization of Gasolines,” *ACS Sustain. Chem. Eng.*, vol. 6, no. 1, pp. 1039–1047, 2018.
- [17] P. Dehury, U. Mahanta, and T. Banerjee, “Comprehensive Assessment on the Use of Boron Nitride-Based Nanofluids Comprising Eutectic Mixtures of Diphenyl Ether and Menthol for Enhanced Thermal Media,” *ACS Sustain. Chem. Eng.*, vol. 8, no. 38, pp. 14595–14604, 2020.
- [18] M. Karibayev and D. Shah, “Comprehensive Computational Analysis Exploring the Formation of Caprolactam-Based Deep Eutectic Solvents and Their Applications in Natural Gas Desulfurization,” *Energy and Fuels*, vol. 34, no. 8, pp. 9894–9902, 2020.
- [19] R. Abedin, S. Heidarian, J. C. Flake, and F. R. Hung, “Computational Evaluation of Mixtures of Hydrofluorocarbons and Deep Eutectic Solvents for Absorption Refrigeration Systems,” *Langmuir*, vol. 33, no. 42, pp. 11611–11625, 2017.
- [20] A. Gutiérrez, S. Aparicio, and M. Atilhan, “Design of arginine-based therapeutic deep eutectic solvents as drug solubilization vehicles for active pharmaceutical ingredients,” *Phys. Chem. Chem. Phys.*, vol. 21, no. 20, pp. 10621–10634, 2019.
- [21] A. K. Jangir, B. Lad, U. Dani, N. Shah, and K. Kuperkar, “In vitro toxicity assessment and enhanced drug solubility profile of green deep eutectic solvent derivatives (DESDs) combined with theoretical validation,” *RSC Adv.*, vol. 10, no. 40, pp. 24063–24072, 2020.
- [22] H. Wang, S. Liu, Y. Zhao, J. Wang, and Z. Yu, “Insights into the Hydrogen Bond Interactions in Deep Eutectic Solvents Composed of Choline Chloride and Polyols,” *ACS Sustain. Chem. Eng.*, vol. 7, no. 8, pp. 7760–7767, 2019.
- [23] G. García, M. Atilhan, and S. Aparicio, “Interfacial Properties of Deep Eutectic Solvents Regarding to CO₂ Capture,” *J. Phys. Chem. C*, vol. 119, no. 37, pp. 21413–21425, 2015.
- [24] H. Ji and P. Lv, “Mechanistic insights into the lignin dissolution behaviors of a recyclable acid hydrotrope, deep eutectic solvent (DES), and ionic liquid (IL),” *Green Chem.*, vol. 22, no. 4, pp. 1378–1387, 2020.
- [25] Q. Xia *et al.*, “Multiple hydrogen bond coordination in three-constituent deep eutectic solvents enhances lignin fractionation from biomass,” *Green Chem.*, vol. 20, no. 12, pp. 2711–2721, 2018.
- [26] R. Verma, M. Mohan, V. V. Goud, and T. Banerjee, “Operational Strategies and Comprehensive Evaluation of Menthol Based Deep Eutectic Solvent for the Extraction of Lower Alcohols from Aqueous Media,” *ACS Sustain. Chem. Eng.*, vol. 6, no. 12, pp. 16920–16932, 2018.
- [27] D. V. Wagle, H. Zhao, C. A. Deakyne, and G. A. Baker, “Quantum Chemical Evaluation of Deep Eutectic Solvents for the Extractive Desulfurization of Fuel,” *ACS Sustain. Chem. Eng.*, vol. 6, no. 6, pp. 7525–7531, Jun. 2018.
- [28] A. Kamgar, S. Mohsenpour, and F. Esmaeilzadeh, “Solubility prediction of CO₂, CH₄, H₂, CO and N₂ in Choline Chloride/Urea as a eutectic solvent using NRTL and COSMO-RS models,” *J. Mol. Liq.*, vol. 247, pp. 70–74, 2017.

REFERENCES

- [29] A. Salamatmanesh, A. Heydari, and H. T. Nahzomi, "Stabilizing Pd on magnetic phosphine-functionalized cellulose: DFT study and catalytic performance under deep eutectic solvent assisted conditions," *Carbohydr. Polym.*, vol. 235, no. October 2019, p. 115947, 2020.
- [30] H. Palmelund, M. P. Andersson, C. J. Asgreen, B. J. Boyd, J. Rantanen, and K. Löbmann, "Tailor-made solvents for pharmaceutical use? Experimental and computational approach for determining solubility in deep eutectic solvents (DES)," *Int. J. Pharm. X*, vol. 1, no. October, p. 100034, 2019.
- [31] H. Li *et al.*, "Theoretical evidence of charge transfer interaction between SO₂ and deep eutectic solvents formed by choline chloride and glycerol," *Phys. Chem. Chem. Phys.*, vol. 17, no. 43, pp. 28729–28742, 2015.
- [32] S. Kaur, A. Malik, and H. K. Kashyap, "Anatomy of Microscopic Structure of Ethaline Deep Eutectic Solvent Decoded through Molecular Dynamics Simulations," *J. Phys. Chem. B*, vol. 123, no. 39, pp. 8291–8299, Oct. 2019.
- [33] S. Kaur, S. Sharma, and H. K. Kashyap, "Bulk and interfacial structures of reline deep eutectic solvent: A molecular dynamics study," *J. Chem. Phys.*, vol. 147, no. 19, pp. 1–10, 2017.
- [34] H. S. Salehi, R. Hens, O. A. Moulτος, and T. J. H. Vlugt, "Computation of gas solubilities in choline chloride urea and choline chloride ethylene glycol deep eutectic solvents using Monte Carlo simulations," *J. Mol. Liq.*, vol. 316, p. 113729, 2020.
- [35] E. S. C. Ferreira, I. V. Voroshylova, N. M. Figueiredo, C. M. Pereira, and M. N. D. S. Cordeiro, "Computational and experimental study of propeline: A choline chloride based deep eutectic solvent," *J. Mol. Liq.*, vol. 298, p. 111978, 2020.
- [36] H. S. Salehi, M. Ramdin, O. A. Moulτος, and T. J. H. Vlugt, "Computing solubility parameters of deep eutectic solvents from Molecular Dynamics simulations," *Fluid Phase Equilib.*, vol. 497, pp. 10–18, 2019.
- [37] S. Mainberger, M. Kindlein, F. Bezold, E. Elts, M. Minceva, and H. Briesen, "Deep eutectic solvent formation: a structural view using molecular dynamics simulations with classical force fields," *Mol. Phys.*, vol. 115, no. 9–12, pp. 1309–1321, 2017.
- [38] V. Migliorati, F. Sessa, and P. D'Angelo, "Deep eutectic solvents: A structural point of view on the role of the cation," *Chem. Phys. Lett. X*, vol. 2, no. December 2018, p. 100001, 2019.
- [39] S. L. Perkins, P. Painter, and C. M. Colina, "Experimental and computational studies of choline chloride-based deep eutectic solvents," *J. Chem. Eng. Data*, vol. 59, no. 11, pp. 3652–3662, 2014.
- [40] A. Van Den Bruinhorst, T. Spyriouni, J. R. Hill, and M. C. Kroon, "Experimental and Molecular Modeling Evaluation of the Physicochemical Properties of Proline-Based Deep Eutectic Solvents," *J. Phys. Chem. B*, vol. 122, no. 1, pp. 369–379, 2018.
- [41] E. O. Fetisov *et al.*, "First-Principles Molecular Dynamics Study of a Deep Eutectic Solvent: Choline Chloride/Urea and Its Mixture with Water," *J. Phys. Chem. B*, vol. 122, no. 3, pp. 1245–1254, 2018.
- [42] S. Kaur, A. Gupta, and H. K. Kashyap, "How Hydration Affects the Microscopic Structural Morphology in a Deep Eutectic Solvent," *J. Phys. Chem. B*, vol. 124, no. 11,

REFERENCES

- pp. 2230–2237, Mar. 2020.
- [43] E. S. C. Ferreira, I. V. Voroshylova, C. M. Pereira, and M. N. D. S. Cordeiro, “Improved force field model for the deep eutectic solvent ethaline: Reliable physicochemical properties,” *J. Phys. Chem. B*, vol. 120, no. 38, pp. 10124–10137, 2016.
- [44] P. Kumari, Shobhna, S. Kaur, and H. K. Kashyap, “Influence of Hydration on the Structure of Reline Deep Eutectic Solvent: A Molecular Dynamics Study,” *ACS Omega*, vol. 3, no. 11, pp. 15246–15255, Nov. 2018.
- [45] Y. Zhang *et al.*, “Liquid Structure and Transport Properties of the Deep Eutectic Solvent Ethaline,” *J. Phys. Chem. B*, vol. 124, no. 25, pp. 5251–5264, 2020.
- [46] O. S. Hammond, D. T. Bowron, and K. J. Edler, “Liquid structure of the choline chloride-urea deep eutectic solvent (reline) from neutron diffraction and atomistic modelling,” *Green Chem.*, vol. 18, no. 9, pp. 2736–2744, 2016.
- [47] M. Saha, M. S. Rahman, M. N. Hossain, D. E. Raynie, and M. A. Halim, “Molecular and Spectroscopic Insights of a Choline Chloride Based Therapeutic Deep Eutectic Solvent,” *J. Phys. Chem. A*, vol. 124, no. 23, pp. 4690–4699, Jun. 2020.
- [48] S. L. Perkins, P. Painter, and C. M. Colina, “Molecular dynamic simulations and vibrational analysis of an ionic liquid analogue,” *J. Phys. Chem. B*, vol. 117, no. 35, pp. 10250–10260, 2013.
- [49] P. K. Naik, M. Mohan, T. Banerjee, S. Paul, and V. V. Goud, “Molecular Dynamic Simulations for the Extraction of Quinoline from Heptane in the Presence of a Low-Cost Phosphonium-Based Deep Eutectic Solvent,” *J. Phys. Chem. B*, vol. 122, no. 14, pp. 4006–4015, 2018.
- [50] T. Banerjee, N. Paul, P. K. Naik, B. D. Ribeiro, P. S. G. Pattader, and I. M. Marrucho, “Molecular dynamics insights and water stability of hydrophobic deep eutectic solvents aided extraction of nitenpyram from an aqueous environment,” *J. Phys. Chem. B*, vol. 124, no. 34, pp. 7405–7420, 2020.
- [51] H. Sun, Y. Li, X. Wu, and G. Li, “Theoretical study on the structures and properties of mixtures of urea and choline chloride,” *J. Mol. Model.*, vol. 19, no. 6, pp. 2433–2441, 2013.
- [52] M. I. Rain *et al.*, “A comprehensive computational and principal component analysis on various choline chloride-based deep eutectic solvents to reveal their structural and spectroscopic properties,” *J. Chem. Phys.*, vol. 155, no. 4, 2021.
- [53] G. García, M. Atilhan, and S. Aparicio, “An approach for the rationalization of melting temperature for deep eutectic solvents from DFT,” *Chem. Phys. Lett.*, vol. 634, pp. 151–155, 2015.
- [54] D. V. Wagle, L. Adhikari, and G. A. Baker, “Computational perspectives on structure, dynamics, gas sorption, and bio-interactions in deep eutectic solvents,” *Fluid Phase Equilib.*, vol. 448, pp. 50–58, 2017.
- [55] C. R. Ashworth, R. P. Matthews, T. Welton, and P. A. Hunt, “Doubly ionic hydrogen bond interactions within the choline chloride-urea deep eutectic solvent,” *Phys. Chem. Chem. Phys.*, vol. 18, no. 27, pp. 18145–18160, 2016.
- [56] D. Shah and F. S. Mjalli, “Effect of water on the thermo-physical properties of Reline: An experimental and molecular simulation based approach,” *Phys. Chem. Chem. Phys.*,

REFERENCES

- vol. 16, no. 43, pp. 23900–23907, 2014.
- [57] I. Zahrina, M. Nasikin, K. Mulia, M. Prajanto, and A. Yanuar, “Molecular interactions between betaine monohydrate-glycerol deep eutectic solvents and palmitic acid: Computational and experimental studies,” *J. Mol. Liq.*, vol. 251, pp. 28–34, Feb. 2018.
- [58] I. Zahrina, K. Mulia, A. Yanuar, and M. Nasikin, “Molecular interactions in the betaine monohydrate-polyol deep eutectic solvents: Experimental and computational studies,” *J. Mol. Struct.*, vol. 1158, pp. 133–138, Apr. 2018.
- [59] R. Stefanovic, M. Ludwig, G. B. Webber, R. Atkin, and A. J. Page, “Nanostructure, hydrogen bonding and rheology in choline chloride deep eutectic solvents as a function of the hydrogen bond donor,” *Phys. Chem. Chem. Phys.*, vol. 19, no. 4, pp. 3297–3306, 2017.
- [60] A. kumar Jangir, D. Patel, R. More, A. Parmar, and K. Kuperkar, “New insight into experimental and computational studies of Choline chloride-based ‘green’ ternary deep eutectic solvent (TDES),” *J. Mol. Struct.*, vol. 1181, pp. 295–299, 2019.
- [61] K. Biernacki, H. K. S. Souza, C. M. R. Almeida, A. L. Magalhães, and M. P. Gonçalves, “Physicochemical Properties of Choline Chloride-Based Deep Eutectic Solvents with Polyols: An Experimental and Theoretical Investigation,” *ACS Sustain. Chem. Eng.*, vol. 8, no. 50, pp. 18712–18728, 2020.
- [62] D. V. Wagle, C. A. Deakyne, and G. A. Baker, “Quantum Chemical Insight into the Interactions and Thermodynamics Present in Choline Chloride Based Deep Eutectic Solvents,” *J. Phys. Chem. B*, vol. 120, no. 27, pp. 6739–6746, 2016.
- [63] M. A. Ali, M. S. Rahman, R. Roy, P. Gambill, D. E. Raynie, and M. A. Halim, “Structure Elucidation of Menthol-Based Deep Eutectic Solvent using Experimental and Computational Techniques,” *J. Phys. Chem. A*, vol. 125, no. 12, pp. 2402–2412, 2021.
- [64] S. Benabid, Y. Benguerba, I. M. AlNashef, and N. Haddaoui, “Theoretical study of physicochemical properties of selected ammonium salt-based deep eutectic solvents,” *J. Mol. Liq.*, vol. 285, pp. 38–46, 2019.
- [65] S. Zhu *et al.*, “Vibrational analysis and formation mechanism of typical deep eutectic solvents: An experimental and theoretical study,” *J. Mol. Graph. Model.*, vol. 68, pp. 158–175, 2016.
- [66] V. P. Nicu, J. Autschbach, and E. J. Baerends, “Enhancement of IR and VCD intensities due to charge transfer,” *Phys. Chem. Chem. Phys.*, vol. 11, no. 10, pp. 1526–1538, 2009.
- [67] M. Losada and Y. Xu, “Chirality transfer through hydrogen-bonding: Experimental and ab initio analyses of vibrational circular dichroism spectra of methyl lactate in water,” *Phys. Chem. Chem. Phys.*, vol. 9, no. 24, p. 3127, 2007.
- [68] T. M. Carlson, K. W. Lam, C. W. Lam, J. Z. He, J. H. Maynard, and S. Cavagnero, “Naked-Eye Detection of Reversible Protein Folding and Unfolding in Aqueous Solution,” *J. Chem. Educ.*, vol. 94, no. 3, pp. 350–355, Mar. 2017.
- [69] D. Gomez, K. Huber, and S. Klumpp, “On Protein Folding in Crowded Conditions,” *J. Phys. Chem. Lett.*, vol. 10, no. 24, pp. 7650–7656, Dec. 2019.
- [70] R. W. Newberry and R. T. Raines, “Secondary Forces in Protein Folding,” *ACS Chem. Biol.*, vol. 14, no. 8, pp. 1677–1686, Aug. 2019.

REFERENCES

- [71] U. Adhikari, B. Mostofian, J. Copperman, S. R. Subramanian, A. A. Petersen, and D. M. Zuckerman, "Computational Estimation of Microsecond to Second Atomistic Folding Times," *J. Am. Chem. Soc.*, vol. 141, no. 16, pp. 6519–6526, Apr. 2019.
- [72] S. Chong and S. Ham, "Protein Folding Thermodynamics: A New Computational Approach," *J. Phys. Chem. B*, vol. 118, no. 19, pp. 5017–5025, May 2014.
- [73] M. Compiani and E. Capriotti, "Computational and Theoretical Methods for Protein Folding," *Biochemistry*, vol. 52, no. 48, pp. 8601–8624, Dec. 2013.
- [74] K. Tamoliūnas and N. Galamba, "Protein Denaturation, Zero Entropy Temperature, and the Structure of Water around Hydrophobic and Amphiphilic Solutes," *J. Phys. Chem. B*, vol. 124, no. 48, pp. 10994–11006, Dec. 2020.
- [75] I. A. Sedov and T. I. Magsumov, "Molecular dynamics study of unfolding of lysozyme in water and its mixtures with dimethyl sulfoxide," *J. Mol. Graph. Model.*, vol. 76, pp. 466–474, Sep. 2017.
- [76] C. Yang, S. Jang, and Y. Pak, "Computational Probing of Temperature-Dependent Unfolding of a Small Globular Protein: From Cold to Heat Denaturation," 2020.
- [77] S. Roy and B. Bagchi, "Comparative Study of Protein Unfolding in Aqueous Urea and Dimethyl Sulfoxide Solutions: Surface Polarity, Solvent Specificity, and Sequence of Secondary Structure Melting," *J. Phys. Chem. B*, vol. 118, no. 21, pp. 5691–5697, May 2014.
- [78] B. Biswas, A. N. Muttathukattil, G. Reddy, and P. C. Singh, "Contrasting Effects of Guanidinium Chloride and Urea on the Activity and Unfolding of Lysozyme," *ACS Omega*, vol. 3, no. 10, pp. 14119–14126, Oct. 2018.
- [79] H. Monhemi, M. R. Housaindokht, A. A. Moosavi-Movahedi, and M. R. Bozorgmehr, "How a protein can remain stable in a solvent with high content of urea: insights from molecular dynamics simulation of *Candida antarctica* lipase B in urea : choline chloride deep eutectic solvent," *Phys. Chem. Chem. Phys.*, vol. 16, no. 28, p. 14882, 2014.
- [80] P. Kumari, M. Kumari, and H. K. Kashyap, "How Pure and Hydrated Reline Deep Eutectic Solvents Affect the Conformation and Stability of Lysozyme: Insights from Atomistic Molecular Dynamics Simulations," *J. Phys. Chem. B*, vol. 124, no. 52, pp. 11919–11927, Dec. 2020.
- [81] S. Sarkar, S. Ghosh, and R. Chakrabarti, "Ammonium based stabilizers effectively counteract urea-induced denaturation in a small protein: insights from molecular dynamics simulations," *RSC Adv.*, vol. 7, no. 83, pp. 52888–52906, 2017.
- [82] M. Shehata, A. Unlu, U. Sezerman, and E. Timucin, "Lipase and Water in a Deep Eutectic Solvent: Molecular Dynamics and Experimental Studies of the Effects of Water-In-Deep Eutectic Solvents on Lipase Stability," *J. Phys. Chem. B*, vol. 124, no. 40, pp. 8801–8810, Oct. 2020.
- [83] Y. P. Mbous, M. Hayyan, W. F. Wong, A. Hayyan, C. Y. Looi, and M. A. Hashim, "Simulation of Deep Eutectic Solvents' Interaction with Membranes of Cancer Cells Using COSMO-RS," *J. Phys. Chem. B*, vol. 124, no. 41, pp. 9086–9094, Oct. 2020.
- [84] A. Triolo, F. Lo Celso, and O. Russina, "Structural Features of β -Cyclodextrin Solvation in the Deep Eutectic Solvent, Reline," *J. Phys. Chem. B*, vol. 124, no. 13, pp. 2652–2660, Apr. 2020.

REFERENCES

- [85] C. Nick Pace, S. Treviño, E. Prabhakaran, and J. Martin Scholtz, “Protein structure, stability and solubility in water and other solvents,” *Philos. Trans. R. Soc. London. Ser. B Biol. Sci.*, vol. 359, no. 1448, pp. 1225–1235, Aug. 2004.
- [86] S. Pal and S. Paul, “Understanding The Role of Reline, a Natural DES, on Temperature-Induced Conformational Changes of C-Kit G-Quadruplex DNA: A Molecular Dynamics Study,” *J. Phys. Chem. B*, vol. 124, no. 15, pp. 3123–3136, Apr. 2020.
- [87] T. Janc *et al.*, “Ion-specificity and surface water dynamics in protein solutions,” *Phys. Chem. Chem. Phys.*, vol. 20, no. 48, pp. 30340–30350, 2018.
- [88] J. A. Harrison, J. D. Schall, S. Maskey, P. T. Mikulski, M. T. Knippenberg, and B. H. Morrow, “Review of force fields and intermolecular potentials used in atomistic computational materials research,” *Appl. Phys. Rev.*, vol. 5, no. 3, p. 031104, Sep. 2018.
- [89] E. G. Lewars, *Computational Chemistry*. Cham: Springer International Publishing, 2016.
- [90] R. F. Nalewajski, *Perspectives in Electronic Structure Theory*, vol. 9783642201. Berlin, Heidelberg: Springer Berlin Heidelberg, 2012.
- [91] R. O. Jones, “Density functional theory: Its origins, rise to prominence, and future,” *Rev. Mod. Phys.*, vol. 87, no. 3, pp. 897–923, Aug. 2015.
- [92] A. J. Cohen, P. Mori-Sánchez, and W. Yang, “Challenges for Density Functional Theory,” *Chem. Rev.*, vol. 112, no. 1, pp. 289–320, Jan. 2012.
- [93] W. J. Hehre, *A Guide to Molecular Mechanics and Quantum Chemical Calculations*. 2003.
- [94] F. Jensen, “Atomic orbital basis sets,” *Wiley Interdiscip. Rev. Comput. Mol. Sci.*, vol. 3, no. 3, pp. 273–295, May 2013.
- [95] F. Pena-Pereira, A. Kloskowski, and J. Namieśnik, “Perspectives on the replacement of harmful organic solvents in analytical methodologies: a framework toward the implementation of a generation of eco-friendly alternatives,” *Green Chem.*, vol. 17, no. 7, pp. 3687–3705, 2015.
- [96] C. J. Clarke, W.-C. Tu, O. Levers, A. Bröhl, and J. P. Hallett, “Green and Sustainable Solvents in Chemical Processes,” *Chem. Rev.*, vol. 118, no. 2, pp. 747–800, Jan. 2018.
- [97] M. L. Harrell, T. Malinski, C. Torres-López, K. Gonzalez, J. Suriboot, and D. E. Bergbreiter, “Alternatives for Conventional Alkane Solvents,” *J. Am. Chem. Soc.*, vol. 138, no. 44, pp. 14650–14657, Nov. 2016.
- [98] D. J. G. P. van Osch, C. H. J. T. Dietz, S. E. E. Warrag, and M. C. Kroon, “The Curious Case of Hydrophobic Deep Eutectic Solvents: A Story on the Discovery, Design, and Applications,” *ACS Sustain. Chem. Eng.*, vol. 8, no. 29, p. accsuschemeng.0c00559, Jul. 2020.
- [99] A. van den Bruinhorst, T. Spyriouni, J.-R. Hill, and M. C. Kroon, “Experimental and Molecular Modeling Evaluation of the Physicochemical Properties of Proline-Based Deep Eutectic Solvents,” *J. Phys. Chem. B*, vol. 122, no. 1, pp. 369–379, Jan. 2018.
- [100] M. J. Frisch *et al.*, “Gaussian 09, Revision D.01,” *Gaussian Inc.*, p. Wallingford CT, 2009.

REFERENCES

- [101] A. Kovács, J. Cz. Dobrowolski, S. Ostrowski, and J. E. Rode, “Benchmarking density functionals in conjunction with Grimme’s dispersion correction for noble gas dimers (Ne 2 , Ar 2 , Kr 2 , Xe 2 , Rn 2),” *Int. J. Quantum Chem.*, vol. 117, no. 9, p. e25358, May 2017.
- [102] E. G. Hohenstein, S. T. Chill, and C. D. Sherrill, “Assessment of the Performance of the M05–2X and M06–2X Exchange–Correlation Functionals for Noncovalent Interactions in Biomolecules,” *J. Chem. Theory Comput.*, vol. 4, no. 12, pp. 1996–2000, Dec. 2008.
- [103] M. A. Halim, D. M. Shaw, and R. A. Poirier, “Medium effect on the equilibrium geometries, vibrational frequencies and solvation energies of sulfanilamide,” *J. Mol. Struct. THEOCHEM*, vol. 960, no. 1–3, pp. 63–72, Nov. 2010.
- [104] A. D. Becke, “Density-functional thermochemistry. III. The role of exact exchange,” *J. Chem. Phys.*, vol. 98, no. 7, pp. 5648–5652, Apr. 1993.
- [105] J. S. Murray and P. Politzer, “The electrostatic potential: an overview,” *WIREs Comput. Mol. Sci.*, vol. 1, no. 2, pp. 153–163, Mar. 2011.
- [106] J. D. Mottishaw, A. R. Erck, J. H. Kramer, H. Sun, and M. Koppang, “Electrostatic Potential Maps and Natural Bond Orbital Analysis: Visualization and Conceptualization of Reactivity in Sanger’s Reagent,” *J. Chem. Educ.*, vol. 92, no. 11, pp. 1846–1852, Nov. 2015.
- [107] A. kumar Jangir, D. Patel, R. More, A. Parmar, and K. Kuperkar, “New insight into experimental and computational studies of Choline chloride-based ‘green’ ternary deep eutectic solvent (TDES),” *J. Mol. Struct.*, vol. 1181, pp. 295–299, Apr. 2019.
- [108] M. Martínez-Martínez *et al.*, “Determinants and Prediction of Esterase Substrate Promiscuity Patterns,” *ACS Chem. Biol.*, vol. 13, no. 1, pp. 225–234, Jan. 2018.
- [109] S. Hayryan, C.-K. Hu, J. Skřivánek, E. Hayryane, and I. Pokorný, “A new analytical method for computing solvent-accessible surface area of macromolecules and its gradients,” *J. Comput. Chem.*, vol. 26, no. 4, pp. 334–343, Mar. 2005.
- [110] R. Fraczkiewicz and W. Braun, “Exact and efficient analytical calculation of the accessible surface areas and their gradients for macromolecules,” *J. Comput. Chem.*, vol. 19, no. 3, p. 319, Feb. 1998.
- [111] B. Qiao, F. Jiménez-Ángeles, T. D. Nguyen, and M. Olvera de la Cruz, “Water follows polar and nonpolar protein surface domains,” *Proc. Natl. Acad. Sci.*, vol. 116, no. 39, pp. 19274–19281, Sep. 2019.
- [112] F. Persson, P. Söderhjelm, and B. Halle, “How proteins modify water dynamics,” *J. Chem. Phys.*, vol. 148, no. 21, p. 215103, Jun. 2018.
- [113] R. Barnes, S. Sun, Y. Fichou, F. W. Dahlquist, M. Heyden, and S. Han, “Spatially Heterogeneous Surface Water Diffusivity around Structured Protein Surfaces at Equilibrium,” *J. Am. Chem. Soc.*, vol. 139, no. 49, pp. 17890–17901, Dec. 2017.
- [114] P. Rani and P. Biswas, “Diffusion of Hydration Water around Intrinsically Disordered Proteins,” *J. Phys. Chem. B*, vol. 119, no. 42, pp. 13262–13270, Oct. 2015.